Titre: Title:	Bio-Sourced Quinones for Sustainable Electrochemical Energy Storage: The Case Studies of Tannins and Sepia Melanin
Auteur: Author:	Molood Alsadat Hoseinizadeh
Date:	2024
Type:	Mémoire ou thèse / Dissertation or Thesis
Référence: Citation:	Hoseinizadeh, M. A. (2024). Bio-Sourced Quinones for Sustainable Electrochemical Energy Storage: The Case Studies of Tannins and Sepia Melanin [Thèse de doctorat, Polytechnique Montréal]. PolyPublie. https://publications.polymtl.ca/61897/

POLYTECHNIQUE MONTRÉAL

affiliée à l'Université de Montréal

Bio-sourced quinones for sustainable electrochemical energy storage: the case studies of Tannins and Sepia melanin

MOLOOD ALSADAT HOSEINIZADEH

Département de génie physique

Thèse présentée en vue de l'obtention du diplôme de *Philosophiæ Doctor*

Génie des matériaux

Décembre 2024

POLYTECHNIQUE MONTRÉAL

affiliée à l'Université de Montréal

Cette thèse intitulée :

Bio-sourced quinone for sustainable electrochemical energy storage: the case studies of Tannins and Sepia melanin

présentée par **Molood Alsadat HOSEINIZADEH**

en vue de l'obtention du diplôme de *Philosophiæ Doctor*

a été dûment acceptée par le jury d'examen constitué de :

Gregory PATIENCE, président
Clara SANTATO, membre et directrice de recherche
Patrice CHARTRAND, membre
Massimo MARCACCIO, membre externe

DEDICATION

To my better half, Hamid, and my little man, Mahan: I couldn't have made it without you.

ACKNOWLEDGEMENTS

First and foremost, I would like to express my deepest gratitude to my supervisor, Prof. Clara Santato, for her unwavering support and her invaluable guidance throughout the past four years. Her tireless efforts toward scientific excellence, with her commitment as a dedicated mother, have always been a source of inspiration and motivation for me.

I would like to thank my jury members, Prof. Patience, Prof. Chartrand, Prof. Marcaccio and Prof. Kummert, for their time and interest in my thesis. Their presence was a great honor for me.

I would like to express my gratitude to all my co-authors, Nila Davari, Dr. Abdelaziz Gouda, Kholoud Salem, Hamza Hyat, Prof. Daniel Belanger, Prof. Daria C.Boffito, and Prof. Mohini Sain, for their invaluable support and contributions.

I wish to truly thank Dr. Denis Rho, Dr. Flavia Visentin, Dr. Josianne Lefevbre, Yves Drolet, and Youssef Ben Mami, for their constant support and assistance with my experiments.

Special thanks to all my dear colleagues and friends: Manuel, Ramin, Anthony, Dieudonne, Ramon, Zhaojing, Youssef, Camille, Keshu, Yasser, Alexandre, Melchiade, Shahid, Hamza, Rebeca, Orlando, Joaquin, Lariel, Luan, Afzal, Omar, Sara, Sadaf, Nila, and Azadeh.

My endless respect and thanks to my mother, my father, and my brothers, *Amir* and *Milad*. They have been my constant source of love and encouragement throughout this journey.

In closing, words cannot fully convey my gratitude to my love *Hamid* and my sweetheart *Mahan*. Their unwavering love and support during the most challenging chapter of my life continually motivated me to persevere and move forward.

RÉSUMÉ

Les technologies de stockage d'énergie électrochimique sont devenues un catalyseur essentiel pour accélérer la transition énergétique verte en promouvant l'intégration des sources d'énergie renouvelables. Cependant, l'adoption des stratégies de décarbonisation, ainsi que la hausse de la demande mondiale pour les appareils électroniques portables, exerce une pression considérable sur la chaîne d'approvisionnement des matériaux stratégiques et critiques (par ex., Co et Li). La chaîne d'approvisionnement de ces éléments critiques, depuis l'extraction minière et le traitement jusqu'à la gestion des déchets, présente des défis environnementaux, sociaux et géopolitiques importants. Par ailleurs, l'accumulation mondiale des déchets d'équipements électriques et électroniques (DEEE) exacerbe cette problématique, notamment dans les pays où les cadres économiques actuels limitent des solutions de recyclage viables. Par conséquent, la transition vers des systèmes de stockage d'énergie éco-conçus s'avère impérative.

L'éco-conception dans les systèmes de stockage d'énergie électrochimique repose sur plusieurs principes clés, parmi lesquels : i) la sélection de matériaux bio-sourcés et abondants dans la croûte terrestre (par ex., extraits de la biomasse) pour remplacer les substances critiques; ii) l'application de techniques de fabrication avancées pour minimiser le *embedded energy* ; et iii) l'évaluation des scénarios de fin de vie dispositifs.

Les molécules organiques bio-sourcées redox-actives présentent des avantages significatifs pour l'éco-conception de systèmes de stockage d'énergie durables, notamment leur abondance, leur faible coût, leur processabilité en solution et leur potentielle biodégradabilité. Lorsqu'elles sont intégrées à des électrodes à base de carbone, ces molécules améliorent la capacité de stockage d'énergie via des mécanismes de transfer de charge Faradaïques. Cependant, l'optimisation des performances de ces systèmes nécessite une ingénierie minutieuse des surfaces/interfaces de l'électrode avec les molécules redox et l'électrolyte, afin d'améliorer, entre autres, la capacité de charge rapide et la stabilité au cyclage.

Dans cette thèse de doctorat, nous étudions l'utilisation de matériaux organiques moléculaires bio-sourcés dans le développement de dispositifs de stockage d'énergie éco-conçus, en adoptant les principes de la chimie verte pour minimiser l'*embedded energy* et l'empreinte environnementale, tout en assurant des performances électrochimiques favorables. Notre étude se concentre sur deux molécules bio-sourcées importantes à base de quinones : la Sépia mélanine et la Catéchine. La

Sépia mélanine peut être extraite de l'encre de seiche, tandis que la Catéchine, un membre de la famille des Tannins (c'est-à-dire une large classe de biomolécules polyphénoliques), peut être obtenue à partir de composants d'arbres (par ex., écorce ou feuilles), de résidus de fruits ou comme sous-produit de l'industrie du bois ou de l'alimentation. Ces deux matériaux moléculaires sont abondants, non toxiques et biodégradables, ce qui en fait des candidats prometteurs pour le développement de systèmes de stockage respectueux de l'environnement.

Dans le **Chapitre 1**, nous définissons le contexte de cette recherche, en mettant en évidence les principaux facteurs accélérant la transition vers l'électronique éco-conçue. Compte tenu de l'importance des molécules bio-sourcées à base de quinones dans le développement de dispositifs de stockage d'énergie durables, le premier objectif de cette recherche doctorale est d'examiner les propriétés redox de la Catéchine, une molécule redox-active de la famille des Tannins, et son impact sur les performances de stockage de charge du papier carbone préalablement traité chimiquement. De plus, en raison de l'importance de l'ingénierie des interfaces/surfaces pour optimiser les propriétés de stockage de charge des supercondensateurs à base de quinones, le deuxième objectif est d'étudier les performances électrochimiques de nouveaux matériaux d'électrodes composites à base de nanotubes de carbone multi-parois et de Sépia mélanine, déposés sur des collecteurs de courant en tissu de carbone flexible via un processus d'ultrasonication éco-énergétique et sans déchets.

Dans le **Chapitre 2**, nous présentons une revue de la littérature sur les supercondensateurs à base de quinones bio-sourcées, en mettant en avant les stratégies les plus efficaces pour améliorer leurs performances de stockage de charge. Dans le **Chapitre 3**, nous détaillons méthodes et techniques employées dans cette recherche, en mettant l'accent sur les techniques de caractérisation électrochimique et les processus d'ultrasonication utilisés pour atteindre nos objectifs de recherche. Dans le **Chapitre 4**, nous démontrons un supercondensateur symétrique semi-solide utilisant la catéchine comme molécule redox-active à base de quinones, déposée sur du papier carbone traité hydro thermiquement via un procédé en solution sans ajout d'additifs conducteurs ni de liants. Les résultats ont montré que la grande surface spécifique et l'architecture poreuse du papier carbone traité ont facilité les interactions électrostatiques et l'accumulation d'ions, améliorant ainsi la contribution de la capacité de double couche électrique. Le traitement hydrothermal de la surface du carbone, qui introduit des sites redox-actifs (c'est-à-dire des fonctionnalités contenant de l'oxygène et de l'azote), ainsi que la modification de surface par la catéchine, ont significativement

amélioré les propriétés de stockage de charge des électrodes via des mécanismes Faradaïques. De plus, les supercondensateurs symétriques semi-solides à base de catéchine ont démontré une remarquable capacité, densité d'énergie et densité de puissance, ainsi qu'une stabilité exceptionnelle au cyclage. Les résultats ont montré que l'électrolyte à base d'hydrogel de PVA limite efficacement la diffusion des molécules de catéchine dans l'électrolyte, contribuant ainsi à la haute stabilité au cyclage des dispositifs.

Dans le **Chapitre 5**, nous rapportons l'utilisation d'un processus d'ultrasonication en une seule étape comme technique d'ingénierie de surface écoénergétique et sans déchets pour la modification de surface du tissu de carbone avec de la Sépia mélanine et des nanotubes de carbone multi-parois (MWCNTs) pour des applications de stockage d'énergie, sans l'utilisation de tensioactifs ou de liants. Les résultats ont montré que le processus d'ultrasonication dans l'eau augmente la surface spécifique et la porosité du tissu de carbone, tout en induisant une fonctionnalisation redox (c'est-à-dire des espèces contenant de l'oxygène). La combinaison de la Sépia mélanine redox-active avec des MWCNTs conducteurs a significativement amélioré les propriétés de stockage de charge des électrodes via un mécanisme Faradaïque, en plus de l'activité électrostatique conventionnelle. De plus, les supercondensateurs symétriques semi-solides à base de MWCNT-mélanine ont atteint une haute capacité, densité d'énergie et densité de puissance, avec une remarquable stabilité au cyclage. Les supercondensateurs ont également démontré une performance constante lorsqu'ils ont été soumis à des flexions mécaniques sous différents angles. Dans le **Chapitre 6**, nous présentons des discussions détaillées sur l'Article 1 et l'Article 2, en soulignant comment cette recherche atteint les objectifs de cette étude doctorale.

Dans le **Chapitre 7**, nous concluons en résumant les enseignements tirés de cette étude et en soulignant l'originalité de l'approche d'ingénierie de surface proposée dans les applications de stockage d'énergie éco-conçues. En outre, nous formulons des recommandations pour les futurs chercheurs afin de faire progresser le développement de systèmes de stockage d'énergie durables bio-sourcés.

ABSTRACT

Energy storage technology has emerged as a critical enabler in advancing the green energy transition by facilitating decarbonization and promoting the integration of renewable energy sources into the global energy landscape. However, the widespread adoption of decarbonization strategies in all sectors, along with the surge in global demand for consumer electronics and portable devices, places considerable strain on the supply chain for strategic and critical battery materials (e.g., Co and Li). The entire supply chain of these critical elements, from mineral extraction and processing to waste management, presents substantial environmental, social, and geopolitical challenges. On the other hand, the global accumulation of waste electrical and electronic equipment (WEEE), and its powering components exacerbates this challenge, especially in countries where current economic frameworks hinder viable recycling solutions. Therefore, the transition to eco-designed energy storage systems is imperative.

Eco-design in electronics and their powering components emphasizes environmental considerations across the device lifecycle. Key principles include: (i) choosing earth-abundant, bio-sourced materials to replace critical or hazardous substances; (ii) employing advanced fabrication techniques to lower embodied energy; and (iii) evaluating end-of-life scenarios to minimize devices' environmental impact.

Organic bio-sourced redox-active molecules present key advantages for eco-design of sustainable energy storage systems, including abundance, cost-effectiveness, solution processability, and potential biodegradability. When integrated with carbon-based electrodes, these molecules enhance energy storage capacitance via Faradaic charge storage mechanisms. Optimizing the performance of these systems requires meticulous surface/interface engineering of the electrode, the redox-active molecule, and the electrolyte to improve among others rate capability and cycling stability.

In this PhD thesis, we investigate the use of organic bio-sourced materials in the development of eco-designed energy storage devices, adopting green chemistry principles to minimize embodied energy and environmental footprint of such devices, while ensuring favorable electrochemical performance. Our study focuses on two important bio-sourced quinone-based redox-active molecular materials: Sepia melanin and Catechin. Sepia melanin can be extracted from the ink sac of cuttlefish, while Catechin, a member of the Tannin family (i.e., a broad class of polyphenolic biomolecules), can be sourced from tree components (e.g., bark or leaves). Both molecules are

abundant, non-toxic, and biodegradable, making them promising candidates for the development of environmentally benign storage systems.

In **Chapter 1**, we outline the context of this research, emphasizing the key drivers potentially accelerating the shift toward eco-designed electronics. Given the significance of bio-sourced quinone-based molecules in the development of sustainable energy storage devices, the first objective of this PhD research is to investigate the redox properties of Catechin, and its impact on the charge storage performance of chemically treated carbon paper. Moreover, considering the importance of surface/interface engineering to optimize the charge storage properties of quinone-based supercapacitors, the second objective is to investigate the electrochemical performance of novel composite electrode materials composed of multiwalled carbon nanotubes and Sepia melanin, deposited onto flexible carbon-based current collectors via an energy efficient and waste-free ultrasonication process.

In **Chapter 2**, we present a comprehensive literature review on bio-sourced quinone-based supercapacitors, highlighting the most effective strategies for enhancing their charge storage performance. In **Chapter 3**, we detail the methods and techniques employed in this research, focusing on electrochemical characterization techniques and ultrasonication processes utilized to achieve our research objectives. In **Chapter 4**, we demonstrate a semi-solid symmetric supercapacitor utilizing Catechin as a redox-active quinone-based molecule, deposited on hydrothermally treated carbon paper through solution processing without involvement of any conductive additives or binders. The results indicated that the high surface area and porous architecture of the treated carbon paper facilitated electrostatic interactions and ion accumulation, thereby enhancing the electric double layer capacitance contribution. The hydrothermal treatment of the carbon surface, which introduced redox-active sites (i.e., O and N-including functionalities), along with surface modification using Catechin, significantly enhanced the charge storage properties of the electrodes through Faradaic mechanisms. Furthermore, Catechin-based semi-solid symmetric supercapacitors demonstrated remarkable capacitance, energy density, and power density, as well as exceptional cycling stability. The findings indicated that the PVA-based hydrogel electrolyte effectively restricts the diffusion and leaching of Catechin molecules, thereby contributing to the high cycling stability of the devices.

In **Chapter 5**, we report on the utilization of a one-pot ultrasonication process as an energy-efficient and waste-free surface engineering technique for surface modification of carbon cloth with redox-active sepia melanin and multiwalled carbon nanotubes (MWCNTs) for energy storage applications, without the use of surfactants or binders. The results indicated that the ultrasonication process in water enhances the surface area and porosity of the carbon cloth, while also inducing redox functionalization (i.e., O-containing species). The combination of redox-active sepia melanin with conductive MWCNTs significantly improved the charge storage properties of the electrodes via Faradaic mechanism, in addition to the conventional carbon-based electrostatic activity. Moreover, MWCNT-sepia-based semi-solid-state symmetric supercapacitors achieved high capacitance, energy density, and power density, along with remarkable cycling stability. The supercapacitors also demonstrated consistent performance when subjected to mechanical bending at various angles. In **Chapter 6**, we provide comprehensive discussions on Article 1 and Article 2, highlighting how this research fulfills the objectives of this PhD study.

In **Chapter 7**, we conclude by summarizing the insights gained from this study and underscoring the originality of the proposed surface engineering approach in eco-designed energy storage devices. Furthermore, we provide recommendations for future researchers to further advance the development of sustainable bio-sourced electrochemical energy storage systems.

TABLE OF CONTENTS

LIST OF TABLES

LIST OF FIGURES

LISTE OF SYMBOLS AND ABBREVIATIONS

BET Brunauer-Emmett-Teller

BJH Barrett-Joyner-Halenda

BSE Backscattered electron

CC Carbon cloth

CE Circular economy

CE Counter electrode

CNF Carbon nanofiber

CNT Carbon nanotube

CP Carbon paper

CQDs Carbon quantum dots

Ctn Catechin

CV Cyclic voltammetry

CVD Chemical vapor deposition

DHI 5,6-dihydroxyindole

DHICA 5,6-dihydroxyindole carboxylic acid

DIW Deionized water

DMSO Dimethyl sulfoxide

EC Electrochemical capacitor

EDLC Electric double layer capacitor

EDS Energy dispersive X-ray spectroscopy

EESD Electrochemical energy storage device

EIS Electrochemical impedance spectroscopy

EPR Electron paramagnetic resonance

GCD Galvanostatic charge-discharge

GO Graphene oxide

H2Q Hydroquinone

HTCC Heat-treated carbon cloth

IoT Internet of things

MWCNT Multi-walled carbon nanotube

PPy Polypyrrole

PVA Polyvinyl alcohol

Q Quinone

RE Reference electrode

rGO Reduced graphene oxide

SC Supercapacitors

SE secondary electron

SEM Scanning electron microscopy

SQ semiquinone

SWNT Single-walled carbon nanotube

TA Tannic acid

TCP Treated carbon paper

TEM Transmission electron microscopy

ULPE Ultrasound-assisted liquid phase exfoliation

UTCC Ultrasound-treated carbon cloth

WE Working electrode

WEC World energy council

WEEE Waste electrical and electronic equipment

XPS X-ray photoelectron spectroscopy

XRD X-ray diffraction

LIST OF APPENDICES

CHAPTER 1 INTRODUCTION

1.1 Context of the research

The availability of raw materials has become a crucial economic and geopolitical concern in the 21st century. The energy transition toward renewable sources is a key driver for the demand of several critical minerals, since it requires the intensive use of minerals and metals, for the production of solar panels, wind turbines, batteries, and other technologies[1-3]. At the same time, the rapid expansion of the Internet of Things (IoT) results in the proliferation of billions of electronic devices globally[4].

The need for *critical* elements is a challenge in the fabrication of electronic devices, and their powering elements (i.e., batteries and supercapacitors). Elements like gallium, cobalt, lithium, have limited and unstable supply chains, with associated significant geopolitical and environmental risks [5, 6]. Manufacturers face the growing need to find alternatives, recycle materials, or reduce reliance on these critical elements, as their limited availability could threaten the production of key technologies like semiconductors, batteries and supercapacitors.

Apart from the materials availability, a significant manufacturing challenge is the high embodied energy (i.e., energy spent in the production phase and stored in inner constituents) required to ensure the quality and miniaturize electronics and their powering components[7].

Finally, as electronic devices become increasingly prevalent in modern lifestyles, the generation and management of waste electrical and electronic equipment (WEEE) at their end of life are emerging as significant environmental challenges. Globally, the production of electronic waste (e-waste) is rising by 2.6 million tonnes annually, a picture expected to rise to 82 million tonnes by 2030[8, 9]. Sadly, a substantial portion of this waste is exported to developing nations, where improper disposal and recycling processes release toxic substances into the environment, threatening ecosystems and human health[9, 10]. E-waste and spent energy storage devices, often contains hazardous metals and chemicals that are non-biodegradable, leading to their long-term persistence in the environment and subsequent harmful ecological and health impacts[11].

In this context, a paradigm shift in how we manage resources, mineral extraction, and electronics disposal is crucial, minimizing the environmental footprint and ensuring sustainability for future generations. This requires a comprehensive rethinking of the entire life cycle of electronic devices

to promote circular economy (CE) and reduce the adverse environmental impacts of e-waste[12, 13]. A key aspect of this shift is the adoption of “eco-design” principles, which emphasize the importance of material efficiency and recyclability, not just at the end of a product's life but, more importantly, incorporating environmental considerations at the initial stage of design[14].

The eco-design approach integrates sustainability from the outset and into every phase of the electronic product life cycle. All in all, eco-design encompasses conducting environmental impact assessments, selecting biodegradable and earth-abundant materials (such as bio-sourced materials from biomass feedstock) to replace critical metals and hazardous substances, and utilizing advanced fabrication technologies to reduce embodied energy[14, 15].

Sustainable organic (i.e., carbon-based) energy storage devices offer a promising approach for the eco-design of powering elements in electronics and reducing the environmental impact of waste electrical and electronic equipment (WEEE). This strategy encompasses: (i) using abundant, low-cost, and solution-processable organic precursors, (ii) employing innovative production schemes with non-toxic solvents and reagents, adhering to green chemistry principles to minimize toxic waste, and (iii) designing devices with environmentally acceptable end-of-life scenarios (e.g. biodegradable devices)[16, 17].

Quinones are a diverse class of organic molecules that are widely found in nature. Quinones undergo rapid two-electron redox reactions via proton-coupled electron transfer in aqueous media. The redox activity of quinone-based molecules permits higher charge storage performance through *pseudocapacitance* in supercapacitors[18, 19]. Given their redox activity, solution processability, abundance, non-toxicity, and potential biodegradability, quinone-based bio-sourced molecules are promising candidates for eco-designed electrochemical capacitors operating in aqueous solutions[20].

Several studies have investigated the integration of bio-sourced quinone derivatives into *pseudocapacitors* (please see Table 2.1 in literature review). Unfortunately, despite intensive studies, quinones often exhibit high contact resistance at their interface with carbon current collectors. This results in limited rate response (i.e., loss of capacitance at higher current densities) and poor cycling stability (i.e., loss of capacitance over long-term charging/discharging cycles) in the corresponding supercapacitors[19, 21].

The need to enhance cycling stability while preserving the mechanical integrity and flexibility of quinone-based electrochemical capacitors favors semi-solid-state gel polymer electrolytes over liquid or solid electrolytes. However, achieving a seamless electrode/electrolyte interface that effectively limits redox-active materials dissolution and ensures optimal ionic conductivity is a challenge.

Carbon-based materials are considered as primary choice for current collectors in energy storage devices due to their low cost, favorable electrical conductivity, and electrochemical stability. However, their inherent limitations, such as low specific surface area and poor electrolyte wettability, necessitate surface treatment processes to optimize their pore structure and modify their surface chemistry, thereby enhancing their electrochemical performance.

However, conventional surface treatment processes are often highly energy-intensive and may involve toxic reagents and strong acid treatments (please see Table 2.2 in the literature review). Consequently, developing energy-efficient and environmentally friendly surface engineering techniques for carbon-based electrodes, without compromising their capacitive performance, poses a substantial challenge.

All in all, if we wish to produce large scale, eco-designed energy storage devices, there is a need to develop sustainable surface engineering approaches that enhance energy storage performance by optimizing the carbon electrode surface and the interfaces between the electrode, the quinone molecules, and the electrolyte.

1.2 Research objectives

Given the importance of bio-sourced redox active molecules in the development of sustainable energy storage devices and the need to minimize the environmental footprint of spent powering components in e-waste, this PhD research focuses on two important quinone-based bio-sourced redox-active (macro)molecules: Sepia melanin and Catechin (i.e., a member of the Tannin family), selected for their abundance, non-toxicity, and biodegradability.

the first specific objective of this PhD thesis is:

1) Investigating the redox properties of Catechin, a quinone-based, bio-sourced molecule, to enhance the charge storage performance of carbon-based electrodes in semi-solid-state electrolytes (Article 1, chapter 4).

Considering the low electronic conductivity of bio-sourced quinone-based molecules and their poor electronic coupling at the interface with carbon-based electrodes, along with the need for the development of energy-efficient and sustainable surface engineering processes, the second objective is

2. Investigating the effect of conductive additives on the electrochemical charge storage of Sepia melanin, (i.e., bi-sourced redox-active macromolecules), in a novel composite electrode material prepared through an eco-designed surface engineering process utilizing ultrasonication technique (Article 2, chapter 5).

The impact of this research is expected to significantly contribute to the development of eco-designed energy storage devices by showcasing the potential of bio-sourced redox-active electrode materials and leveraging innovative surface/interface engineering techniques. Our original insights into the modification processes of carbon-based electrodes through ultrasonication underscore a key paradigm shift that integrates electrochemical performance with sustainability, taking into account the environmental impacts of modification processes.

1.3 Structure of the thesis

This PhD thesis is arranged into eight chapters that go as follows:

Chapter 1 provides the research context and thesis' objectives. Chapter 2 presents a literature review on electrochemical energy storage systems, focusing on state-of-the-art bio-sourced quinone-based supercapacitors. It also discusses the most effective strategies for improving their electrochemical performance, particularly melanin-based and Tannin-based supercapacitors. Additionally, this chapter includes a review of biodegradable and compostable supercapacitors.

Chapter 3 details the methodological framework of this research, with a focus on electrochemical characterization techniques. These include cyclic voltammetry (CV), galvanostatic charge-discharge (GCD), and electrochemical impedance spectroscopy (EIS), alongside a discussion of the electrochemical signatures of pseudocapacitive and battery-like behaviors. This chapter covers the working principles of the ultrasonication technique used for electrode modification, as applied in Article 2. Chapter 4 presents the first publication of this Ph.D. thesis (Article 1), entitled “Tannins for Sustainable Semi-solid-state Supercapacitors”, published in *Waste and Biomass Valorization* in 2023.

Chapter 5 includes the second publication of this PhD thesis (Article 2) entitled “Ultrasound-Assisted Deposition of Sepia Melanin and Multiwalled Carbon Nanotubes on Carbon Cloth: Toward Sustainable Surface Engineering for Flexible Supercapacitors”, published in *Advanced Sustainable Systems* in 2024. Chapter 6 provides a general discussion of the results and insights presented in Chapters 4, 5. Chapter 7 concludes the PhD thesis by summarizing the accomplishments in meeting the research objectives and offering perspectives for future investigations in the eco-design of sustainable bio-based energy storage systems.

CHAPTER 2 LITERATURE REVIEW

2.1 Energy issue and sustainable resources

The World Energy Council (WEC) projects that global energy consumption will double by 2050 compared to current levels [22]. Rising global energy demands, coupled with increasing greenhouse gas emissions, have accelerated the shift toward energy transition, emphasizing low-carbon approaches and the use of renewable energy sources. The inherent intermittency of these renewable sources underscores the need for energy storage systems. Additionally, rapid advancements in electronics, especially the miniaturization and functional integration of smart devices (e.g., laptops, smartphones, sensors, and implantable medical technologies) further push the growing demand for the development of novel, biocompatible, low-cost, and sustainable energy storage solutions beyond conventional electrochemical energy storage devices (EESDs). Such miniaturized devices require compact, high energy and power density, safe, and environmentally benign energy storage systems that conventional EESDs alone are unable to adequately provide [23-25].

2.2 Electrochemical energy storage systems

The primary goal of developing an energy storage system is to capture energy and effectively deliver it for future use [26]. Two main systems for electrochemical energy storage are i) batteries, and ii) electrochemical capacitors (ECs), also known as supercapacitors (SCs).

From an electrochemical point of view, the major similarities of these two systems are that both systems go through the storage and shuttling of ions between two electrodes along with the flow of electrons in an external circuit. Moreover, electron and ion transport occur independently. In other words, the electrolyte facilitates the efficient transfer of ions into the electrode, while the electrode provides a conductive pathway for electrons to the external circuit [27, 28]. Ideally, an electrochemical energy storage device should exhibit both high specific energy (i.e., its capacity to store substantial amounts of energy), and high specific power, (i.e., enabling rapid charge and discharge cycles)[29].

To get a better grasp of the opportunities for ECs development, it is important to consider power vs. energy diagrams for each type of devices (Figure 2.1). ECs are seen as a middle ground between traditional capacitors, characterized by high power density but low energy density, and

batteries, which offer moderate power density alongside high energy density. In this context, ECs function as a middle ground between traditional dielectric capacitors and batteries. [24, 30, 31]. Batteries are employed in a diverse range of short- to mid-term energy storage applications, such as power distribution to remote locations, electric vehicles, off-grid storage for residential or commercial buildings, and portable electronic devices, etc. In contrast, ECs are classified as high-power density devices, making them particularly suitable for short-term applications that often require bursts of energy. These applications include, but are not limited to, regenerative braking systems in electric vehicles, grid stabilization, backup power for uninterruptible power supplies (UPS), energy harvesting systems, and pulse power applications in telecommunications[32].

Compared with conventional dielectric capacitors, supercapacitors current collectors or electrodes are typically built of large specific surface areas, and hollow and porous conductive materials, such as carbon-based materials. Thus electrode/electrolyte interfaces are significantly larger than conventional capacitors resulting in greater specific capacitance and energy density[32, 33].

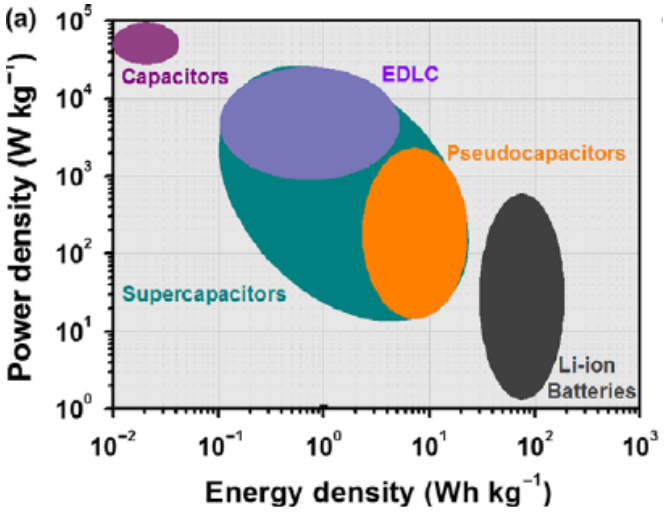

Figure 2.1 Power density vs. energy density for
various electrochemical energy storage devices [24].

2.3 Electrochemical capacitors (ECs)

ECs, also known as supercapacitors (SCs) or ultracapacitors, have significantly higher capacitance and energy density than conventional dielectric capacitors [34]. SCs are made up of two electrodes

separated by an ion-permeable separator membrane and an electrolyte that connects the two electrodes ionically [35]. SCs have a higher specific power (1000-1500 W kg^{-1}) and a longer cyclic life (up to 100 000 cycles) than batteries, but they have a lower energy density (up to 10 W h kg^{-1}) than batteries [36].

Based on energy storage mechanisms, SCs generally can be classified into three types i) electrical double layer capacitors (EDLCs) ii) *pseudocapacitors* and, iii) hybrid capacitors. These mechanisms are referred to i) electrostatic, ii) Faradaic and iii) combination of Faradaic and non-Faradaic, respectively [37, 38]. Figure 2.2 compares schematically the energy storage mechanisms of EDLCs, pseudocapacitors and batteries.

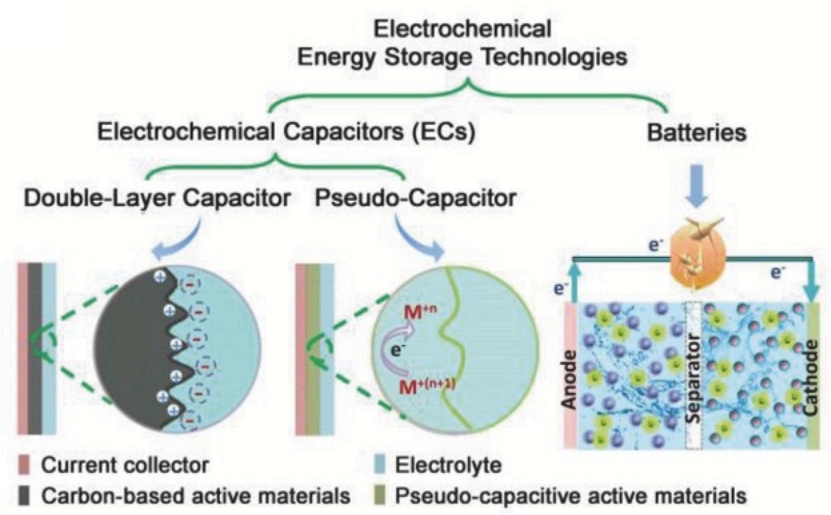

Figure 2.2 Schematic of working principles of electrochemical energy storage systems [39].

2.3.1 Electric double layer capacitors (EDLCs)

Electrostatic interactions between ions and polarised electrodes are the basis of EDLCs. In EDLCs, ions accumulate in a thin layer (i.e., a few nanometers) to counterbalance the charge of an electrode that is oppositely polarised. In other words, surface charges are distributed at the interface between the surface of the conductive electrode and the electrolyte without contribution of any chemical processes or Faradic reactions [31, 39]. Typically, carbon-based porous materials such as activated carbon, xerogels, carbon nanotubes (CNTs), carbon nanofibers (CNFs), graphene, and its

derivatives exhibit EDLC-type behavior due to their high specific surface area and excellent conductivity[40].

2.3.2 Pseudocapacitors

The term *pseudocapacitor* originates from the ancient Greek word *pseudés*, meaning “false” or “appears like”. This term captures the unique nature of pseudocapacitors, which mimic the behavior of traditional capacitors. Actually, pseudocapacitors exhibit electrochemical characteristics similar to those of capacitive electrodes, specifically showing a linear or dependence of stored charge on the applied potential within a defined potential window. However, in pseudocapacitors, charge storage is driven by electron-transfer reactions rather than solely by ion accumulation, as observed in EDLCs[41, 42].

Pseudocapacitors are a type of electrochemical capacitor in which reversible Faradaic reactions take place at or near the electrode/electrolyte interface due to the presence of redox-active materials (e.g., transition metal oxides/hydroxides, conducting polymers, MXenes, heteroatom-based functionalities, etc.) in which higher capacitance and energy density can be attained in comparison to EDLCs [43, 44]. This means that pseudocapacitors can store charge by electrostatic, redox reactions, and/or intercalation, due to ions moving through (or diffusing into) the electrode materials without any phase transformation. Such that, electrochemical features of pseudocapacitive materials are neither purely capacitive nor bulk Faradaic process[45].

The charge storage mechanisms in pseudocapacitive materials can involve various Faradaic processes (Figure 2.3) including:

I. *Underpotential deposition*, where ions are adsorbed onto the electrode surface (i.e., form an adsorbed monolayer) at potential less negative than their redox potential (e.g., deposition of Pb on Au or Pt electrodes, Figure 2.3a).
II. *Redox pseudocapacitance*, which involves fast and reversible redox reactions at or near the electrode surface and is the most common pseudocapacitive charge storage mechanism in metal oxides (e.g., RuO_2, MnO_2, etc., Figure 2.3b).
III. *Intercalation pseudocapacitance*, where ions are intercalated into the electrode material's structure accompanied by Faradaic charge-transfer with no crystallographic phase transformations (Figure 2.3c)[40, 43].

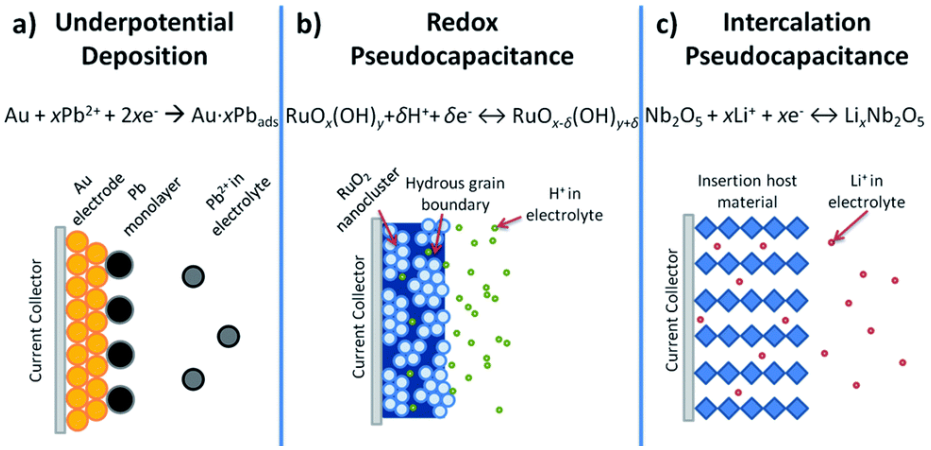

Figure 2.3 Various Faradaic processes contribute to pseudocapacitance; a) underpotential deposition; b) redox pseudocapacitance; c) intercalation pseudocapacitance [43].

In the case of redox pseudocapacitance, the total charge stored results from a combination of mechanisms, including pseudocapacitive contribution from surface redox reactions, and EDL contribution arising from electrostatic ion adsorption/desorption at the electrode/electrolyte interface[42, 46]. This case is pivotal to this PhD research and will be discussed in detail in Article 1 and Article 2.

2.3.3 Hybrid capacitors

As indicated by their name, hybrid capacitors combine the features of both EDLCs and pseudocapacitors, typically demonstrating performance characteristics that reside between these two types. Based on their electrode configuration, they can be categorized into three types: asymmetric hybrids, battery-type hybrids, and composite hybrids. Charge storage in hybrid supercapacitors are based on both Faradaic and non-Faradaic mechanisms[47, 48]. For example, in battery-type hybrid capacitors, the intercalation mechanism involves crystallographic phase transitions, which extend charge storage from the electrode surface into the electrode bulk, resulting in an increase in energy density [38, 49].

It is worth noting that to differentiate between battery-like energy storage processes (i.e., involving crystallographic phase transformations of the electrode materials during charge/discharge), pseudocapacitive mechanisms, and EDLCs, specific electrochemical signatures (e.g., CV and GCD

curves), along with quantitative kinetic analyses, should be considered. These distinctions are discussed in detail in section 3.2.

2.4 Quinone-based molecules for supercapacitors

Quinones are a diverse class of organic molecules commonly found in nature, known for their redox activity, consisting in rapid two-electron redox processes through proton-coupled electron transfer in aqueous media[20, 50]. The primary motivation for incorporating bio-sourced quinone derivatives into supercapacitors is to enhance their charge storage performance by integrating Faradaic contributions to the electrostatic one.

Modifying carbon-based electrodes with quinone-based molecules combines non-Faradaic and Faradaic mechanisms, resulting in a hybrid electrode with improved energy density [25, 51]. Tunable redox-activity with the molecular structure, abundance, low cost and environmentally friendliness, make quinone-based species relevant materials for the development of sustainable energy storage devices[32, 52].

The application of quinone molecules as electroactive materials in supercapacitors was first proposed by Naoi et al.[53] in 2000. They prepared a polymer using the 1,5-diaminoanthraquinone monomer and suggested that quinone-based moieties could serve as potential candidate for electrochemical capacitors.

Milczarek et al.[54] in 2012 explored the redox-active quinone groups found in lignin derivatives (extracted from by-products of pulp and paper industry) for potential use in electrochemical energy storage. Subsequently, numerous researchers have reported significant advancements in utilizing bio-sourced quinone-based materials (e.g., emodin, juglone, humic acid, lignin, Tannins, and melanin) to modify carbon electrodes (Table 2.1) [21, 55-59].

Although quinone-based molecules have garnered considerable interest, they still exhibit several limitations: (i) high contact resistance at its interface with carbon current collectors, resulting in poor rate capability (i.e., capacitance loss at high current densities), and (ii) dissolution in the electrolyte, bringing about cycling stability losses [25, 50, 60].

For the large scale production, it is essential to meticulously control various aspects of both materials and devices, including: (i) the supramolecular aggregation of the redox-active molecules, to ensure electronic conductivity and ion transport, (ii) the carbon electrode surface where the

quinones are deposited, in terms of surface area, porosity and electrolyte wettability, and (iii) the quality of the immobilization of the quinone at the carbon surface, to limit the leaching of the molecules in the electrolyte[61, 62]. Thus, the development of versatile structural design strategies is deemed imperative to optimize the utilization of quinone and its derivatives in energy storage systems.

Table 2.1 Electrochemical performance of state-of-the-art of bio-sourced-based supercapacitors in the literature.

Electrode material	***Electrolyte***	***Performance***				***Capacitance retention***	***Year***	***Ref.***
		Capacitance	***Charging voltage***	***Energy Density***	***Power density***			
Juglone modified CNT/bacterial cellulose	H_2SO_4/PVA hydrogel	NA	2 V	40 W h kg^{-1} at 10 A g^{-1}	1 000 W kg^{-1} at 10 A g^{-1}	80% after 10 000 cycles	2020	[58]
Juglone modified activated carbon/activated carbon	H_2SO_4 1M	66 F g^{-1} at 0.3 A g^{-1}	1.2 V	12 W h kg^{-1} at 3 A g^{-1}	180 W kg^{-1} at 3 A g^{-1}	77% after 3 000 cycles	2019	[63]
Emodin and graphene nanosheet/ Caffeic acid-graphene hydrogel	H_2SO_4 1M	88 F g^{-1} at 10 mV s^{-1}	1.8 V	33 W h kg^{-1} at 0.5 A g^{-1}	800 W kg^{-1} at 0.5 A g^{-1}	80% after 7 000 cycles	2021	[64]
Lignin-based carbon nanofiber-SnO_2	Na_2SO_4 1M	NA	1.8 V	11 W h kg^{-1} at 1 A g^{-1}	451 W kg^{-1} at 1 A g^{-1}	91% after 10 000 cycles	2020	[65]
Polydopamine supported on functionalized carbon cloth	H_2SO_4/PVA hydrogel	61 F g^{-1} at 1 A g^{-1}	1.2 V	11 W h kg^{-1} at 1 A g^{-1}	6400 W kg^{-1} at 1 A g^{-1}	81% after 10 000 cycles	2021	[57]
Tannic acid/ graphene	H_2SO_4 /PVA hydrogel	195 F g^{-1} at 0.5 A g^{-1}	1 V	37 W h kg^{-1} at 20 A g^{-1}	4476 W kg^{-1} at 20 A g^{-1}	84% after 8 000	2018	[66]

Electrode material	*Electrolyte*	*Performance*				*Capacitance retention*	*Year*	*Ref.*
		Capacitance	*Charging voltage*	*Energy Density*	*Power density*			
						cycles		
Tannic acid/reduced graphene oxide	$EMIMBF_4$ 2 M	525 mF cm^{-2} at 0.5 mA cm^{-2}	3 V	72 mWh cm^{-2} at 0.5 mA cm^{-2}	250 mW cm^{-2} at 0.5 mA cm^{-2}	91% after 10000 cycles	2024	[67]
Tannin/reduced graphene oxide	H_2SO_4/PVA hydrogel	40 mF cm^{-2} at 0.5 mA cm^{-2}	0.8 V	3.6 W h cm^{-2} at 0.5 mA cm^{-2}	107 W cm^{-2} at 0.5 mA cm^{-2}	92% after 10000 cycles	2021	[68]
PANI and Tannic acid/ reduced graphene oxide	H_2SO_4 /PVA hydrogel	56 F g^{-1} at 0.5 A g^{-1}	1.6 V	1.6 W h kg^{-1} at 0.5 A g^{-1}	115 W kg^{-1} at 0.5 A g^{-1}	NA	2019	[69]
Catechin and tannic acid/treated carbon paper	Na_2SO_4 0.5 M	300 F g^{-1} at 10 A g^{-1}	1.6 V	23 W h kg^{-1} at 10 A g^{-1}	26 kW kg^{-1} at 10 A g^{-1}	100% after 10 000 cycles	2022	[19]
Sepia melanin/treated carbon paper	Na_2SO_4 0.5 M	452 F g^{-1} at 10 A g^{-1}	1.6 V	20 W h kg^{-1} at 10 A g^{-1}	46 kW kg^{-1} at 10 A g^{-1}	100% after 50 000 cycles	2022	[19]
Sepia melanin and carbon Quantum dots/carbon paper	Na_2SO_4 0.5 M	180 mF cm^{-2} at 0.5 mA cm^{-2}	1 V	11 W h cm^{-2} at 0.5 mA cm^{-2}	102 W cm^{-2} at 0.5 mA cm^{-2}	92% after 10 000 cycles	2021	[70]

2.5 Carbon electrodes for quinone-based supercapacitors

The conductivity of carbon, combined with its tunable porosity and electrochemical stability, makes it a key component in energy storage. The deposition of quinone-based materials on conductive carbon substrates (e.g., activated carbon, carbon paper, 2D graphene and its derivatives, carbon clothe, etc.) leads to enhanced energy storage performance. This enhancement arises from the synergistic effect of superimposing pseudocapacitance on the traditional electrical double-layer capacitance (EDLC)[60].

The EDLC of the carbon materials is typically low due to the rather low capacitance contribution per surface area (i.e., specific areal capacitance)[62]. The formation of EDLC in carbon materials is primarily governed by the kinetics of in-pore ion transport.

Materials such as graphene and other nanocarbons derive much of their surface area from their unique morphology, often referred to as the outer surface area[71]. For instance, the theoretical specific areal capacitance of graphene is calculated to be only about 0.21 F m^{-2} [72]. This relatively low value highlights the challenge in maximizing capacitance in carbon-based materials, despite their high surface area and conductivity.

Moreover, from the electron transport point of view, porous or activated carbons exhibit relatively low conductivity due to their amorphous structures and presence of numerous defects. The formation of pores in these materials disrupts the sp^2 conjugated carbon structure, further hindering fast electron transport and limiting the efficient utilization of energy storage sites. As the mass loading of active materials on electrode or electrode thickness increases, the conductivity becomes even more an issue[62, 73].

To address these challenges, many strategies have been developed, including: (i) introducing surface electroactive sites on the carbon (e.g., functional groups, heteroatoms) and (ii) compositing the conductive carbon materials (e.g., carbon nanotubes (CNTs), conductive polymers, etc.) with redox-active moieties.

2.5.1 Design of active sites

In order to enhance the capacitance of the carbon substrate beyond its EDLC, it is crucial to control its surface chemistry. The introduction of heteroatoms and functional groups has been extensively investigated.

Doping carbon materials with certain heteroatoms (e.g., N, O, B, P, S, etc.) influences physicochemical properties such as, (i) surface wettability (i.e., electrolyte affinity), (ii) electronic conductivity, and (iii) pseudocapacitive behavior of the electrodes, owing to the electron donor-acceptor characteristics [74-76].

A summary of the most prevalent oxygen- and nitrogen-containing surface functional groups that enhance the electrochemical performance of carbon-based electrodes in supercapacitors is provided in Figure 2.4.

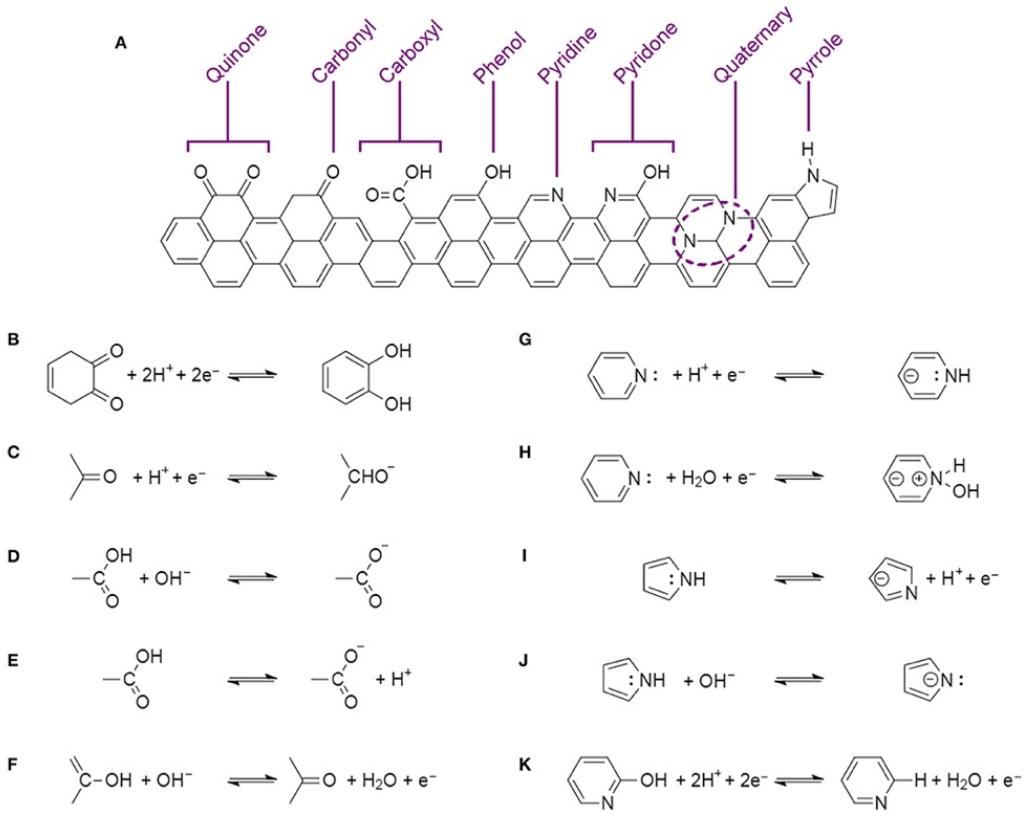

Figure 2.4 O and N-including functionalities associated with the charge storage in carbon-based electrodes in aqueous medium [32].

N-doped carbon electrodes can achieve significant capacitance values despite having relatively low surface areas. Given that N possesses a higher electronegativity ($\chi = 3.04$) than carbon ($\chi = 2.55$), N-doping enhances the asymmetric valence charge, thereby improving the electron transfer capabilities of carbon materials [76, 77]. Moreover, the pyridinic-N and pyrrolic-N placed at the edges of carbon plane, can provide additional pseudocapacitance contribution through protonation and deprotonation, as represented by reactions (1) and (2) [78].

(1)

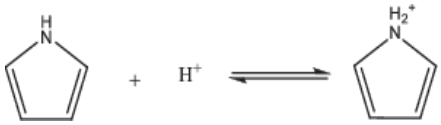

(2)

Huang *et al*.[79] synthesized N-doped, ordered, mesoporous, few-layer carbon (OMFLC-N) via chemical vapor deposition (CVD). The incorporation of pyrrolic-N (N-5) and pyridine-N (N-6) resulted in an N-doped carbon electrode with improved electronic conductivity (σ = 360 S cm^{-1}), hydrophilicity and specific capacitance of 790 F g^{-1} at 1 A g^{-1} in a 0.5 M H_2SO_4 electrolyte (Figure 2.5).

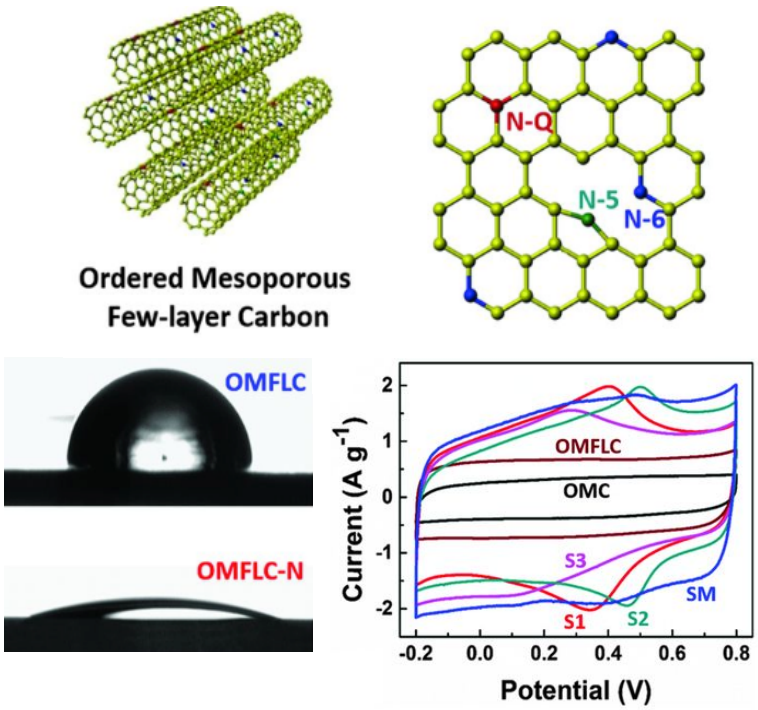

Figure 2.5 Schematic illustration of nitrogen functionalities on a carbon substrate; b) Contact angles of 0.5 M H_2SO_4 droplet on OMFLC and OMFLC-N; c) CV profiles of corresponding electrodes at 2 mV s^{-1} [79].

O-functionalities are commonly present in porous carbon materials. O-functionalities can be introduced into the carbon matrix through treatment of the carbon electrode, including chemical oxidation treatments, thermal activation under controlled atmosphere, hydrothermal activation, electrochemical treatment, microwave irradiation, plasma functionalization, etc. Table 2.2 provides a summary of the electrochemical performance of *carbon cloth* electrodes treated with conventional methods.

Table 2.2 Summary of the electrochemical performance of carbon cloth electrodes treated with some conventional methods.

Activation method	*Electrolyte*	*Potential (V)*	*Electrode capacitance*	*Energy density of the device*	*Ref.*
Electrochemical oxidation at 3V	5 M LiCl	-1 to 0 V vs. Ag/AgCl	756 mF cm^{-2} [2]	1.5 mW h cm^{-2}	[80]
Electrochemical oxidation (CV rate 5 mV s^{-1})	1 M Na_2SO_4	-1 to 1 V vs. Ag/AgCl	1548 mF cm^{-2}	239 mW h cm^{-2}	[81]
Electrochemical oxidation (CV rate 20 mV s^{-1})	5 M LiCl	-0.8 to 0 V vs. Ag/AgCl	143 mF cm^{-2}	NA	[82]
Hummer's oxidation and two-step reduction in hydrazine and NH_3	1 M H_2SO_4	-1 to 1 V vs. Ag/AgCl	88 mF cm^{-2}	31 mW h cm^{-2}	[83]
Hummer's oxidation	1M Na_2SO_4	-0.5 to 1 V vs. Ag/AgCl	5310 mF cm^{-2}	31 mW h cm^{-2}	[84]
Plasma functionalization	1 M KOH	0 to 0.6 V vs. Ag/AgCl	391 mF cm^{-2}	NA	[85]
Thermal activation	6 M KOH	0 to 1 V vs. Ag/AgCl	1136.7 mF cm^{-2}	70 mW h cm^{-2}	[86]

The incorporation of oxygen-including groups enhances surface wettability by increasing the number of hydrophilic polar sites, thereby improving carbon electrode-electrolyte interactions in aqueous electrolytes. More importantly, oxygen functionalities (e.g., C–OH and O=C–OH) contribute to pseudocapacitance through redox reactions with OH^- ions in the electrolyte. The potential redox reactions are represented by reaction (1) and (2) below:

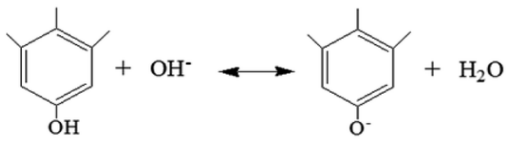

(1)

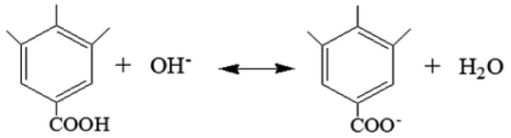

(2)

Notably, an excess of oxygen groups, particularly epoxy (C–O) groups, can reduce the electronic conductivity of carbon materials by trapping localized electrons [87]. Therefore, it is crucial to precisely regulate the type and distribution of O-functionalities on carbon surfaces.

Doping carbon with heteroatoms such as F, B, P, and S significantly enhances the charge storage capability of carbon-based supercapacitors, owing to the distinct electronegativities and atomic sizes of these elements relative to carbon. In comparison to N-doping, F, B, P, and S exhibit stronger electron-donating capabilities and pronounced n-type behavior, making them good candidates for doped carbons. Moreover, co-doping strategies (dual-element, triple-element), such as N/S [88], N/B[89], and N/P/O[90] co-doping, have been widely studied and demonstrate superior electrochemical properties over single-atom doping due to the synergistic interactions between the different heteroatoms[91]. Figure 2.6 illustrates a schematic representation of the carbon structure doped with different heteroatom.

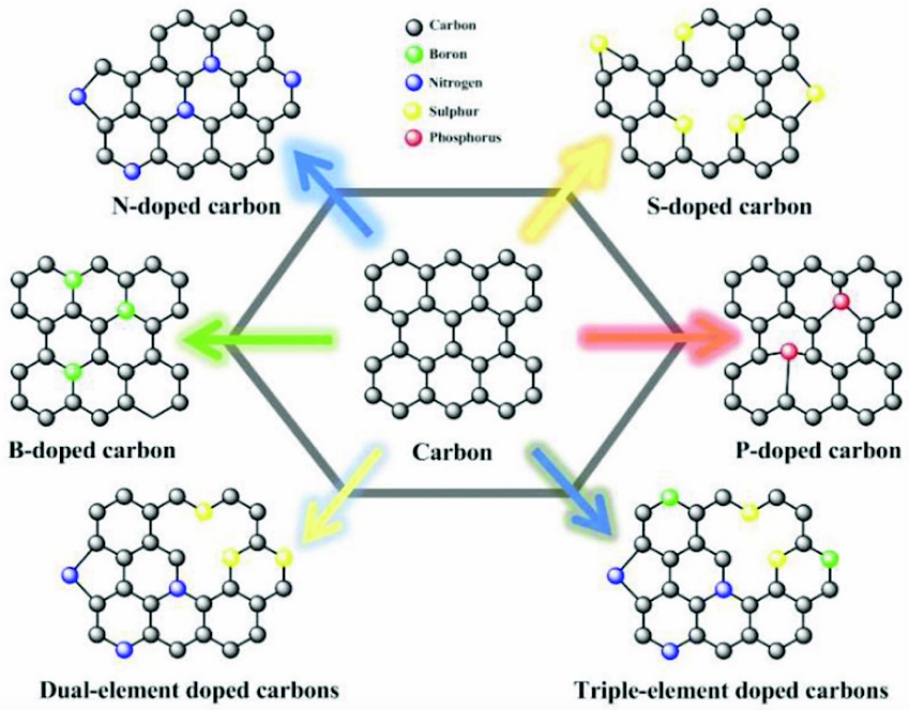

Figure 2.6 Schematic illustration of carbon structure doped with different heteroatom [91].

Li *et al*. [92] fabricated N, P co-doped carbon quantum dots (CQDs)/reduced graphene oxide (rGO) composite aerogels (N, P-CQDs/rGO) using a hydrothermal method (180 °C, 24 h) with $(NH_4)_2HPO_4$ serving as the N and P source (Figure 2.7). Thanks to the synergistic effect of N and

P co-doping, the electrodes demonstrated a remarkable enhancement in specific capacitance, achieving 453.7 F g^{-1} at 1 A g^{-1}. This value significantly surpassed the capacitances of GO (110.4 F g^{-1}), rGO (217.4 F g^{-1}), N, P-rGO (272.9 F g^{-1}), and CQDs/rGO (297.4 F g^{-1}).

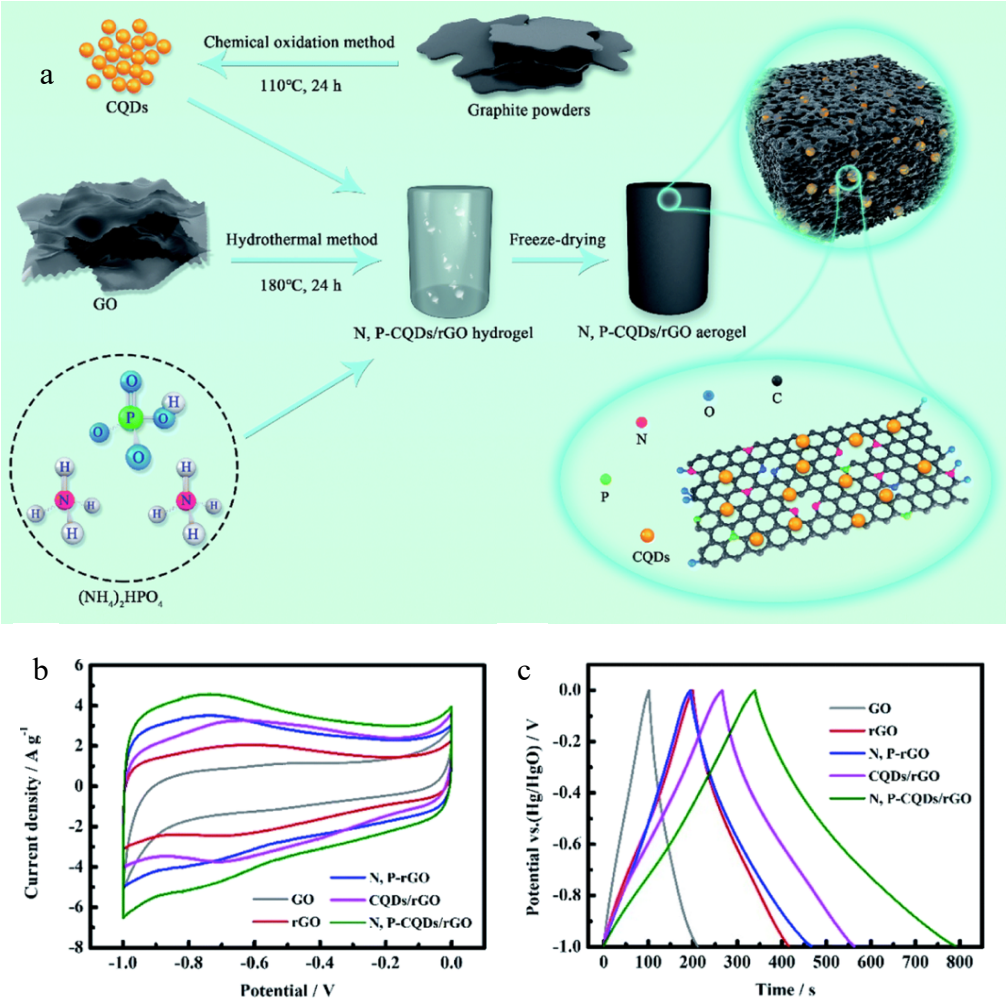

Figure 2.7 a) Schematic of the fabrication process of the N, P-CQDs/rGO composite aerogel; b) CV profiles at 10 mV s^{-1}, and (c) GCD curves at 1 A $g^{-}1$ of the GO, rGO, N, P-rGO, CQDs/rGO, and N, P-CQDs/rGO electrodes [92].

It is worth noting that while the treatment processes of carbon electrodes could potentially improve their electrochemical performance, such treatment processes are often highly energy-intensive (e.g., prolonged high-temperature treatment in controlled atmosphere) and sometimes rely on toxic reagents and strong acid treatments. As a result, developing energy-efficient and environmentally benign surface engineering techniques for carbon-based electrodes, without compromising its capacitive performance, is essential.

2.5.2 Design of conductive network

Given the high contact resistance between redox-active molecules and carbon current collectors, it is essential to not only design porous structures and dope carbon electrodes but also to build highly conductive networks throughout the electrode materials. This approach will help achieve high power densities and improve the rate capability of supercapacitors. Recently, composite electrode materials combining quinone moieties with highly conductive carbon-based materials have been developed, specifically for flexible supercapacitors [93, 94]. To enhance charge transport within quinone-based electrode materials, a three-dimensional conductive network can be established by incorporating high aspect-ratio nanocarbons, such as graphene derivatives, CNTs and carbon quantum dots (CQDs)[94, 95]. Compared to traditional carbon black or graphite, these nanocarbons provide more contact sites at their interface due to their larger surface area, leading to enhanced electrical conductivity and overall improved electrode performance. In such systems, quinones can hybridize with carbon structures through non-covalent interactions [62, 96].

However, this approach faces several challenges, such as the agglomeration or entanglement of conductive nanocarbons, which results in inhomogeneous dispersion of active materials and conductive agents within the electrode materials leading to poor cycling stability and rate capability[93, 97].

Jia *et al*.[98] reported on flexible electrodes composed of carbonized cotton fiber, graphene oxide hydrogel, and juglone (CCF/GH-JUG) through carbonization (900 C^o, 2 h) and a hydrothermal (180 C^o, 12 h) process for supercapacitor applications (Figure 2.8). Juglone was immobilized onto reduced graphene oxide sheets via non-covalent bonding (i.e. π-π interactions between its aromatic structure and the carbon scaffold). The integration of juglone's redox activity with graphene's high electrical conductivity led to a conductive, redox-active electrode material. The cyclic voltammogram of the CCF/GH-JUG 8:3 (mass ratio) electrode exhibited two distinct redox peaks within the potential range of -0.05 to 0.4 V vs Ag/AgCl, corresponding to double-electron/proton redox reaction (Figure 2.7). Symmetric supercapacitors utilizing CCF/GH-JUG 8:3, 316L stainless steel fabrics (as current collectors), and a Polyvinyl alcohol (PVA)/H2SO4 electrolyte, exhibited capacitance of 453 F g^{-1} (based on the total mass of active material). However, the cycling stability was relatively low, with capacitance retention of 87% after 10,000 cycles.

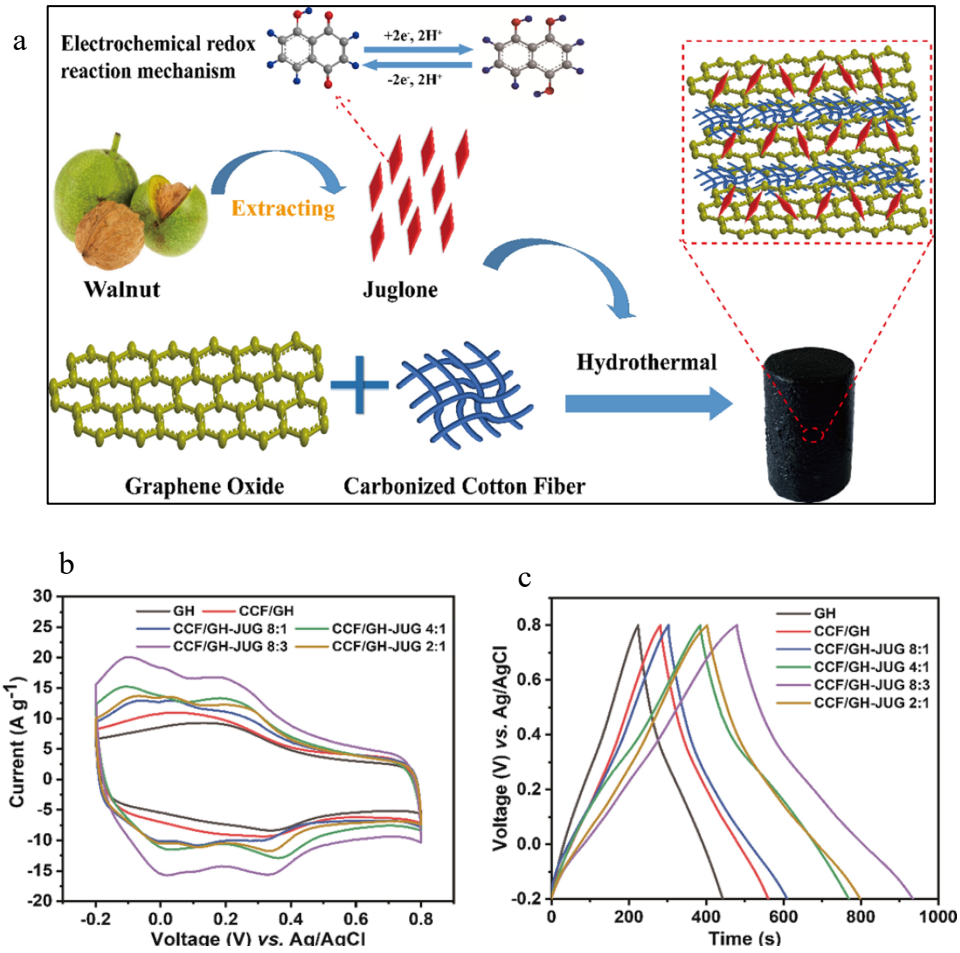

Figure 2.8 a) Schematic of fabrication process of carbonized cotton fiber, graphene oxide hydrogel, and juglone (CCF/GH-JUG) electrodes; b) CV curves of fabricated electrodes at 25 mV s^{-1}; d) GCD curves of fabricated electrodes [98].

The observed poor cycling stability, as reported in several studies involving quinones combined with conductive additives (please see Table 2.1), is attributable to the interactions between the electroactive molecules, rich in oxygen-containing functional groups, and the organic solvent-based electrolytes[32, 93].

The solubility issues of quinone compounds can be effectively addressed through several strategies, including but not limited to: i) surface engineering (e.g., the incorporation of specific functionalities), ii) the use of semi-solid-state or all-solid-state electrolytes, and iii) modifications with binders or separators[25, 99, 100].

2.6 Melanin-based supercapacitors

Melanin, a class of naturally occurring polyphenolic bio-pigments, found in various biological systems from bacteria to mammals, exhibits unique physicochemical properties such as UV absorption, metal ion-binding affinity, hydration-dependent electrical response, and redox activity [101, 102].

Natural melanins are categorized into five primary types: (i) eumelanin, responsible for black and brown pigmentation; (ii) pheomelanin, associated with red and yellow hues; (iii) neuromelanin, found in specific brain regions, including the *substantia nigra*; (vi) allomelanin, derived from plant and fungal sources; and (v) pyomelanin, produced by certain bacteria[101, 103].

Each type of melanin exhibits distinct structural and functional characteristics. Despite decades of research, the structure-property-function relationship of melanins is still not fully elucidated. Nevertheless, this complexity enables melanin to be adapted for a wide range of applications, including biosensors[104], gating medium in transistors[105], pH sensors[106], and energy storage[107].

The type of melanin that has been studied extensively by materials scientist is eumelanin, which will be referred to as melanin for simplicity. Melanin results from of 5,6-dihydroxyindole (DHI) and 5,6-dihydroxyindole carboxylic acid (DHICA) building blocks that, in parallel with covalent polymerization, hierarchically assemble through π–π stacking and hydrogen bonding interactions to form granules approximately of 150-200 nm in size. The building blocks of the melanin macromolecule can adopt various redox states, including hydroquinone (reduced form), semiquinone (intermediate form), and quinone (oxidized form) (Figure 2.9)[102, 103].

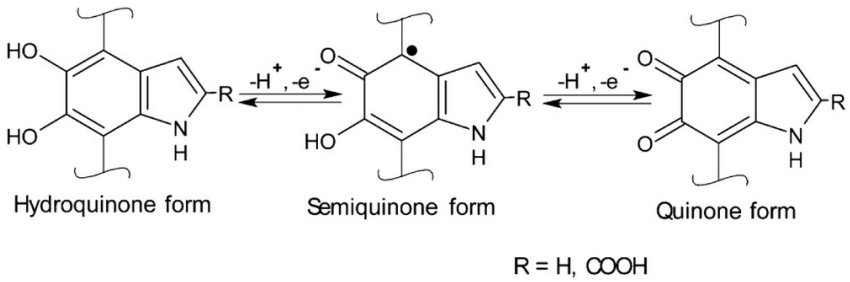

Figure 2.9 5,6-dihydroxyindole (DHI) and 5,6-dihydroxyindole-2-carboxylic acid (DHICA) building blocks of Sepia in their different redox states: hydroquinone, semiquinone, and quinone. R is -H in DHI whereas R is the -COOH group in DHICA [103].

The synergy between the intrinsic redox activity of melanin's building blocks and its ability to reversibly bind multivalent cations forms the foundation for its application in pseudocapacitive energy storage systems.

In contrast to conventional capacitors that utilize carbon electrodes and store energy exclusively through electrostatic mechanisms, the integration of redox-active melanin with carbon electrodes introduces pseudocapacitive behavior, leading to significant improvements in both specific capacitance and energy density.

In 2013, Bettinger *et al*. [107] reported the first use of biologically derived melanin pigments, isolated from *Sepia officinalis*, as anode materials for aqueous sodium-ion energy storage devices. The charge storage capacity of melanin anodes with sodium ions (NatMel-Na), measured at the discharge rate of 10 mA g^{-1}, was 30 mAh g^{-1}. This value was comparable to those of polyaniline/carbon nanotube composite electrodes (i.e., 12 mAh g^{-1}) and PPy/carbon fiber electrodes (i.e., 23 mAh g^{-1}). These results suggested that naturally occurring melanin, with minimal post-processing, could be used for energy storage applications, offering the key advantage of eco-friendliness for green energy storage systems.

Several studies have since explored melanin-based supercapacitors [70, 100, 103, 108-110]. Generally, two main approaches have emerged for incorporating natural melanin into supercapacitors: (i) converting natural melanin to carbonaceous electrode materials through carbonization, and (ii) directly using purified natural melanin as the redox-active electrode material without further carbonization.

Liu *et al*. [108] reported the preparation of supercapacitor electrode materials by extracting melanin from squid ink (Figure 2.10). After carbonization (700°C, 1 h in N_2), followed by activation using potassium hydroxide (KOH), the resulting carbon materials exhibited a hierarchically porous structure with 2 wt% nitrogen doping. When used as electrode materials for supercapacitors, the as-obtained samples demonstrated a capacitance of 329 F g^{-1} (at 0.50 A g^{-1}), maintaining nearly 100% retention over 10,000 cycles. While the electrochemical performance is notable, the report highlighted the need for more energy-efficient processes carried out at room temperature.

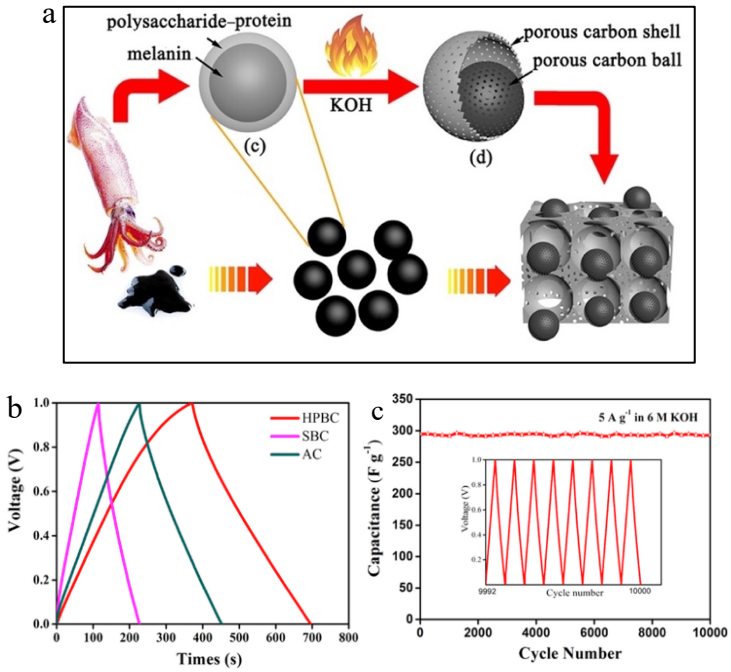

Figure 2.10 Illustration of fabrication process of hierarchically porous bio-carbon materials (HPBC) extracted from squid inks; b) GCD curves of HPBC, spherical bio-carbon materials (SBC) and activated carbon (AC); c) Capacitance retention vs. cycle number for HPBC at 5 A g^{-1}; The inset of (c) shows the GCD curves in the last 8 cycles [108].

Our group has conducted several studies where the redox properties of natural melanin have been leveraged for the development of flexible micro supercapacitors light-assisted supercapacitors [109], electrochemical capacitors operating in aqueous solutions[70, 100]. Natural melanin extracted from the ink sac of cuttlefish can be solution-processed at ambient conditions, enabling its direct application to modify the surface of the carbon-based current collectors.

Kumar *et al.*[103] investigated the charge storage properties of natural melanin (commercially available eumelanin polymers) in supercapacitor configurations without any thermal treatment. A gravimetric specific capacitance of up to 167 F g^{-1}, was reported for melanin deposited on carbon paper electrodes in $NH_4CH_3COOH_{(aq)}$ electrolyte. The capacitance of melanin-based supercapacitors can be enhanced through surface engineering by introducing additional active sites on carbon paper (as discussed in detail in the section 2.5.1). To further enhance the capacitance of carbon paper electrode beyond its EDLC, Gouda *et al.*[100] employed a two-step treatment process on carbon substrate. First, the carbon paper was subjected to hydrothermal treatment with sulfuric acid and nitric acid (120 °C, 2 h, in autoclave), followed by a secondary hydrothermal treatment

with ammonium phosphate ($(NH4)_3PO_4$, 180 °C, 24 h, in an autoclave). Melanin processed in dimethyl sulfoxide (DMSO) and deposited on as-prepared hydrothermally treated carbon paper electrodes, exhibited a capacitance of 452 F g^{-1} in $Na2SO_{4(aq)}$ electrolyte.

Unfortunately, like many other bio-sourced redox-active molecules, melanin typically suffers from high contact resistance at the interface with carbon current collectors, limiting its rate performance and cycling stability. Therefore, designing a conductive network within electrode materials is crucial (as described in detail in section 2.5.2). For example, Gouda *et al.*[70] demonstrated that a composite of melanin and N- and S-doped graphitic carbon quantum dots (N, S GCQDs) deposited on carbon paper electrodes achieved a notable areal capacitance of up to 180 mF cm^{-2} in $Na_2SO_{4(aq)}$ (Figure 2.11). Additionally, the melanin/N,S GCQD symmetric supercapacitor, when operated in $Na_2SO_{4(aq)}$, demonstrated 92% capacitance retention and 100% coulombic efficiency over 10,000 cycles at a current density of 5 A g^{-1}.

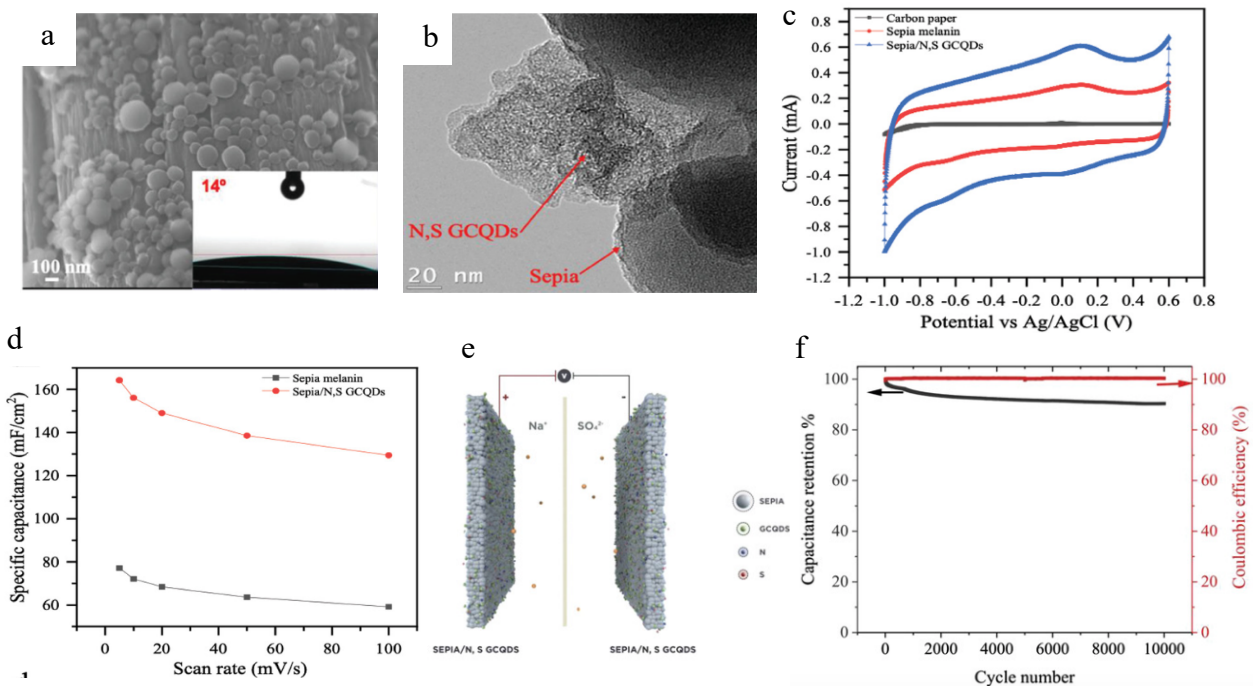

Figure 2.11 a) sepia/N,S GCQD composite electrode materials on carbon fiber; b) TEM images of sepia/N,S GCQD; c) CV curves of sepia melanin, sepia/N,S GCQDs, and bare carbon paper at 5 mV s^{-1} ; d) areal capacitance for both sepia and sepia/N,S GCQDs at different scan rates; e) schematic illustration of the symmetric supercapacitor; f) capacitance retention and coulombic efficiency for 10,000 cycles of GCD at 5 A g−1; Insets (a) contact angle measurements for sepia/N,S GCQD mixture [70].

2.6.1 Working principle of melanin-based supercapacitors

The working principle melanin-based supercapacitors in a symmetric configuration consists of identical positive and negative carbon paper electrodes operating in an aqueous electrolyte (e.g., $NH_4CH_3COOH_{(aq)}$), can be described as follows (Figure 2.12).

During the charging process, at the positive electrode, hydroquinone (H2Q) and semiquinone (SQ) groups are rapidly oxidized, leading to an increase in quinone (Q) groups. Simultaneously, H^+ and NH_4^+ are released into the solution, while anions are absorbed into the electrode material. At the negative electrode, Q and SQ groups are reduced, resulting in a higher concentration of H2Q groups. Anions are released into the solution, and H^+ and NH_4^+ are incorporated into the electrode material. These processes are reversible during discharge[103].

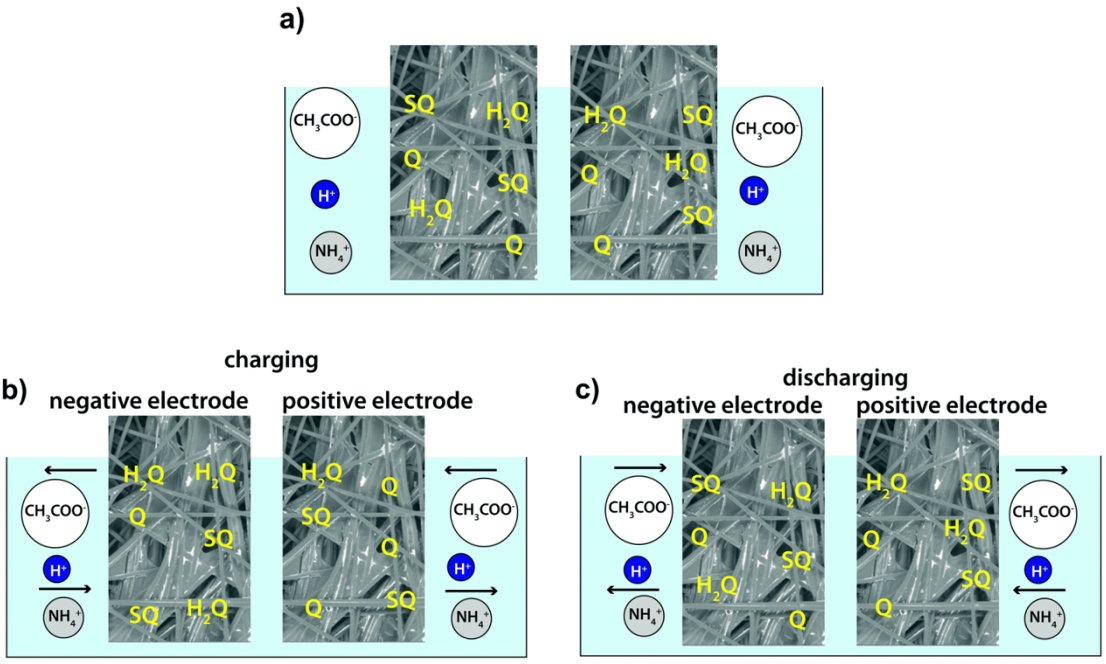

Figure 2.12 Working principle of melanin-based symmetric supercapacitors operating in $NH_4CH_3COOH_{(aq)}$; a) before applying potential; b) during charging; c) during discharging [103].

2.7 Tannins

Tannins are abundantly available in nature and considered among nature's most versatile redox active biopolymers, created through natural plant biosynthesis[111]. Tannins can be extracted from tree bark (e.g., pine, oak, mimosa), fruit residues (e.g., persimmon, grape) or by-product of wood or food industries by using eco-friendly and sustainable process in aqueous solvents (e.g., solid-liquid extraction) allowing isolate Tannin fractions with a high phenolic content [55, 112].

The solid-liquid extraction method entails dissolving Tannins in water at a moderate temperature (60-70 °C). Subsequently, the solution is concentrated and spray-dried to yield a red/yellow powder rich in phenolic content [32, 113]. The chemical composition of the final powder is greatly influenced by the plant species and the specific part of the plant from which the Tannin is extracted. Tannins exhibit molecular weights ranging from 500 to 20,000 Da and possess the highest phenol concentration (5.56 mol g^{-1}) among natural phenolic biopolymers, even up to 5,000 times more than lignin[111].

The Tannin family exhibits significant structural diversity and based on their structural characteristics, Tannins can be categorized into four major groups: gallotannins, ellagitannins, complex Tannins, and condensed Tannins (Figure 2.13)[114].

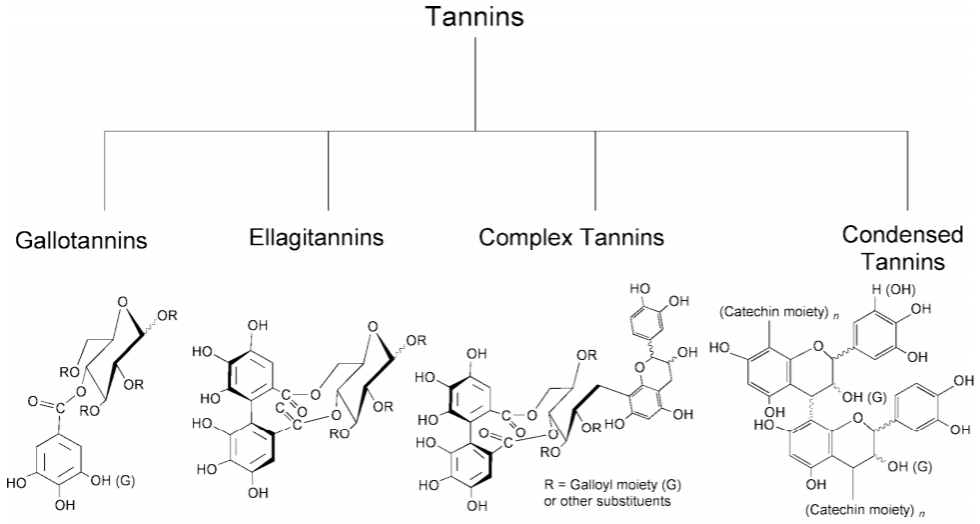

Figure 2.13 Classification of Tannins based on their structural characteristics [114].

Tannins have a variety of structural features, including phenolic, hydroxyl, ester, and ether functional groups. These diverse components play a crucial role in determining their unique chemical properties and reactivity[115]. Gallotannins, ellagitannins and complex Tannins are

considered as hydrolysable Tannins and naturally occur as single molecules. In contrast, condensed Tannins occur as oligomers composed of their constituent Tannin units [116].

Gallotannins are found in berries, grapes, persimmons, and pomegranates, whereas ellagitannins are abundant in coffee, fruits, nuts, tea, and wine fermented in oak barrels [117]. Tannic Acid is another example of hydrolysable Tannin and can be found in practically all plant tissues [118]. Examples of condensed Tannins are Catechin, epicatechin, and gallocatechin. They can be extracted from chocolate, cocoa, coffee, cranberries or tea [117]. Condensed Tannins (i.e., composed of flavonoid units linked together by carbon-carbon bonds) are of significant interest for the synthesis of carbon-based materials due to their high polyflavonoid content (i.e., 70-80 %) and their notable carbon yield of approximately 50% through pyrolysis[32]. Condensed Tannins currently account for over 90% of the global industrial extraction of tannins, which exceeds 220,000 tons annually[119].

Tannins generally have a wide range of applications, including their traditional use in the tanning of leather, as additives in wine and food to improve flavor and stability, and as active ingredients in the cosmetic industry due to their antioxidant[115]. Tannins are also employed in water treatment for their ability to bind heavy metals, in the production of adhesives and resins, as natural dyes in textiles[120].

2.7.1 Tannin-based supercapacitors

Tannins are rich in phenolic content, providing them with active functional groups that facilitate redox reactions. Tannins may undergo two-electron proton-coupled electron transfer in aqueous media [21, 55]. Figure 2.14a represents chemical structure of ellagitannins and figure 2.14b demonstrates reversible redox reaction between phenol and quinone during charge and discharge process. Given their redox activity, abundance, accessibility, and non-toxicity, Tannins are excellent candidates for eco-friendly electrochemical energy storage solutions [32, 100].

The diversity within the Tannin family and the heterogeneity in their structures depending on the source, present both opportunities and challenges. Each Tannin is expected to have its own redox activity and electrochemical signature. Tannins offer a broad selection of potential molecules and sources, but also make complicate the choice of the ideal candidate in energy storage applications in terms of electrochemical performance.

Generally, the theoretical capacitance of organic molecular electrode materials is highly influenced by the number of redox-active sites available per unit of molecular weight [60, 121]. It means that, enabling multi-electron Faradaic reactions at lower molecular weights enhances electron transfer

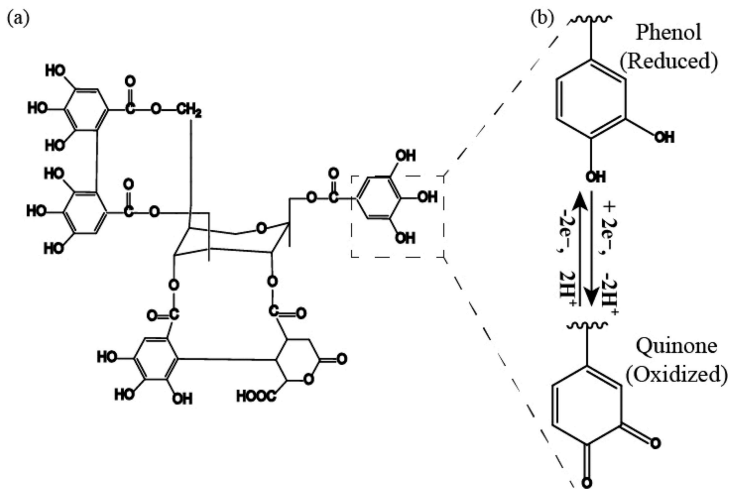

Figure 2.14 representative of possible redox reaction in tannin; a) the molecular structure of ellagitannins; b) redox reaction between phenol and quinone in aqueous medium [55].

per unit mass, thereby increasing energy density. Although the presence of more oxygen-containing functional groups in the molecular structure may theoretically enhance redox activity in aqueous electrolytes, it also increases water solubility, resulting in poor cycling stability[122-124].

Many studies have explored the redox activity of Tannins, as redox active electrode materials in supercapacitors and as cathode in lithium-ion and or sodium-ion batteries [21, 54, 55, 68, 125, 126]. Mukhopadhyay *et al*. [55] in 2017 reported Tannin-based electrodes based on extracted Tannin from bark and polypyrrole (PPy) on carbonized wood as a freestanding electrode. An areal capacitance of 4.6 F cm^{-2} at 0.5 mA cm^{-2} was reported for the composite electrode in $HClO_4$ 0.1 M aqueous electrolyte. The observed improvement in electrochemical performance of the electrode compared to bare carbonized wood electrode was attributed to three contributing factures including: (i) high surface area and *cellular* porosity of wood-derived substrate, (ii) presence of the conductive polymer PPy and (iii) pseudocapacitive contribution from Tannin. However, the electrode exhibited poor cycling stability, and a notable decline in capacitance was observed during the stability test, likely due to the leaching of Tannin in aqueous electrolytes.

Given the potential of Tannins as bio-sourced redox-active molecules for the development of sustainable supercapacitors, our group has investigated the electrochemical properties of various tannins. For example, Lemieux *et al*. [21] studied electrochemical performance of the two Tannins namely Tannic acid (TA) and Catechin (Ctn) deposited on galvanostatically treated carbon paper (gCP) as current collector, in 0.5 M H_2SO_4 electrolyte (Figure 2.15). A capacity increase of 32% compared to that of bare activated CP electrodes was reported due to pseudocapacitive contribution of tannic acid and Catechin deposited on activated carbon paper (TA/pre-gCP and Ctn/pre-gCP). Interestingly, over 5,000 cycles, the capacity retention dropped rapidly to around 80% and 76%, for TA/pre-gCP and Ctn/pre-gCP, respectively. This capacity loss and the limited cyclability of Tannin-based electrodes were anticipated, primarily due to the high solubility of Tannin. Additionally, the anchoring mechanism of these molecules on the carbon surface, which is assumed to be through weak π–π interactions of the aromatic rings, further contributes to leaching in aqueous electrolytes.

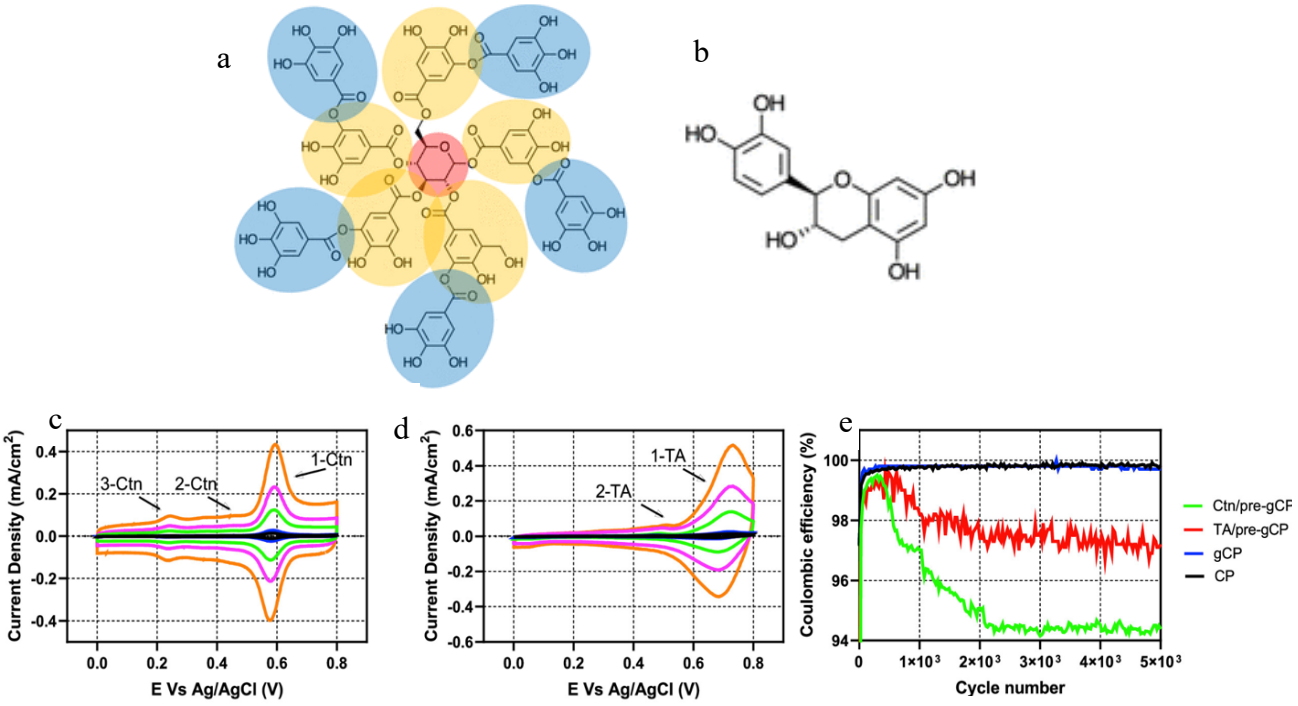

Figure 2.15 Schematic representation of the molecular structure of (a) tannic acid(TA) and (b) catechin (Ctn); CV profiles of (c) Ctn/gCP; (d) TA/gCP, at different scan rates in 0.5 M H_2SO_4; e) Coulombic efficiency of samples [21].

One approach to reducing the solubility of Tannins and simultaneously increase conductivity within electrode materials is utilizes graphene sheets to stabilize tannic acid by π–π interactions. Meng *et al.* [127] reported the fabrication of a composite electrode materials made of graphene, carbonized paper, and tannic acid (GN/CP/TA) for energy storage applications. The composite electrode demonstrated around 86% capacitance retention over 10,000 cycles. Additionally, the corresponding supercapacitors achieved an energy density of 36.82 μW h cm^{-2} and power density of 1372.73 μW cm^{-2}.

Another study reported that modifying reduced graphene oxide (rGO) sheets with tannic acid enhanced the overall electrochemical performance of the electrode[67]. The abundant redox-active functional groups in tannic acid not only help prevent the restacking of rGO sheets in aqueous media and promote the in-situ reduction of graphene oxide (GO), but also provide additional pseudocapacitance to the electrode. Specifically, symmetric supercapacitors making use of tannic acid and GO in a 6 M KOH electrolyte delivered an areal capacitance of 525 mF cm^{-2} at 0.5 mA cm^{-2}, energy density of 72 μWh cm^{-2} and, power density of 250 μW cm^{-2}. The device also showed improved capacitance retention up to 91% after 10,000 charge/discharge cycles.

Following the same strategy, in the study by Oh *et al*.[128], it was demonstrated that tannic acid can also self-assemble on the surface of carbon nanotubes (CNTs) through the formation of metal-phenolic coordination bonds (Figure 2.16). Specifically, the phenolic groups of tannic acid undergo dehydroxylation, forming a tannic acid-Fe^{3+} complex. This complex generates metal-phenolic compounds on the surface of single-walled carbon nanotubes (SWNTs) via π–π interactions between the aromatic rings of the tannic acid and the carbon nanotubes. The resulting flexible metal-phenolic carbon nanocomposites electrode exhibited a gravimetric capacitance as high as 147.4 F g^{-1} and retained 97% of its capacitance over 1000 cycles.

Tannic acid plays two key roles in this system, (i) it acts as both a dispersant and a cross-linker, while simultaneously (ii) providing redox-active sites, improving the overall electrochemical performance of the electrode.

Our group investigated Catechin-based electrodes in aqueous medium[100]. Catechin (Ctn), a member of the Tannin family and classified as a condensed Tannin, was mixed with tannic acid as a binder -following the previous strategy-and deposited on hydrothermally treated carbon paper (TCP) electrodes. These electrodes exhibited a capacitance of approximately 300 F g^{-1} in aqueous

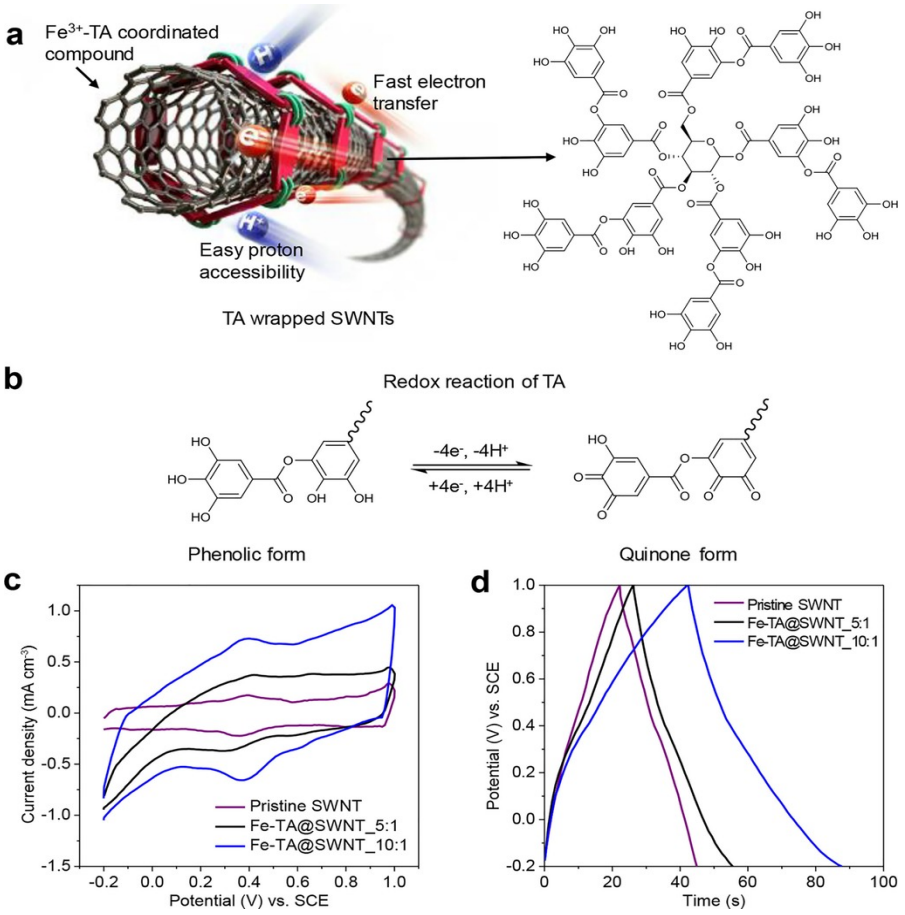

Figure 2.16 Schematic representation of tannic acid (TA) on the conductive single-walled nanotubes (SWNTs); b) representation of the redox reaction in TA; c) CV profiles at a scan rate of 10 mV s^{-1} and d) GCD plots at 1 A g^{-1} for samples at different mass ratio [128].

electrolyte (0.5 M $Na_2SO_{4(aq)}$) thanks to pseudocapacitive contribution of Tannins. Interestingly, Catechin/Tannic acid (Ctn/TA)-based supercapacitors exhibited 100% capacitance retention and 100% coulombic efficiency over 10,000 cycles at a current density of 10 A g^{-1}. This improved cycling stability is attributable to the introduction of tannic acid as a binder with hydrogen-bonding capability, which helps to limit the solubility of Catechin in aqueous electrolytes. This underscores the dual functionality of tannic acid as an organic bio-sourced binder, along with its redox activity.

Despite the great potential of Tannin molecules in the development of sustainable electrochemical energy storage applications, the electrochemical characteristics of the Tannin family are not well understood due to the large variety of molecular structures and arrangements.

CHAPTER 3 METHODOLOGICAL ASPECTS

3.1 Electrochemical characterization

Electrochemistry probes electron transfer processes at interfaces between metal or semiconductor electrodes and electrolytes. Various electrochemical methods have been developed to investigate the behavior of electrode materials and energy storage devices, with each technique relying on different input parameters such as current, voltage, resistance, frequency, and power. Based on the specific application needs, common methods are cyclic voltammetry (CV), galvanostatic charge/discharge (GCD), and electrochemical impedance spectroscopy (EIS)[129, 130]. In this PhD project, CV, GCD and EIS techniques have been utilized to evaluate the electrochemical energy storage performance of the electrode materials and their corresponding symmetric supercapacitors.

3.1.1 Cyclic voltammetry

CV test can be applied in both three-electrode setup and two-electrode configurations (e.g., in device configuration). Figure 3.1 shows the schematic of a CV experimental setup[131].

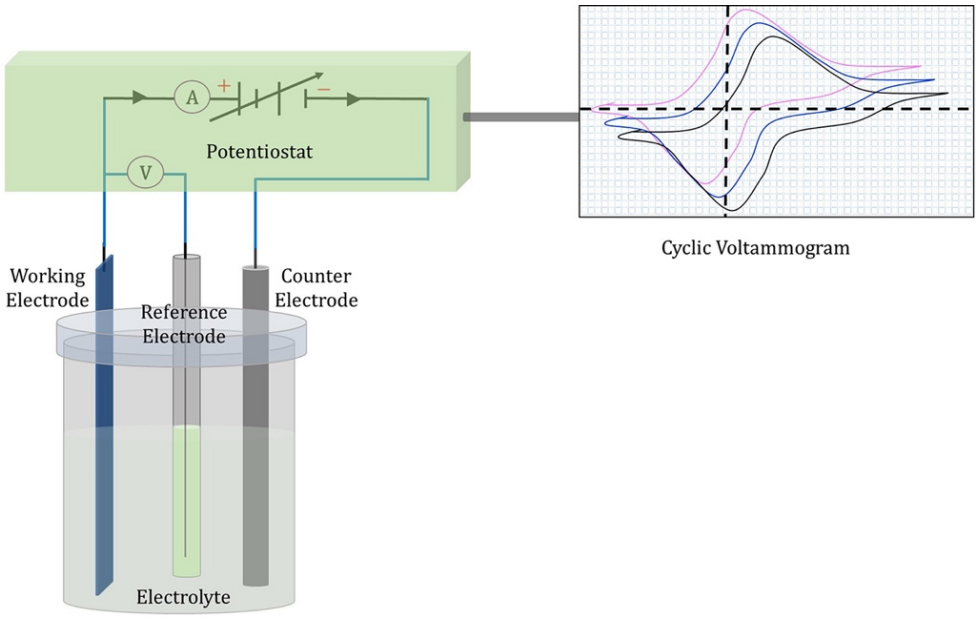

Figure 3.1 Schematic representation of an electrochemical cell used for cyclic voltammetry (CV) [131].

The three-electrode configuration include: (i) the working electrode (WE, i.e., where the electrochemical process under investigation occurs), (ii) the counter electrode (CE, the current flows between the working and counter electrodes); (iii) the reference electrode (RE, to provide a reference point against which the potentials of other electrodes can be measured).

During a CV experiment, the potential is repeatedly swept between two extremes (i.e., operating potential or potential window) at a given scan rate (i.e., sweeping rate at which the potential changes). During CV, the electron transfer takes place while electroneutrality is maintained through the movement of ions in the electrolyte solution (i.e., a mixture of solvent and salt). As electrons move from the analyte (i.e., the substance being studied, usually immobilized on the working electrode) to the electrode, electron transfer occurs in the external circuit, while ions move within the solution to balance the charge and complete the electrical circuit[129].

During a CV test, the electrochemical potential is varied between RE and WE, while the corresponding change in current through the outer circuit is measured. The current plotted versus the potential is known as a CV profile or cyclic voltammogram[132]. CV analysis relies on the characteristics of the CV profile, including but not limited to (i) the shape of the CV, (ii) the enclosed area of the CV, (iii) peak currents values, and iv) peak position[131, 133]. Moreover, CV analysis is used to determine the potential window for a specific electrode material.

By integrating enclosed area under the CV curve, the gravimetric specific capacitance (C, $F\ g^{-1}$) can be calculated using equation 3.1[40]:

$$C_s = \frac{\int Idv}{2\upsilon \Delta \mathrm{Vm}} \qquad 3.1$$

where $\int IdV$ is the integral area of the CV curve, υ is the scan rate ($mV\ s^{-1}$), m is active material on the current collector (g) or, and ΔV is the potential window (V).

3.1.2 Galvanostatic charge/discharge (GCD)

During GCD in two-electrode configurations, the electrodes are alternately charged and discharged between two defined potentials (i.e., cut-off potentials) under a constant applied current. GCD is the most widely used method for calculating the specific capacitance of a device (C_{GCD} , $F\ g^{-1}$),

as well as its energy density (E, $Wh\ kg^{-1}$), power density (P, $W\ kg^{-1}$), and cycle stability (i.e., running GCD over thousands of cycles) as follows:

$$C_{GCD} = I \int \left(\frac{1}{V_{(t)}}\right) dt \quad 3.2$$

$$E = \frac{I_{dis} \int v dt}{3600} \quad 3.3$$

$$P = \frac{E}{t_{dis}} \quad 3.4$$

where I is the applied constant-current density, t is the discharge time, and $V_{(t)}$ is the potential as a function of t, I_{dis} represents the constant discharg current density ($A\ g^{-1}$), $\int v dt$ is the integral area of the GCD discharge cycle, and t_{dis} denotes discharge time (s) [134, 135].

3.1.3 Electrochemical impedance spectroscopy (EIS)

Electrochemical Impedance Spectroscopy (EIS) is one of the most versatile electrochemical techniques, widely employed in various fields such as energy storage, corrosion studies, and sensors. In EIS, a low-amplitude alternating potential is applied to the system, and the resulting changes in both the amplitude and phase of the current are measured across a range of frequencies (e.g., from 0.01 to 100 kHz). The impedance spectrum (i.e., Nyquist plot), illustrates the relationship between the imaginary component of the impedance (Z_{im}) and the real component (Z_{re})[136, 137]. In a Nyquist plot of a typical pseudocapacitor, each frequency range is attributable to a distinct process. The low-frequency range reveals processes related to mass transport, such as ion diffusion (e.g., pure capacitive behavior). The medium-frequency range (10 mHz to 1 kHz) typically reflects processes occurring at the electrode/electrolyte interface, including charge transfer process and EDL formation. The high-frequency range (≥1 kHz) primarily is attributable to total cell resistance, including electrolyte and electrode resistances (Figure 3.2)[44, 138].

By fitting the impedance data to an equivalent circuit model, various impedance elements can be distinguished, enabling a more detailed understanding of the contributions of each component to the overall electrochemical behavior.

The appearance of a semicircle in the high-frequency region of a Nyquist plot indicates charge transfer resistance and can be associated to a pseudocapacitive behavior. This phenomenon was observed during the EIS characterization of semi-solid-state devices in this PhD project and is discussed in Articles 1 and 2.

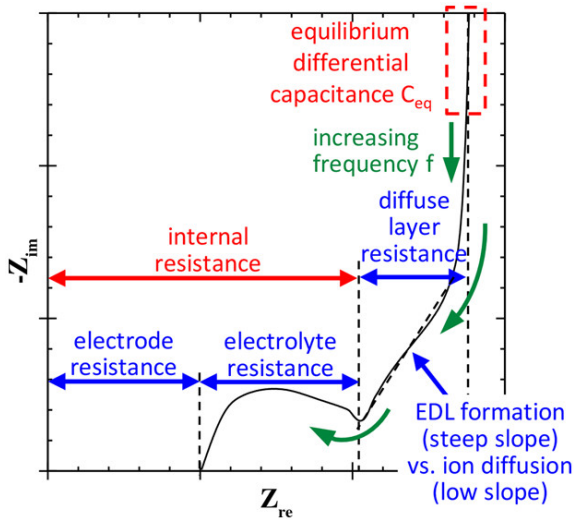

Figure 3.2 Schematic illustration of a typical Nyquist plots of a pseudocapacitor [136].

3.2 Electrochemical signature of pseudocapacitive and battery-like behavior

To differentiate between the energy storage mechanisms (EDLC, pseudocapacitive and battery-type behavior), it is essential to analyze the electrochemical signatures obtained from CV and GCD tests.

In EDLCs, the cyclic voltammogram typically displays a rectangular shape with constant current plateaus and absence of redox peaks, signifying purely capacitive charge storage mechanism. The GCD profile of EDLCs consistently displays a triangular shape and a linear voltage-time response, with a constant slope during both charging/discharging (Figure 3.3)[138, 139].

For an ideal EDLC, the Helmholtz model provides the simplest representation of this process, applying the parallel-plate capacitor equation for specific capacitance (C, F g^{-1}).

$$C = \frac{\varepsilon_0 \varepsilon_r A}{d} \qquad 3.5$$

Where ε_r represents the relative permittivity, ε_o denotes the absolute permittivity (F m^{-1}) in a vacuum, A (m^2 g^{-1}) indicates the specific surface area of the electrode accessible to the ions, and d (m) refers to the effective thickness of the EDL[42].

Unlike EDLCs, pseudocapacitive materials exhibit a semi-rectangular CV curve with multiple superimposed broad peaks, corresponding to charge generation from redox reactions. The GCD profile of pseudocapacitive materials typically shows a nearly triangular shape with slight

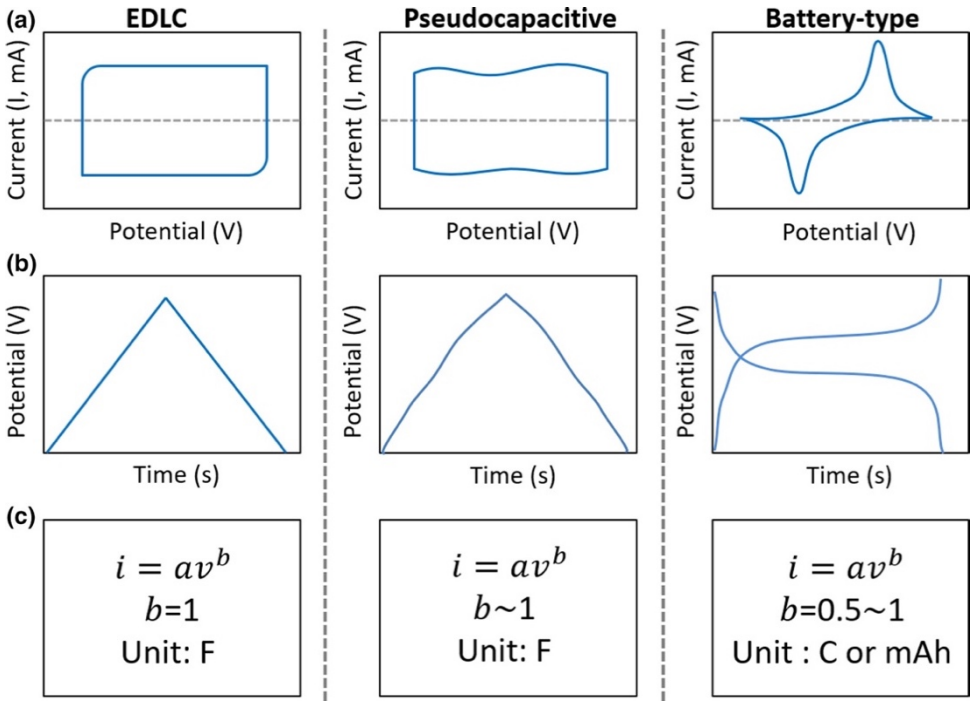

Figure 3.3 The electrochemical signatures for different charge storage mechanisms, a) Cyclic Voltammetry (CV), b) Galvanostatic charge/discharge (GCD), c) Power law analysis [24].

deviations from linearity, indicating the occurrence of surface redox reactions (Figure 3.3)[29, 131]. As discussed earlier in Section 2.3.2, the similarity of the cyclic voltammograms and GCD profiles of the electrode materials in both Article 1 and Article 2 features pseudocapacitive signatures, indicating that the charge storage mechanism in both cases involves a combination of surface redox reactions and electrostatic contributions.

A battery-type electrode exhibits distinct and sharp peaks in its CV profile, indicative of Faradaic reactions, and shows plateaus in the corresponding GCD profiles, which are attributed to phase transitions or specific redox reactions occurring within the material (Figure 3.3). These features

highlight a storage mechanism that is fundamentally different from electrostatic or pseudocapacitive processes, reflecting the electrode's capacity to store and release energy through bulk diffusion-controlled reactions, which are characteristic of battery-like energy storage mechanisms[49, 140].

The power law method provides a complementary tool for investigating charge transfer processes occurring at the electrode, enabling distinction between surface-controlled and diffusion-limited contributions in a charge storage system. In this method, the current is assumed to vary with the scan rate according to the following:

$$i = av^b \quad 3.5$$

Where, i is the current (mA), and v is the scan rate (mV s^{-1}). The value of b lies between 0.5 and 1. If the b value is close to 0.5, stands for the diffusion-controlled reaction (i.e., battery-type behavior) where the charge storage mechanism relies on the bulk diffusion of ions within the electrode material. This behavior suggests that the rate of charge transfer is limited by the movement of ions through the electrolyte and the solid-state diffusion in the electrode, leading to slower charge and discharge rates [43, 47].

Conversely, if b is close to 1, it signifies a surface-controlled reaction, typical of capacitive or pseudocapacitive processes. In this case, charge storage occurs predominantly at the electrode surface, where fast electrochemical reactions can take place without the need for significant ion diffusion into the bulk of the electrode material, resulting in rapid charge and discharge capabilities compare to that of diffusion-controlled systems (i.e., battery-type behavior).

3.3 Ultrasonication

Ultrasonication is recognized as a green technology with diverse applications across several domains, including food processing, metal extraction, stabilization, cleaning processes, and large-scale production of organic and inorganic 2D mono/multilayer materials, etc. The ultrasonication process is non-invasive, energy-efficient and up-scalable and as such it is attractive for sustainable practices[141, 142].

The ultrasonication is based on utilizing ultrasound waves to induce physical and mechanical effects in the liquid. Through ultrasonic irradiation in a liquid medium, sound waves interact with micro/nanobubbles, triggering the process of acoustic cavitation[143]. During this process,

cavitation bubbles expand and eventually collapse implosively within the medium, generating shock waves and microjets, which in turn lead to intensified shear forces. Such significant locally concentrated energy leads to the formation of local hotspots, reaching local temperature up to 10,000 K and pressure up to 10 000 atm, inducing the generation of radicals (e.g., H and OH radicals) through the homolytic cleavage of water molecules[144]. Figure 3.4 schematically represents an ultrasonication setup[145].

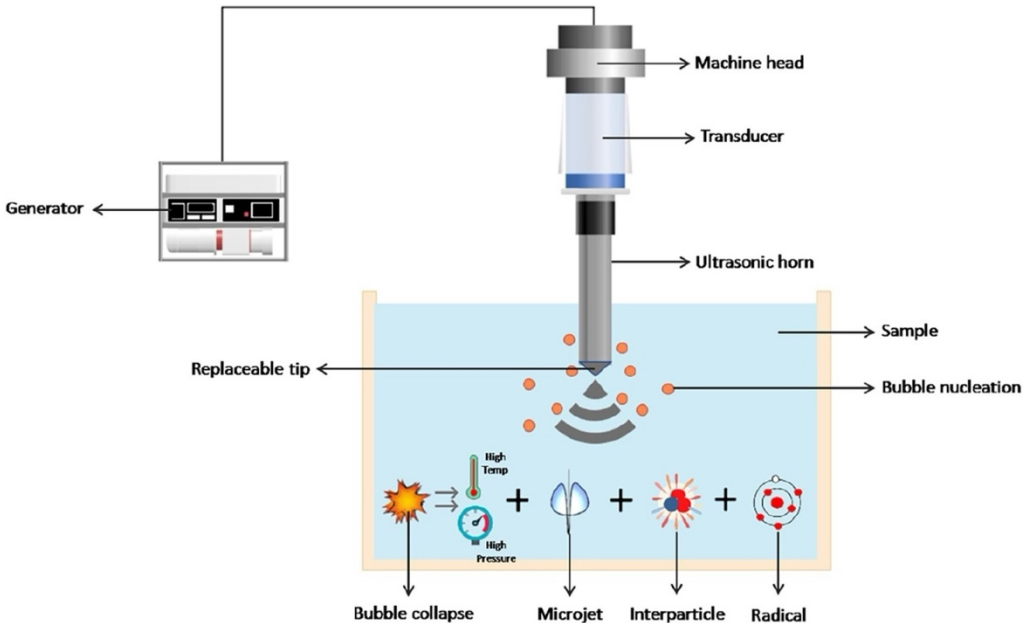

Figure 3.4 Schematic representation of an ultrasonication setup [145].

The effect of cavitation is governed by several key parameters, including, but not limited to, temperature, ultrasonication frequency, and time. Therefore, careful optimization of these parameters is essential to obtain the desired outcomes based on the ultrasonication application.

In this PhD thesis, we utilized the ultrasonication process for the surface modification of carbon cloth using sepia melanin (i.e., a redox-active bio-sourced molecule) and multi-walled carbon nanotubes (MWCNTs) as electrode materials (please see Article 2). This study represents the first report of employing ultrasonication in an aqueous medium (i.e., deionized water) for the surface activation of electrode materials for energy storage application.

During the process, Sepia melanin granules and MWCNTs were anchored onto the carbon fibers of the carbon electrodes without the use of any binders or surfactants. Moreover, the cavitation-induced shear forces inhibited the agglomeration of sepia melanin granules and MWCNTs during ultrasonication. Additionally, cavitation-induced radicals facilitated the generation of oxygen-containing functionalities on the surface of carbon electrodes, enhancing their wettability and redox activity.

We optimized the ultrasonication conditions (time, temperature, and output power) to achieve the highest capacitance in the resulting modified carbon cloth (supplementary note of Article 2)The results of this PhD thesis confirmed that employing the ultrasonication technique for the activation of carbon-based electrodes can significantly reduce operating time and energy consumption while also mitigating chemical usage.

CHAPTER 4 ARTICLE 1: TANNINS FOR SUSTAINABLE SEMI-SOLID-STATE SUPERCAPACITORS

Article 1 was published in the Waste and Biomass Valorization on April 07, 2023. The supplementary information is provided in Appendix A.

4.1 Authors

Molood Hoseinizadeh[1], Kholoud Salem[2], Abdelaziz Gouda[1,3], Daniel Belanger[4], Clara Santato[1, *]

[1]Department of Engineering Physics, Polytechnique Montreal, Canada

[2]Energy Materials Laboratory (EML), School of Sciences and Engineering, The American University in Cairo, New Cairo, Egypt

[3]Solar Fuels Group, Department of Applied Chemistry and Chemical Engineering, University of Toronto, Canada

[4]Département de Chimie, Université du Québec à Montréal, Canada

*Corresponding author: Clara Santato

Keywords

Supercapacitors, Redox-active organic molecules, Tannins, Hydrogel electrolytes, Cycling stability

4.2 Abstract

Organic redox-active molecules extracted from natural sources (bio-sourced) are relevant for sustainable storage of renewable, yet intermittent, energy. When deposited on electrode surfaces, redox-active molecules bring about an increase of the energy density of the electrodes since the Faradaic storage mechanism adds to the electrostatic one. The engineering of the electrode surface and the interfaces between the electrode surface with the molecules and the electrolyte is key to optimization of storage. Here, we report on (i) electrodes prepared by depositing onto chemically modified surfaces of carbon paper solutions of the redox-active Catechin (Ctn) molecule, a member of the Tannin family, and (ii) its use in symmetric electrochemical capacitors assembled by interfacing them to the polyvinyl alcohol (PVA)-based hydrogel electrolyte. Ctn-based supercapacitors reach capacitance values as high as 202 $F\ g^{-1}$ at 1 $A\ g^{-1}$ (based on the mass of

Ctn). They feature 99.6% capacitance retention and 99.8% Coulombic efficiency, after 20 000 cycles. The devices exhibit an energy density of 55 $Wh\,kg^{-1}$ and power density of 660 $W\,kg^{-1}$ (based on the mass of Ctn). Our work contributes to the development of eco-designed, low-cost, and potentially biodegradable electrochemical supercapacitors based on redox-active Tannin materials.

4.3 Graphical abstract

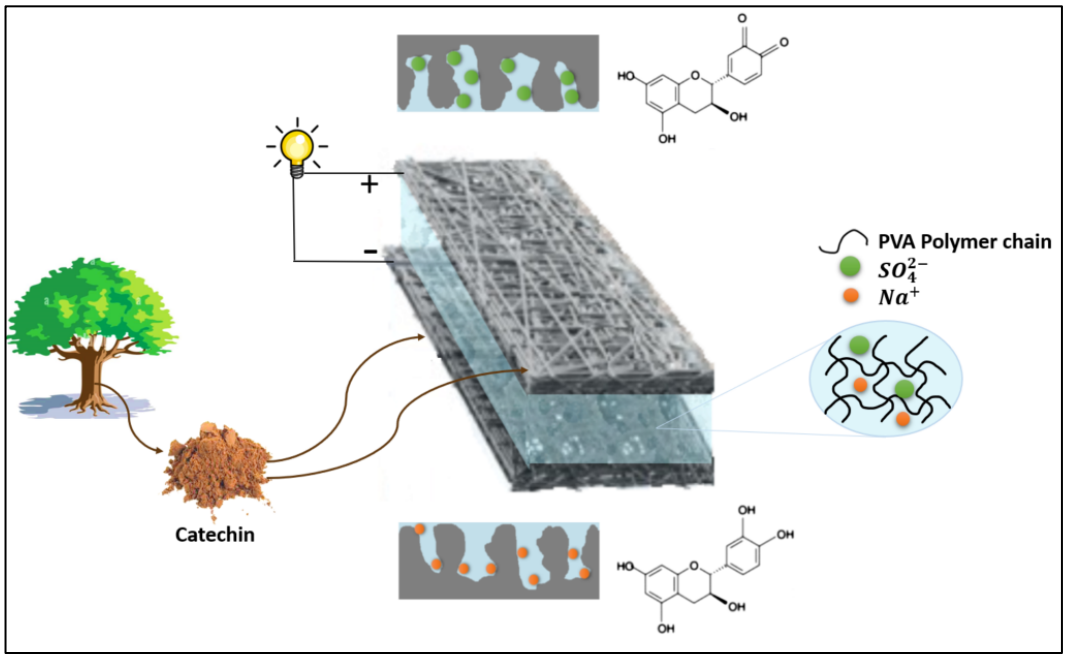

Figure 4.1 Graphical abstract of Article1.

4.4 Statement of Novelty

Carbon-based electrode materials surface-modified with abundant and biodegradable redox-active organic molecules are relevant to the development of sustainable electrochemical devices to store renewable, intermittent, energy. We report on electrochemical capacitors (supercapacitors) based on electrodes made up of chemically treated carbon paper surface-modified with Catechin, a redox-active molecule member of the Tannin family. No toxic or expensive binder or conductive additive was used in this process. Electrostatic and Faradaic (charge transfer) processes occur together in the supercapacitors. The use of a semi-solid-state electrolyte (hydrogel) that effectively prevents leaching of the water-soluble Catechin molecules into the electrolyte is key to the cycling stability of the supercapacitors.

4.5 Introduction

Reliance on fossil fuels is driving global warming to a critical level. Renewable energy sources, such as solar and wind, are essential for net-zero greenhouse gas emissions by 2050[146, 147]. Considering the intermittency of renewables, it is imperative to couple them to energy storage technologies, such as electrochemical ones. The increasing demand for electric vehicles and wearable electronics further drives the development of sustainable and biocompatible electrochemical energy storage devices (EESDs) [148, 149]. EESDs can be divided into two main categories: (1) electrochemical capacitors also known as supercapacitors or ultracapacitors, and (2) batteries. The former exhibit high power density and low energy density, while the latter exhibit moderate power density and high energy density[30, 150].

Electrochemical double layer capacitors (EDLCs) are an important category of electrochemical capacitors. Their working principle relies on the formation of electrical double layers at the electrode/electrolyte interfaces. They exhibit excellent cycling performance (up to 500 000 cycles) and fast charge/discharge rates (up to 10 times faster than commercially available lithium-ion batteries). Unfortunately, their energy densities are quite low (5 to 10 $Wh\ kg^{-1}$)[151, 152].

Carbon-based materials have been extensively used as electrode materials in EDLCs since they feature good chemical and thermal stability, electronic conductivity, and porosity[32, 153]. Further, they do not require the use of critical or toxic elements for electrodes' fabrication. The charge storage performance of EDLCs can be dramatically enhanced if Faradaic processes take place along with the electrostatic processes. This can be achieved through the modification of the surface of the electrodes of the capacitor by redox-active species, such as transition metal oxides/hydroxides[154, 155], conducting polymers[156], MXenes[157] and heteroatom-based functionalities[25, 52, 158]. *Pseudocapacitors* are electrochemical capacitors in which fast and reversible Faradaic reactions occur at the electrode/electrolyte interface and the bulk electrode materials such that their energy density and specific capacitance increase with respect to EDLCs[43, 51, 70].

Efforts are currently ongoing to eco-design of pseudocapacitors, making use of abundant, organic redox-active electrode materials, rather than critical and toxic elements. Such devices are potentially biodegradable and may be employed along with aqueous-based electrolytes[16, 70, 159].

Quinones are a class of redox-active organic compounds containing two carbonyl groups in an unsaturated six-member ring structure[20, 50, 160]. Milczarek et al. investigated the redox-active quinone moiety present in lignin derivatives for electrochemical energy storage [54]. Several studies which followed reported on the integration of bio-sourced quinone derivatives into pseudocapacitors[21, 55, 66, 70, 103]. Unfortunately, despite intensive studies, the quinone layers usually exhibited low electronic conductivity, and the supercapacitors incorporating them exhibited limited cycling stability[32, 70]. If we wish to produce large scale, commercial devices, it is imperative to control several aspects of the materials and of the devices incorporating them, including: (i) the supramolecular aggregation of the redox-active molecules, to improve electronic conductivity, (ii) the electrode surface, to optimize surface area, porosity and electrolyte wettability and impart Faradaic activity, and (iii) the quinone/electrolyte interface, to limit the leaching of the redox-active molecules in the electrolyte [100, 161].

Tannins are quinones that can be found in a wide variety of natural materials throughout the plant kingdom, such as tree bark (e.g., pine, oak, mimosa)[56, 111, 113], leaves (e.g., tea leaves)[162, 163], fruit residues (e.g., persimmon, grape)[112, 164] and typically are extracted as by-product of wood or food industries[55]. Tannins have been used in leather processing[165], as wine additives, food supplements, and cosmetic ingredients[25, 166]. Tannins are diverse, with molecular weights ranging from 200 to 20 000 Da. They have the highest phenol concentration (5.56 mol g^{-1}) of any phenolic biosourced polymer, 5 000 times higher than lignin[21, 32]. Based on their structural characteristics, they are divided into major groups: gallotannins, ellagitannins, complex Tannins, and condensed Tannins[114]. Catechin (Ctn, molecular weight of about 290 Da) is a basic unit of condensed Tannins (Figure 1). Its molecular structure includes O-containing functional groups, which may undergo two-electron proton-coupled electron transfer in aqueous media[117, 167]. Hydroquinone (H2Q), semiquinone (SQ), and quinone (Q) are the redox forms of Ctn (Figure 1). Considering redox activity, abundance, accessibility and non-toxicity, Tannins are attractive candidates for eco-designed EESDs. Our group has studied Ctn-based electrodes for electrochemical capacitors operating in aqueous solutions[21, 100]. When mixed with a binder (tannic acid), Catechin, deposited on chemically treated carbon paper electrodes, exhibited capacitance of ca. 300 F g^{-1} in aqueous electrolyte (0.5M $Na_2SO_{4(aq)}$)[100], whereas in absence of binder, cycling stability was limited, due to dissolution in the water-soluble Catechin in the electrolyte.

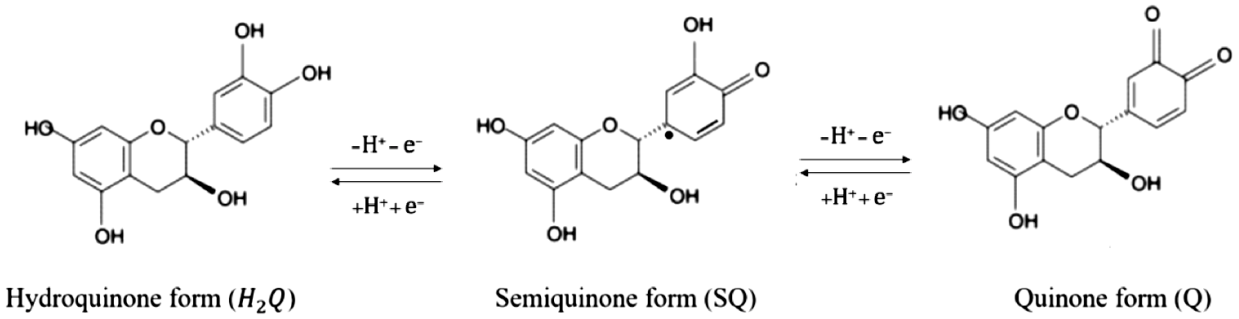

Figure 4.2 Hydroquinone (H2Q), semiquinone (SQ), and quinone(Q) redox forms of Catechin.

The need to extend cycling stability, while simultaneously ensuring mechanical integrity and flexibility of the quinone-based EESDs, point to the use of semi-solid state gel polymer, rather than liquid or solid electrolytes[168, 169]. Gel polymer electrolytes are expected to form seamless interfaces with the electrodes. Environmental considerations favor hydrogels (water-based gels) compared to organic solvent-containing gel polymers[170, 171]. Several polymer hosts have been investigated for formulating gel polymer electrolytes. Among those, polyvinyl alcohol PVA-based hydrogels offer good ionic conductivity and biodegradability by certain microorganisms in aerobic and anaerobic conditions[57, 172-174].

Here, we report on the integration of Catechin as a redox-active molecule from the Tannin family on chemically treated carbon paper in the fabrication of semi-solid-state symmetric supercapacitors making use of a PVA-based hydrogel for the electrolyte. The long-term objective of our study is to fabricate biodegradable energy storage devices based on abundant, bio-sourced materials. The treatment of the carbon paper is expected to increase the surface area available for ion adsorption (and then charge stored) and introduce redox active heteroatoms at the surface. From the methodological point of view, the Brunauer-Emmett-Teller (BET) and Barrett-Joyner-Halenda (BJH) techniques were employed to determine the surface area, pore size, and pore volume distribution of electrodes. Afterward, the morphology of electrode materials was studied by scanning electron microscopy (SEM). Energy dispersive X-ray spectroscopy (EDS) and X-ray photoelectron spectroscopy (XPS) were used for the elemental and chemical characterization of the electrodes. Finally, the electrochemical energy storage performance of the electrode materials and corresponding symmetric supercapacitors were investigated via cyclic voltammetry (CV), galvanostatic charge/discharge (GCD), and electrochemical impedance spectroscopy (EIS). The

use of biodegradable gel polymer electrolytes is expected to ensure the mechanical integrity of the devices and prolonged cycling stability. The latter is an essential aspect toward the demonstration of a novel, high-performance sustainable energy storage devices that avoid the use of critical and toxic chemical compounds.

4.6 Experimental

4.6.1 Carbon paper

Commercial carbon paper Spectracarb 2050A-1550 (electrical resistivity 5.4 mΩ cm and density of 0.50 g/cm^3) was purchased from Fuel Cell Store. After cleaning in acetone (Honeywell, VLSI, 100%) and ethanol (Commercial Alcohols, Ontario, Canada) in an ultrasonic bath (Eumax-4L) for 10 min at 40 kHz, it was dried under vacuum for 30 min at 60 °C. Then, the surface underwent a three-step chemical treatment[92, 100]: (i) immersing and sonicating the paper for 2 h in an acidic solution 3:1 (v/v) sulphuric acid (Sigma-Aldrich ACS reagents 98%):nitric acid (16M Fischer Chemical, ACS plus); (ii) transferring the paper into an autoclave for thermal treatment in the same acidic solution, at 120 °C, for 20 min, then allowed to cool overnight; (iii) immersing the paper in ammonium phosphate 7M $(NH_4)_3PO_4$ (Sigma-Aldrich, ACS reagents > 98%), in the autoclave at 180 °C, for 24 h, followed by cooling down to room temperature (5 h). Finally, the paper was rinsed with deionized water and dried under vacuum for 6 h at 60 ˚C. The resulting material is indicated in what follows as treated carbon paper (TCP), and compared with untreated carbon paper (CP).

4.6.2 Catechin solution

Catechin (Ctn) was purchased from Sigma-Aldrich (ACS reagents > 98%) and used as received. Solutions of Ctn (40 g L^{-1}) were prepared using a mixture of water:ethanol 2:1 (v/v). Ctn solution (50 µL) were deposited on the surface of CP and TCP (5 cm×0.5 cm) via drop casting (mass loading of 0.8 mg cm^{-2}). Catechin-loaded TCP (Ctn/TCP) and TCP were vacuum dried for 30 min at 60 °C before morphological, chemical, and electrochemical characterizations.

4.6.3 Hydrogel fabrication

Polyvinyl alcohol (PVA) was purchased from Sigma-Aldrich (purity > 99% hydrolyzed, molecular weight 89,000‑98,000 Da) to prepare a hydrogel, according to previous study[175], 2 g of PVA were dissolved in 80 mL of deionized water at 90 °C and stirred for 30 min to obtain a homogeneous and transparent solution. Then, 20 mL of 2.5M $Na_2SO_{4(aq)}$ (Sigma-Aldrich, purity > 99%) were

added to the solution to obtain 100 mL of 0.5M $Na_2SO_{4(aq)}$ and form the hydrogel. A thin film (~ 0.5 mm-thick) of hydrogel was fabricated under a pressure of 700 Pa, then cut into 0.5 cm×5 cm and sandwiched between the two electrodes of the supercapacitor.

4.6.4 Electrochemical characterization

Electrochemical characteristics were investigated by cyclic voltammetry (CV), galvanostatic charge/discharge (GCD), and electrochemical impedance spectroscopy (EIS), using a biologic potentiostat (SP-300). A three-electrode cell configuration was used for the electrochemical characterization of single electrodes. CP and TCP were modified with Ctn and used as working electrodes, platinum (Pt) mesh as the counter electrode, and $Ag/AgCl_{(aq)}$ in 3M NaCl as the reference electrode[129]. For the electrochemical characterization of symmetric semi-solid-state supercapacitors, EIS measurements were conducted in a two-electrode configuration in the frequency range 10^{-1} – 10^5 Hz, with a 10 mV sinusoidal perturbation, at 0 V bias. The electrode gravimetric specific capacitance (C_s, Fg^{-1}) was calculated at $5\,mVs^{-1}$, based on the cyclic voltammetry, using equation (1):

$$C_s = \frac{\int Idv}{2\mu\,\Delta V\,m} \tag{4.1}$$

where $\int Idv$ is integral CV curve area, μ is the scan rate (mV/s), m is the mass (g) of the active material on the electrode, and ΔV (V) is the potential window. Full device specific capacitance (C_{GCD}, Fg^{-1}), energy density (E, $Wh\,kg^{-1}$), power density (P, Wkg^{-1}), and Columbic efficiency (CE) were estimated from the GCD curves, as in Equation 2.

$$C_s = I\int(1/V(t))dt\ , E = \frac{I_{dis}\int vdt}{3600}, P = \frac{E}{t_{dis}} \text{ and CE} = \frac{\int I_{dis}dt}{\int I_{ch}dt} \tag{4.2}$$

where I is the applied constant-current density, t is the discharge time, and V(t) is the potential as a function of t. I_{ch} and I_{dis} represent the current of charge and discharge (mA), $\int vdt$ is the integral area of the GCD discharge cycle, and t_{dis} denote discharge time (s), respectively[134, 135]. We note that calculating the energy and power density based on the mass of the active material alone might not provide a realistic assessment of the performance of an assembled supercapacitor: the weight of other device components (e.g. current collectors, electrolyte and packaging) should be considered, as well[176]. For commercial carbon-based supercapacitors, the carbon-based electrode accounts for approximately 1/3 of the total device weight. Consequently, active material-

based values need to be reduced by a factor of 3 to get the energy and power density of the device (*device-level performance*) from the performance of the electrode (*material-level performance*)[135].

4.6.5 Morphological and structural characterization

The morphology of the electrodes was examined using scanning electron microscopy (SEM, JEOL JSM7600F) at an acceleration voltage of 5 kV in backscattered electron (BSE) and secondary electron (SE) imaging modes. Ctn on carbon cannot be easily identified by SEM due to the lack of contrast between Ctn and carbon[55]. Tannins can chemically reduce metallic cations like Ag^+ [177]. Therefore, after drop casting of the Ctn solution on TCP, the sample was immersed in $AgNO_3$ 0.1M (ACS reagent > 99%) for 24 h. Reduced Ag atoms on Ctn provide the required contrast for SEM imaging of Ctn on carbon. For chemical characterization of the electrode surface, we employed energy dispersive X-ray spectroscopy (EDS) using the same SEM equipment described above, with Aztec software (detector x-Max, Oxford, 80 mm^2, 5 kV). We utilized X-ray photoelectron spectroscopy (XPS) (VG ESCALAB 250Xi) for surface chemical analysis of CP and TCP electrodes. The X-ray source was monochromatic Al Kα, and pressure in the analysis chamber was $10^{-8}\ Torr$. Survey scans and high-resolution scans were carried out with 1 eV and 0.1 eV energy steps, respectively. Brunauer-Emmett-Teller (BET) and Barrett-Joyner-Halenda (BJH) techniques were used to determine the surface area, pore size, and pore volume distribution of CP and TCP by N_2 adsorption/desorption measurement (Micromeritics, model TriStar 3000). Samples were degassed at 120 ℃ under vacuum overnight, while analysis was carried out using N_2 as an adsorbate gas at -196 ℃; the volume of the adsorbate gas was determined at standard temperature and pressure (STP, 273 K and atmospheric pressure). We performed contact angle measurements for CP and TCP, according to sessile methods, using a Data Physics contact angle measuring device, with deionized water droplets (2 μL).

4.7 Results and discussion

4.7.1 Morphological characterization of Carbon Paper (CP) and Treated Carbon Paper (TCP)

Initially, we proceeded with the morphological characterization of the carbon surfaces prior to deposition of the redox-active Tannins. SEM images of CP and TCP reveal that the chemical

treatment causes grooves on the carbon surface, potential adsorption sites for grafting of bio-sourced molecules (Figures A1a and A1b in Appendix A).

BET and BJH techniques show that surface area increases from 0.13 m^2g^{-1} to 83.20 m^2g^{-1} and the total pore volume increased by 65% after treatment (Table A1 in Appendix A). The higher surface area available for ion adsorption in TCP compared to CP is expected to bring about an increase in the charge stored in TCP[64, 178]. N_2 adsorption/desorption measurements revealed the co-existence of micropores (pore width, w, < 20 Å) and mesopores ($20 < w < 500$ Å, Figure A2a), in TCP,[179] along with a small number of macropores ($w > 500$ Å , Figure A2b). We note that the average pore width of TCP (about 33 Å) is appropriate to enable hosting of hydrated sodium ions (3.6 Å)[180] and hydrated sulfate ions (3.8 Å)[32, 181]. Micropores provide sites for ion adsorption and charge accumulation[182]. Mesopores act as short pathways or channels for rapid ion diffusion onto the inner surface of the porous electrode and may serve as reservoirs for electrolyte, enabling high-rate capability[52]. Macropores serve as ion-buffering reservoirs and minimize ion diffusion distances to the internal surfaces [183].

Water contact angle measurements show that while CP has a hydrophobic surface with contact angle of 130°, water drops are absorbed rapidly by TCP, indicating hydrophilic behavior (inset Figure A1a, movie A1).

4.7.2 Elemental analysis and surface chemistry characterizations of CP and TCP

EDS mapping of TCP reveals the uniform distribution of O and N heteroatoms on the carbon surface, after chemical treatment (Figure A3). The presence of such heteroatoms is expected to increase charge storage performance of the electrodes in at least two ways: enhanced wettability (electrolyte affinity) of the carbon surface and charge transfer processes involving heteroatoms[32, 76].

CP, TCP and Ctn/TCP were also characterized by XPS to gain insight into the effect of the treatment on the surface chemical composition and bonding. Survey and core level spectra (Figures A4, A5, A6 and Table A2 in Appendix A) show that CP contains carbon (96.5 at.%) and oxygen contamination (3.5 at.%). In contrast, the surface of TCP includes nitrogen (8.9 at.%) and oxygen (15.5 at.%), in addition to carbon. For TCP, the high resolution C1s peak may be deconvoluted into seven components, attributable to graphitic carbon (284.4 eV), sp3 carbon (285.0 eV), C-N (286.1

eV), O=C-N and C=O (287.7 eV) , O-C=O (288.8 eV), RCO_3 (290.1 eV), and a shake-up satellite peak (291.1 eV) (Figure A5)[70]. The high resolution N1s XPS peak for TCP can be curve-fitted with three components, including pyridine (398.8 eV), lactam (399.9 eV), and quaternary N and/or N substituting carbon and/or protonated pyridine (401.6 eV) (Figure A5)[184]. The O1s peak can be deconvoluted into seven components, including O=C-N (530.9 eV), O=C (531.0 eV), O-C=O* (531.5 eV), O-(C=O*)-O (531.8 eV), O*-C=O (532.9 eV), O*-(C=O)-O* (534.0 eV) and a shake-up satellite at 536.7 eV (stars indicate the position of the associated bonding)[100].

4.7.3 Catechin-loaded treated carbon paper (Ctn/TCP)

After the morphological characterization of CP and TCP, we considered Catechin (Ctn) on TCP. To observe the presence of Ctn on TCP, the Catechin moieties were stained with a silver nitrate solution. SEM images of TCP and stained Ctn/TCP electrodes show the open networked structure of the carbon fibers making up the TCP (Figure 4.3a) and the homogeneous distribution of Ctn on TCP (Figures 4.3b and 4.3c).

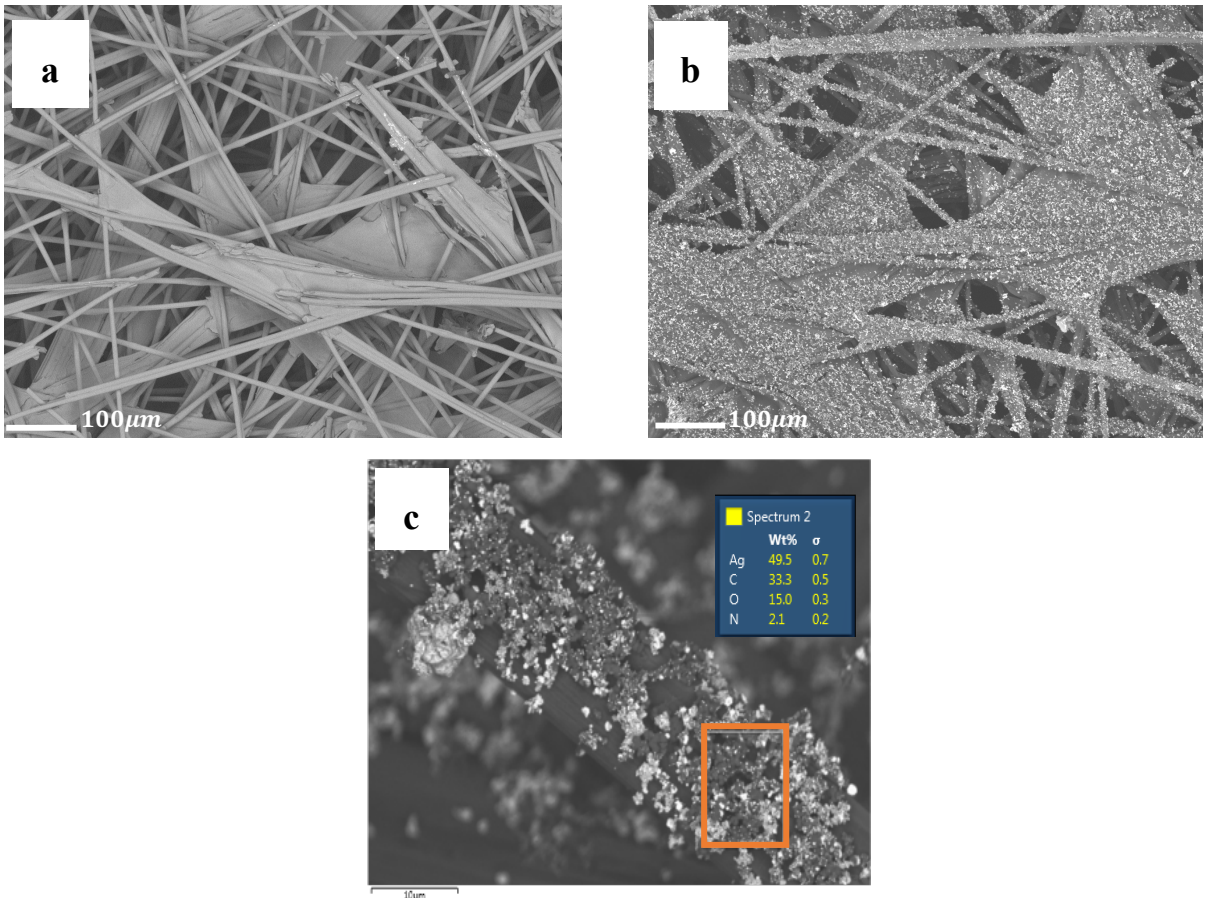

Figure 4.3 SEM images of a) Treated Carbon Paper (TCP); b) and c) stained (with silver nitrate, $AgNO_3$) Catechin-loaded TCP, at 5 kV.

The presence of (stained) Ctn is observable as bright spots of metallic silver obtained from the chemical reduction of silver cations by Ctn (see Experimental). The XPS survey of Ctn/TCP (Table A2 in Appendix A) shows 3.5 at.% N and 20.1 at.% of O, compared to that of TCP (8.9 at.% of N and 15.5 at.% of O. A lower content of N and a higher one of O are expected considering the surface modification with the polyphenolic Ctn molecules[21].

4.7.4 Electrochemical characterization of bare CP and TCP

We performed a series of cyclic voltammetry characterizations using a three-electrode cell configuration and 0.5M $Na_2SO_{4(aq)}$ as the electrolyte. The cyclic voltammograms obtained with CP at a scan rate of 5 mV/s show a smaller area compared to that of TCP bringing about specific capacitances of 0.24 and 103 F/g, respectively (based on the mass of electrode, Figure 4.4a). The increased surface area, suitable porosity, and hydrophilicity of TCP with respect to CP contribute to the enhanced charge storage performance of TCP through the electrostatic capacitive mechanism. In addition, N and O surface functionalities serve as redox-active sites, resulting in the pseudocapacitance contribution of TCP[70, 100].

4.7.5 Electrochemical characterization of Ctn/TCP

The cyclic voltammogram of Ctn/TCP shows a sloped quasi-rectangular shape with a larger area compared to TCP onto which are superimposed oxidation and reduction waves at 0.5 and 0.3 V vs. Ag/AgCl, at 5 mV/s, respectively (Figure 4.4a). The latter can be associated with the redox activity of the quinone/hydroquinone couple of Ctn [21, 55, 70].

The adsorption of quinone moieties on carbon is due to a combination of hydrogen bonding and π-π interactions between the treated carbon surface and the quinone-based molecules [20, 185]. The affinity of Ctn for the carbon surface, among other factors, affects the mass loading of Ctn. It is important to prevent the agglomeration of the Ctn molecules to achieve low charge transfer resistance within the Ctn-based molecular material deposited on TCP [186].

As expected for surface-bound redox species, the peak current for Ctn/TCP rises with the increase of the scan rate[187]. The relatively large peak-to-peak potential separation suggests slow redox kinetics of Ctn/TCP electrode at high scan rates (Figure 4.4b)[51]. The specific capacitance obtained at 5 mV/s is as high as 287 F g^{-1} (based on mass of Ctn) for Ctn/TCP, indicating the beneficial Faradaic contribution of Ctn on the charge storage performance of TCP (Figure 4.4a).

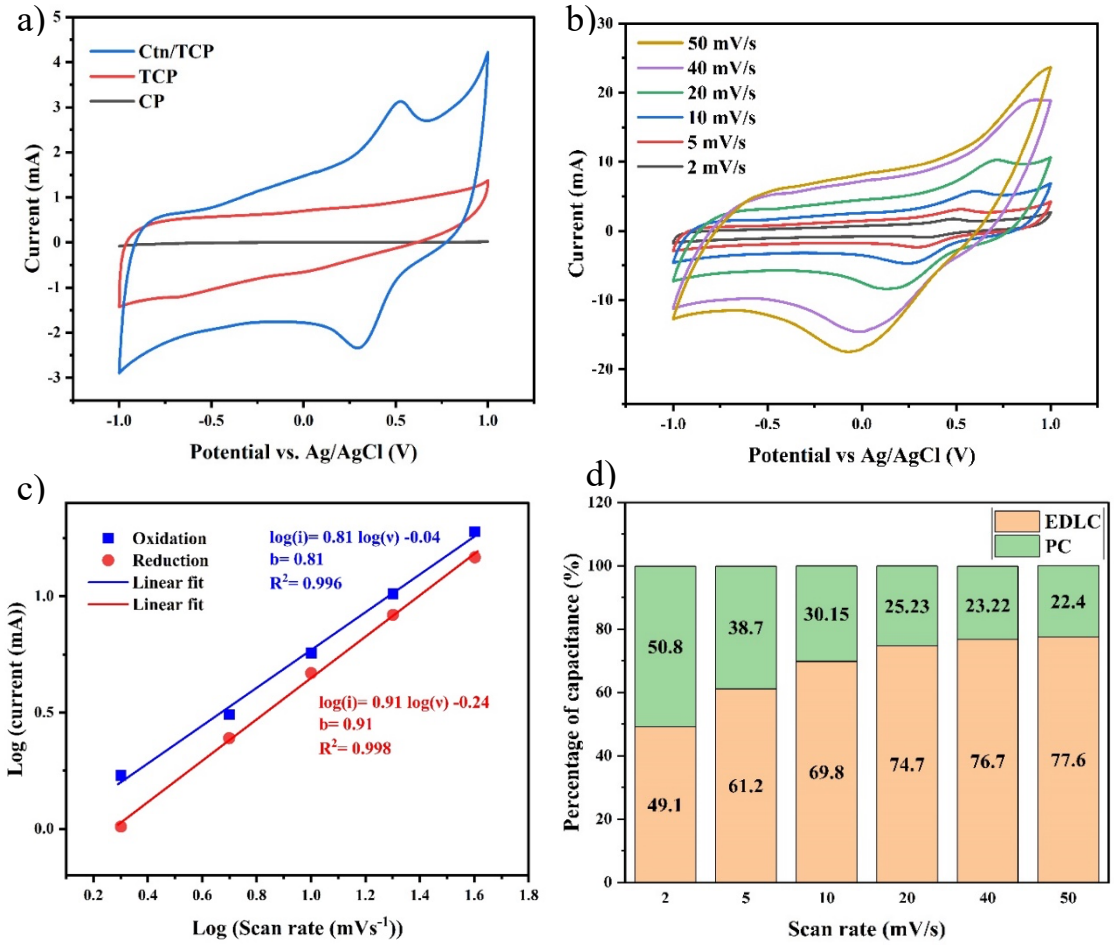

Figure 4.4 a) Cyclic Voltammetry (CV) for Carbon Paper (CP), Treated Carbon Paper (TCP) and Catechin-loaded TCP (Ctn/TCP) in a three-electrode cell set-up, at scan rate 5 mV/s; b) CV of Ctn/TCP at different scan rates; c) Plots of log (current) against log (scan rates in the 0.5M $Na_2SO_{4(aq)}$; d) Percentage of the capacitance contribution evaluated for Ctn/TCP electrodes at different scan rates and based on Trasatti analysis.

To shed light onto the charge transfer processes taking place at the Ctn/TCP electrode, we explored the relationship between the peak current (i) and the scan rate (v) using the power-law equation as in equation (4.3):

$$i = av^b \tag{4.3}$$

where a and b are constants. A value of b close to 1 indicates a surface-controlled processes, whereas a value of b close to 0.5 indicates the presence of diffusion-controlled charge transfer processes[43]. The calculated b values are 0.81 and 0.91, for the cathodic and anodic peaks,

respectively (Figure 4.4c). These results indicate that the behavior is dominated by surface-controlled processes (electrostatic and faradic mechanisms).

To deconvolute faradaic versus non-faradaic contributions to the total charge stored in the Ctn/TCP electrodes, we used the Trasatti method (please see supplementary note 2 in Appendix A and Figure A8)[188]. The results indicate that the pseudocapacitance (PC) contribution (i.e., mainly from Catechin) to the total capacitance is about 50%, at 2 mV/s (Figure 4.4d, the difference being attributable to the electric double layer capacitance (EDLC) from TCP). The pseudocapacitance contribution decreases with scan rate increases and drops to 22% at 50 mV/s likely due to sluggish redox kinetics at the Ctn/TCP electrode.

4.7.6 Electrochemical characterization of Ctn-based symmetric semi-solid-state supercapacitors

Following the electrochemical characterization of the Ctn/TCP electrodes, we proceeded to the fabrication of symmetric semi-solid-state supercapacitors using them. The electrochemical performance of supercapacitors was evaluated in a two-electrode set-up. The cyclic voltammogram of Ctn/TCP-based supercapacitors, at 5 mV/s, exhibits a quasi-rectangular shape with two broad oxidation and reduction peaks attributable to the quinone/hydroquinone redox couple (Figure 4.5a). These redox peaks are not observed for the TCP-electrode device. Figure 4.5b reports the cyclic voltammograms at different scan rates where the broad redox waves are absent at high scan rates, possibly due to the relatively low surface concentration of the Catechin molecules and slow redox kinetics of Ctn/TCP electrode at high scan rates (Figure 4.4d).

The broad anodic peak centered at about 1.0 V for the 2-electrode device (Figure 4.5a) is related to the oxidation peak observed at 0.5 V in the three-electrode configuration. In this case, the potential of the negative electrode would be about – 0.5 V (Figure 4.4a). An additional feature of the cyclic voltammograms of the 2-electrode device is their sloped shape due to resistive effects and the significant increase of the current at the positive voltage limit at high scan rates (Figure 4.5b). This increment is related to those observed at the positive potential of the 3-electrode system (Figure 4.4b). This demonstrates that a slightly lower cell voltage limit (1.5 V) should be set for GCD tests (Figure 4.5c).

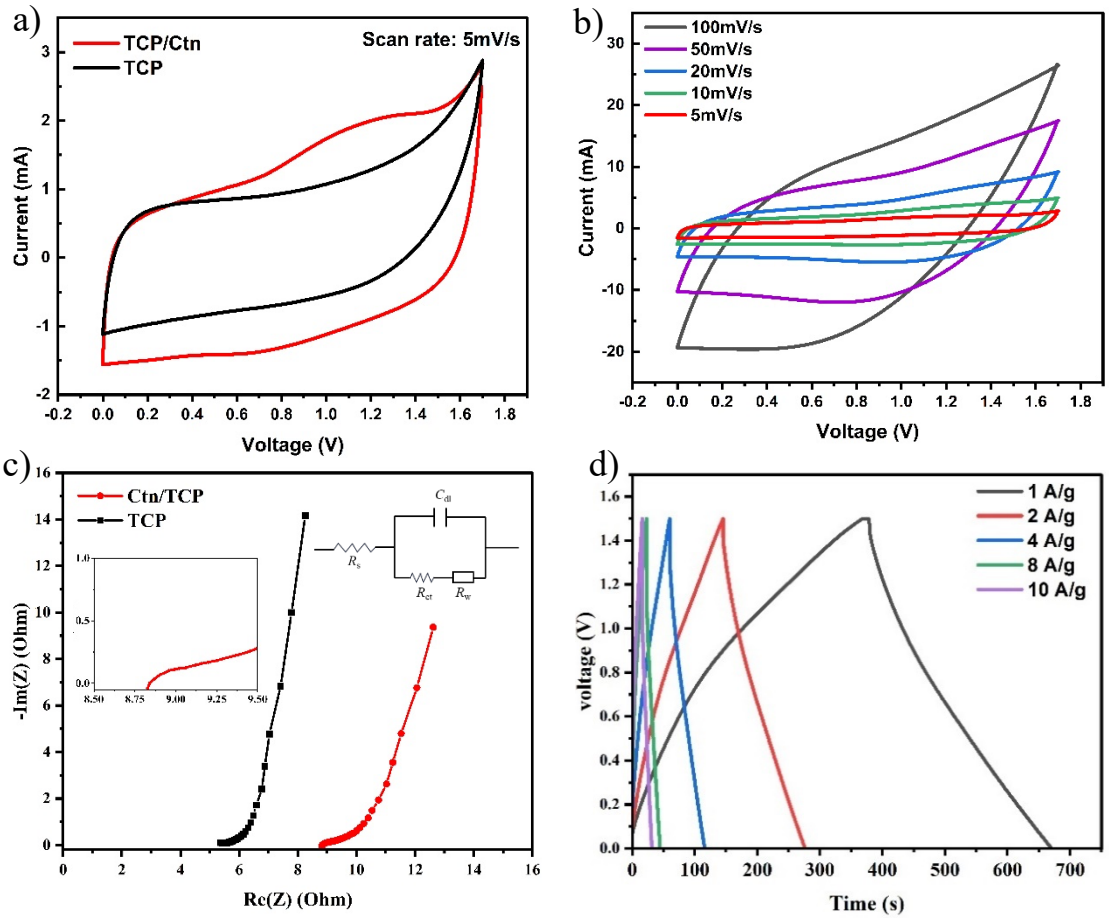

Figure 4.5 Electrochemical characterization of semi-solid-state symmetric supercapacitors: a) Cyclic Voltammograms of Treated Carbon Paper (TCP) and Catechin-loaded TCP (Ctn/TCP) at scan rate 5 mV s^{-1} ; b) Cyclic Voltammograms of Ctn/TCP symmetric supercapacitors at different scan rates; c) Nyquist plot of TCP and Ctn/TCP symmetric supercapacitors in the frequency range 10^5 and 10^{-1} Hz at an applied voltage of 0 V; the insets show an expanded view of the Nyquist plot for high frequency (left hand side) and the equivalent circuit (right hand side); d) Galvanostatic charge/discharge of Ctn/TCP symmetric supercapacitor curves at different current densities.

Ctn/TCP devices employing PVA-Na_2SO_4-based hydrogel as the electrolyte can reach a potential window of 2 V (Figure A10). However, we restricted the operating potential window to 1.7 V to prevent cycling-induced oxidation/reduction processes involving the electrolyte that could compromise long-term stability.

EIS measurements were carried out to investigate charge transfer kinetics at the electrode/electrolyte interface. The Nyquist plot of Ctn/TCP supercapacitors between 10^5 to 10^{-1}

Hz features a semicircle in the high-frequency region attributable to Faradaic processes associated with quinone/hydroquinone couple in Ctn and chemical species including the O and N heteroatoms (Figure A9 and inset of Figure 4.5c). The charge transfer resistance (R_{CT}), estimated from the semicircle diameter of the Ctn/TCP device, is about 0.2 Ω. The Nyquist plot of the TCP devices shows the typical behavior for a capacitive electrode. The steep slope (>75°) of Nyquist plots of TCP and Ctn/TCP in the low-frequency region indicates the capacitive behavior of the devices[189]. The solution resistance (Rs) retrieved from the high-frequency intercept of the Nyquist plots (affected by the electronic resistance of the electrode, bulk electrolyte resistance, and device geometry) for Ctn/TCP is 8.8 Ω. In turn, TCP possesses lower R_s of about 5.2 Ω. Given that the electrolyte and device geometry for Ctn/TCP and TCP are identical, the higher solution resistance of Ctn/TCP device could originate from low electronic conductivity and high contact resistance of Ctn on carbon substrates[55, 103].

GCD curves of Ctn/TCP supercapacitors at different current densities (1, 2, 4, 8, and 10 Ag^{-1}) exhibit a nearly triangular shape with a small ohmic drop (Figures 4.5d and S11). The slight deviation from the linear behavior in GCD charge/discharge profiles comes from pseudocapacitive electrodes, in agreement with the occurrence of redox reactions[55]. Further, the symmetric charge/discharge profiles are in agreement with the symmetric cyclic voltammograms of the devices (Figure 4.5a), both indicating the reversibility of the charge/discharge behavior.

The specific capacitance of Ctn/TCP devices was calculated from the GCD profiles using integration area under the discharge line at different current densities (equation 4.2, Figure 4.6a). The highest specific capacitance is 202 Fg^{-1}, based on the Ctn mass only, and 70 Fg^{-1} , based on the total mass of electrode, observed, at 1 Ag^{-1}. However, the specific capacitance decreases with increasing current density, due to sluggish kinetics of ion diffusion within the hydrogel electrolyte at high current densities (Figure 4.6a)[21, 190].

Energy density and power density are key metrics to evaluate the performance of supercapacitors. The Ragone plot of Ctn/TCP supercapacitors indicates that the device achieved an energy density as high as 55 $Wh\ kg^{-1}$ (about 18 $Wh\ kg^{-1}$, based on the total mass of the electrode) and power density of 660 $W\ kg^{-1}$ (about 220 $W\ kg^{-1}$, based on the total mass of the electrode) evaluated at 1 Ag^{-1}(Figure 4.6b).

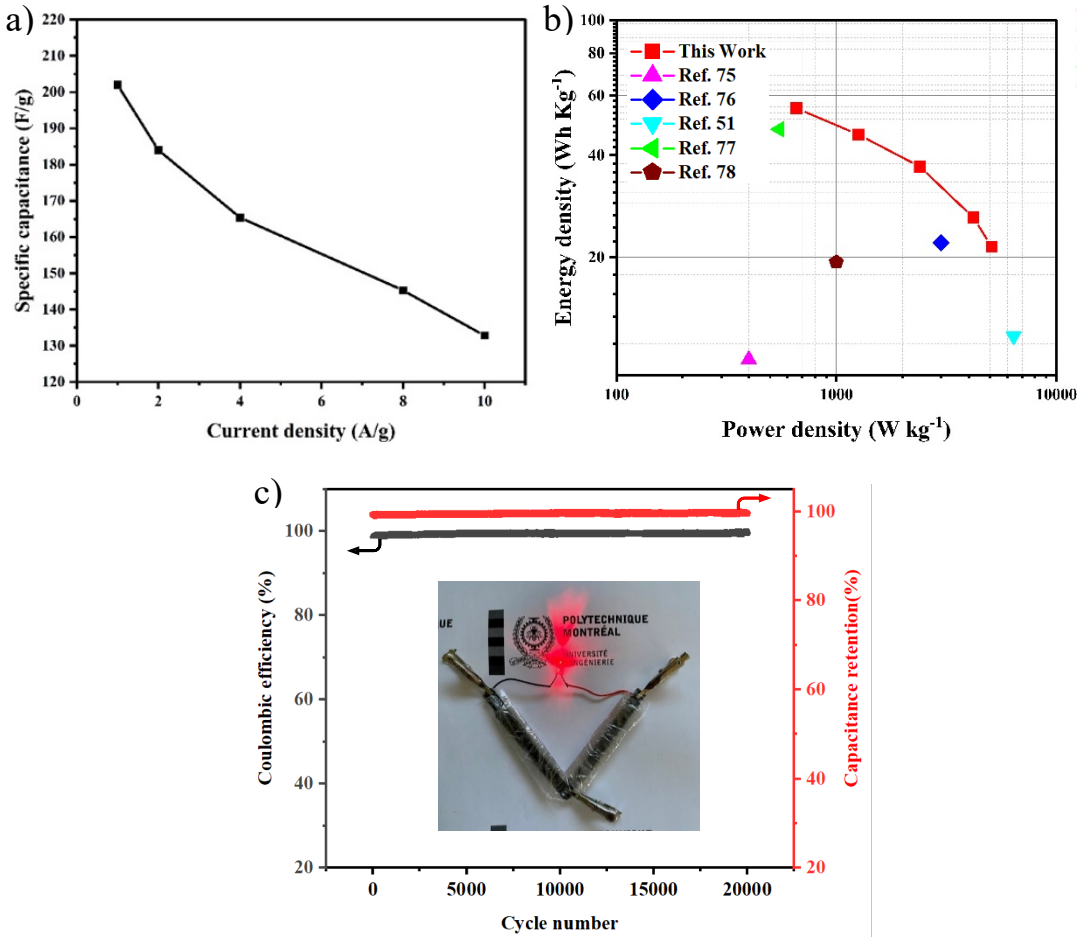

Figure 4.6 Relationship between specific capacitance and corresponding current density evaluated from galvanostatic charge/discharge curves of Catechin-loaded Treated Carbon Paper (Ctn/TCP) symmetric supercapacitors; b) Ragone plots extracted from galvanostatic charge/discharge cycles at different current densities; c) Coulombic efficiency and capacitance retention for 20 000 cycles of galvanostatic charge/discharge at 10 A g^{-1} and the picture of two all-solid-state supercapacitors connected in series lighting up a LED (insets).

As may be concluded from Figure 5.6b and Table A3 in Appendix A, the device described here outperforms both recently reported bio-sourced molecule-based supercapacitors and symmetric solid-state supercapacitors making use of metal oxide redox species[57, 191-194]. All reported energy and power densities in the Ragone plot are based on the mass of the active materials.

We propose the following two mechanisms for charge storage in Ctn-based supercapacitors. At the positive electrode, during charging, the redox-active groups that are in the (semi) reduced form

(semiquinone (SQ), hydroquinone, (H2Q), and O and N-including species) are oxidized, leading to an increase in the density of oxidized species (e.g., quinones). At the same time, protons and sodium cations move towards the gel electrolyte and anions and are incorporated into the electrode material. At the negative electrode, Q, SQ, and oxidized O and N-including species are reduced, anions (sulfate) are released into the hydrogel and cations are incorporated into the electrode material. These processes are reversed during discharging (Figure 4.7).

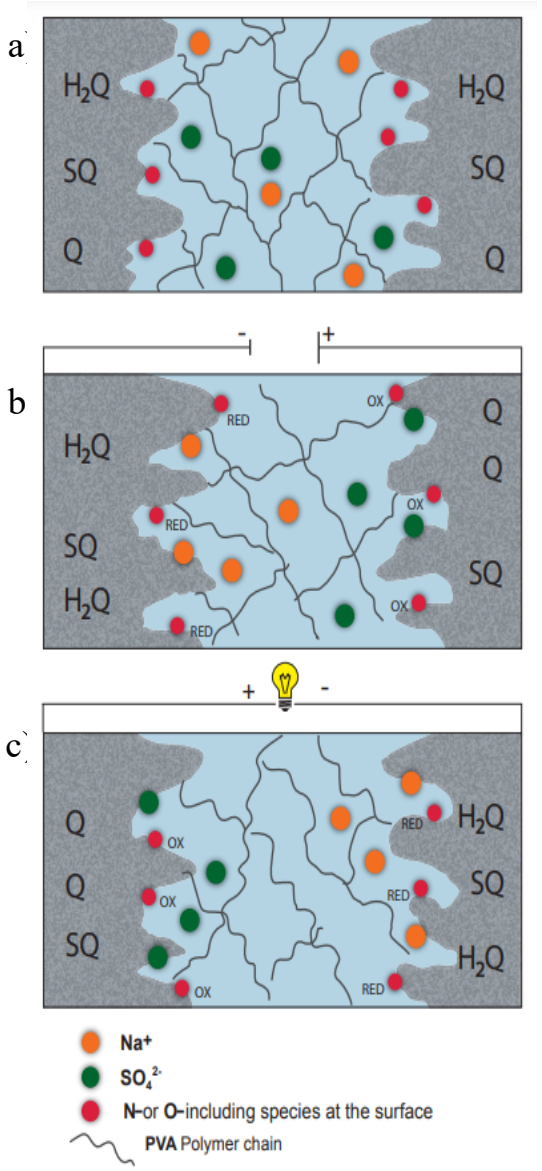

Figure 0.1 Working principle of Catechin based supercapacitors (a) before applying potential; (b) during charging; (c) during discharging.

The second charge storage mechanism that co-occurs is by compensation of the electrode charge by electrolyte ions at the carbon/electrolyte interface. The simultaneous pseudocapacitive and electrostatic mechanisms are responsible for charge storage in Ctn/TCP supercapacitors.

The stability test of the Ctn/TCP semi-solid-state supercapacitors carried out at 10 Ag^{-1} (Figure 4.6c) exhibits a 99.6% capacitance retention and Coulombic efficiency of 99.8% over 20 000 charging/discharging cycles. The cycling stability could be ascribed to the affinity of Ctn for the surface of TCP and to the semi-solid nature of the hydrogel electrolyte that likely limits the loss of Ctn into the electrolyte[64]. Intra-gel diffusion models based on obstruction effects describe how cross-linked polymer chains retain the diffusion of molecules. Solute particles must detour around the gel scaffold or threads, thereby causing an effective increase in path length for the diffusing solute and/or an effective decrease in the coefficient of diffusion[195, 196]. Accordingly, polymer chains would effectively hinder the dissolution of quinone-based molecules into the hydrogel over prolonged cycling, enabling the device to sustain 20 000 cycles with a negligible drop in capacitance retention (0.4%) and Coulombic efficiency (0.2%).

Based on the electrochemical performance of Ctn/TCP semi-solid-state supercapacitors, we connected in series two of them to power a LED bulb (2 V), as an example for their practical application (inset of Figure 4.6c).

4.8 Conclusions and Perspectives

We have demonstrated a semi-solid symmetric supercapacitor making use of Catechin (Ctn) as a redox-active quinone-based Tannin bio-sourced molecule deposited on chemically treated carbon paper by solution-processing from a Ctn aqueous solution. No conductive additives or binder were used to fabricate the electrode material. The high surface area and porous architecture of treated carbon paper promote electrostatic interaction and ion accumulation at the electrode/hydrogel interface, supporting high EDLC contribution. The modification of the carbon surface with redox active chemical species including O and N heteroatoms, followed by the deposition on the surface of Ctn, increase the charge storage properties of the electrodes via Faradaic reactions. Ctn-based semi-solid symmetric supercapacitors reach capacitance values as high as 202 $F\ g^{-1}$ at 1 $A\ g^{-1}$. Devices featured notable energy density (55 $Wh\ kg^{-1}$) and power density (660 $W\ kg^{-1}$). Devices also feature remarkable cycling stability: their capacitance retention and Coulombic efficiency are as high as 99.6% and 99.8%, over 20 000 cycles. The PVA-based hydrogel electrolyte not only

allow to sustain a wide operating electrochemical potential window of the devices but also limits diffusion and leaching of Ctn molecules in the electrolyte enabling, among others, high cycling stability.

Work is in progress to assembly and characterize EESDs based on bio-sourced Catechin extracted from oak bark and printed over large area flexible carbon cloths, and to explore the EESDs' compostability at the end-of-life. With the aim to assess the interest of the Tannin family (beyond Catechin) of molecules for electrochemical energy storage applications, we plan to extend the Catechin studies to other members of the Tannin family, such as pyrogallol and epicatechin gallate.

CHAPTER 5 ARTICLE 2: ULTRASOUND-ASSISTED DEPOSITION OF SEPIA MELANIN AND MULTIWALLED CARBON NANOTUBES ON CARBON CLOTH: TOWARD SUSTAINABLE SURFACE ENGINEERING FOR FLEXIBLE SUPERCAPACITORS

Article 2 was published in "Advanced Sustainable Systems" on July 26, 2024. The supplementary information is provided in Appendix B

5.1 Authors

Molood Hoseinizadeh[1]*, Nila Davari[2], Abdelaziz Gouda[3]*, Hamza Hyat[1], Mohini Sain[3], Daria C.Boffito[2], Clara Santato[1]*

[1]Department of Engineering Physics, Polytechnique Montreal, H3T 1J4, Canada

[2]Department of Chemical Engineering, Polytechnique Montreal, H3T 1J4, Canada

[3]Department of Applied Chemistry and Chemical Engineering, University of Toronto, M5R 0A3, Canada

* Corresponding authors: Molood Hoseinizadeh; Abdelaziz Gouda; Clara Santato

5.2 Graphical abstract

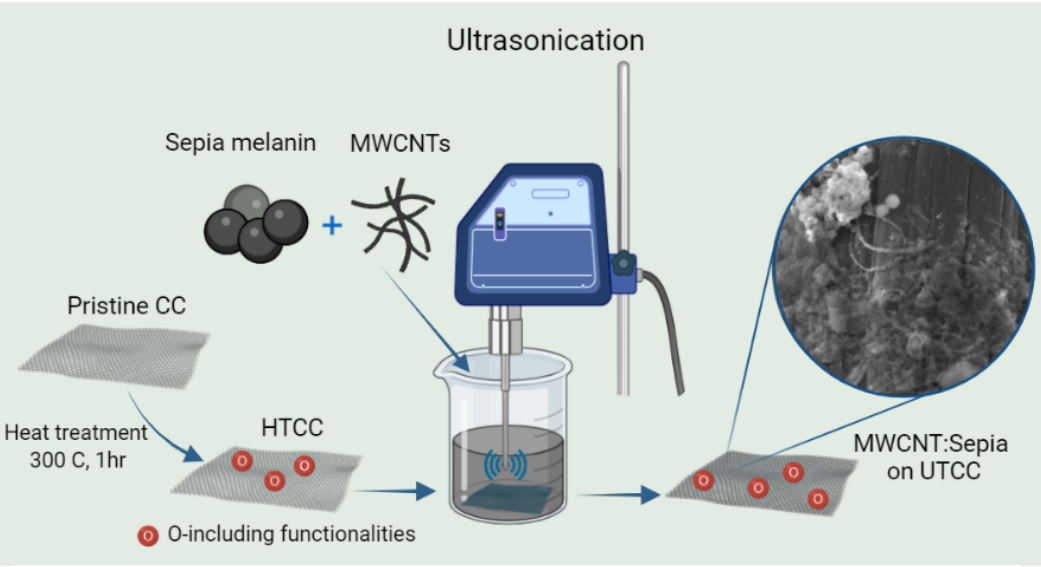

Figure 5.1 Graphical abstract of Article 2

5.3 Keywords

Flexible supercapacitors, Redox-active organic molecules, Sepia melanin, Ultrasonication, Surface engineering, Hydrogel electrolytes

5.4 Abstract

The rising global demand for energy requires, among others, sustainable energy storage devices. Bio-sourced redox-active molecules are interesting for eco-designed electrochemical energy storage as they increase the energy density of the electrodes adding the Faradaic (redox) storage mechanism to the electrostatic one. The engineering of the electrode surface and electrode surface/molecule interface is key to optimizing storage. Here, we report on (i) electrodes prepared by ultrasound-assisted modification of carbon cloth in the presence of Sepia melanin, a quinone macromolecule, and multiwalled carbon nanotubes (MWCNTs) and (ii) their use in flexible symmetric electrochemical capacitors assembled with polyvinyl alcohol (PVA)-based hydrogel electrolyte. Electrodes exhibit an areal capacitance as high as 274 mF cm^{-2}. Corresponding semi-solid-state symmetric supercapacitors feature high energy density of 18 W*h* kg^{-1}, power density up to 221 W kg^{-1} (evaluated at 0.5 Ag^{-1}), outstanding cycling stability (100% capacitance retention and 100% Coulombic efficiency after 10,000 cycles) along with excellent flexibility. Our work contributes to the development of sustainable surface engineering approaches for environmentally benign electrochemical energy storage devices.

5.5 Introduction

The global energy landscape is shifting towards renewable sources, such as solar and wind[147, 197]. However, these energy sources are intermittent, such that it is important to coupling them with energy storage devices, such as electrochemical energy storage devices (EESDs)[198].

The burgeoning demand for wearable and portable electronics further accelerates the development of flexible EESDs combining charge storage capacity and appropriate mechanical properties[199].

Carbon-based materials are attractive for flexible electrodes. They feature low cost, high surface area, and electrical conductivity[200]. Among carbon-based electrodes are carbon paper[61, 100], porous carbon nanofibers[201], carbon nanotubes[202-204], exfoliated graphite sheets[205], and carbon cloth (CC). Despite their flexibility[206], pristine CC electrodes exploiting the principle of electrical double-layer capacitance (EDLC), suffer from limitations, including low specific surface

area (10 m^2 g^{-1}) and electrolyte wettability, leading to relatively low areal capacitances (0.1 to 5 mF cm^{-2})[207],[208]. Various techniques have been developed to increase the surface area of CC and introduce surface functional groups (e.g., O, N, etc.) including chemical oxidation[57, 209], electrochemical oxidation/exfoliation[81, 210], thermal activation[86, 208], plasma modification[85, 211], and strain modulation[212].

Shen et al.[213] fabricated wearable supercapacitors by a two-step chemical (20 M KOH) and thermal (800℃, 30 min in N_2 atmosphere) activation process of CC, and observed an areal capacitance of 300 mF cm^{-2}, corresponding to an energy density of 42 μWh cm^{-2}. Wang et al.[214] employed combined thermal (400 ℃, 12 h in air) and electrochemical activation (2 V, 1 M $Na_2SO_{4(aq)}$) processes to obtain a capacitive performance of 1548 mF cm^{-2}.

Despite the improved technical performance, the environmental impact of those modifications is often overlooked. Further, CC modifications often involve conductive additives, requiring the use of toxic reagents and solvents[209, 215, 216]. Hence, there is a need to develop sustainable surface engineering approaches for CC, while simultaneously ensuring its high capacitive performance.

Ultrasound-assisted Liquid Phase Exfoliation (ULPE) in water can be a *quasi* waste-free surface engineering approach. ULPE has been employed for the scalable production of graphene and other 2D large-size monolayer or multilayer sheets[217, 218] and to increase the surface area of layered-graphitic materials[219]. Ultrasound waves induce cavitation bubbles in liquids, and their implosion generates shear forces weakening van der Waals interactions, thus facilitating the exfoliation[220]. Further, the rapid collapse of cavitation bubbles (generates high temperatures (10,000 K) and high pressures (up to 10,000 atm) at localized spots, promoting water homolysis with the generation of reactive H· and OH· radicals. Using ULPE, we expect to increase the surface area and wettability of the CC, bringing about improved EDLC[144, 221].

To further enhance capacitance while keeping in mind sustainability, electrode surfaces can be modified with abundant and potentially compostable organic materials featuring redox-active groups, such as quinone and amine[21, 50, 55, 70]. Melanins, lignins, Tannins, emodin, juglone, and humic acid are examples of bio-sourced quinone-based molecules whose redox properties have been exploited in pseudocapacitors[66, 100] [16, 222].

Sepia melanin is a quinone-based member of the melanin family of biopigments. It is extracted from the ink sac of cuttlefish[102]. Melanin builds up from 5,6-dihydroxyindole (DHI) and 5,6-

dihydroxyindole carboxylic acid (DHICA) building blocks (monomers)[223], that can be found in different redox states (Figure 5.2). Sepia melanin develops hierarchically from the building blocks to form about 150-200 nm-sized granules[102]. It is notable for its array of distinctive properties, such as redox activity, hydration-dependent electrical response, and thermal and photo-stability [224, 225].

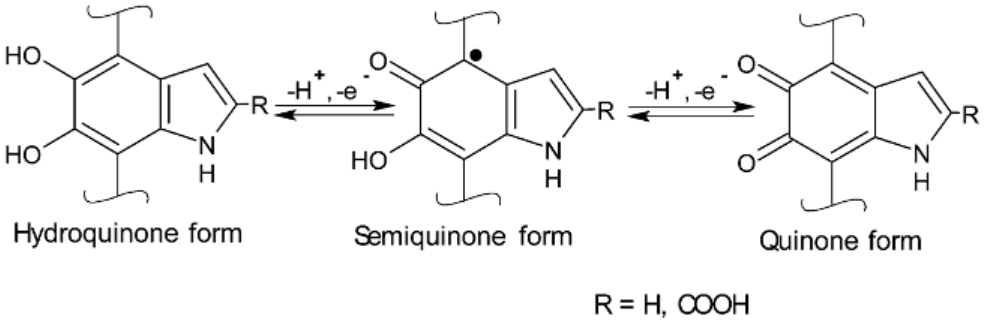

Figure 5.2 5,6-dihydroxyindole (DHI) and 5,6-dihydroxyindole-2-carboxylic acid (DHICA) building blocks of Sepia in their different redox states: hydroquinone (H2Q, reduced redox form), semiquinone (SQ, intermediate redox form), and quinone (Q, oxidized form). R is R is -H in DHI and R is the -COOH in DHICA.

The hydroquinone-quinone redox couple in Sepia melanin (indicated as Sepia from here on) and its ability to reversibly bind multivalent cations, along with its potential biodegradability, motivate its use in eco-designed electrochemical energy storage systems.

Our group studied Sepia-based electrodes for flexible micro supercapacitors[103], light-assisted supercapacitors[109, 226] and electrochemical capacitors operating in aqueous solutions[70, 100]. Sepia processed in dimethyl sulfoxide (DMSO) and deposited on hydrothermally treated carbon paper electrodes, exhibited a capacitance of ca. 452 F g^{-1} in 0.5 M $Na_2SO_{4(aq)}$[100]. Unfortunately, Sepia commonly exhibits high contact resistance at its interface with carbon current collectors, resulting in limited rate response and cycling stability[70, 100], such that the engineering of such interfaces is deemed imperative. For instance, we reported on Sepia combined with nitrogen- and sulfur-doped graphitic carbon quantum dots (N, S GCQDs) deposited on carbon paper electrodes, featuring an areal capacitance as high as 180 mF cm^{-2} in 0.5 M $Na_2SO_{4(aq)}$ [70].

Recently, composite electrode materials made up of (i) high-electronic conductivity carbon nanotubes (CNTs) and (ii) redox-active molecules have been developed for flexible supercapacitors [227-229].

In this work, we present a novel pseudocapacitive electrode material based on a composite from biosourced, redox-active Sepia melanin and conductive MWCNTs, deposited on CC through ULPE in water. The composite Sepia melanin:MWCNTs has been designed to promote (i) the formation of efficient conductive pathways between Sepia granules thanks to the presence of MWCNTs, and (ii) the efficiency of the electronic coupling between the CC and the Sepia melanin granules. The fabrication process of the composite electrode material has been eco-designed in terms of energy-efficiency, chemical waste mitigation and absence of surfactants and organic/inorganic binders. Furthermore, the MWCNTs used in this study are by-products of a photocatalytic process. From the methodological point of view, we initially determined the surface area, pore size, and pore volume distribution of the electrodes. Afterwards, we studied the morphology, structure, and (surface) chemical composition of the electrode materials. Finally, we investigated the electrochemical energy storage performance of the electrode materials and corresponding symmetric supercapacitors.

5.6 Result and discussion

5.6.1 Preparation and characterization of ultrasound-treated carbon cloth

Ultrasound-treated carbon cloth electrodes were obtained through a heat-treatment process followed by ultrasonication in deionized water (DIW). Firstly, a moderate temperature (300 $°C$, 1 h, in air) was selected for the preparation of heat-treated carbon cloth (HTCC). This pre-treatment process is anticipated to introduce minimal O-containing groups into the surface pores of pristine carbon cloth (CC), in turn enhancing the wettability of the electrode, and improving the effectiveness of the ultrasonication process[81]. Afterwards, we used ultrasound-assisted liquid phase exfoliation (ULPE) in DIW as a waste-free surface engineering technique. ULPE serves the double purpose of (i) enhancing the surface area of HTCC and (ii) introducing O-containing functional groups onto the surface HTCC [144].

We studied the effect of the ultrasonication parameters on the areal capacitance of HTCC electrodes. As key parameters, we considered ultrasonication time (1-5 min), temperature (20-60 ℃), and power (40-80 W, supplementary note 1 in Appendix B, Table B1, Figure B1) [218, 230,

231]. The ultrasonication parameters leading to optimized capacitance values were: 60 W for the actual ultrasound power, 40 °C for the temperature, and 5 min for the ultrasonication time. Such ultrasonication conditions led to electrodes indicated from now on as UTCC.

The formation of hydroxyl radicals during the ultrasound treatment in DIW can lead to the introduction of surface oxygen-containing functional groups[221]. To detect hydroxyl radicals, we employed EPR. The EPR spectrum of the water sample (i.e. exposed to 5 min of ultrasonic irradiation with DMPO (5,5-Dimethyl-1-pyrroline N-oxide), power of 60 W, and temperature of 40 °C), exhibits a characteristic four-peak pattern with an intensity ratio of 1:2:2:1, indicative of DMPO-OH radicals[232] (Figure B2). No signal indicative of hydrogen radicals was detected.

SEM images of pristine CC and UTCC show that the interlaced structure of the CC remains intact after heat treatment and subsequent ultrasound treatment (Figure 5.3a and Figure 5.3b). Notably, SEM images of UTCC show the rough surface of the carbon fibers making up the UTCC, suggesting the effect of ultrasounds on carbon fibers possibly through the cavitation[233] (Figure 5.3c and Figure 5.3d). The increased surface roughness on carbon fibers facilitates the grafting of redox-active molecules.

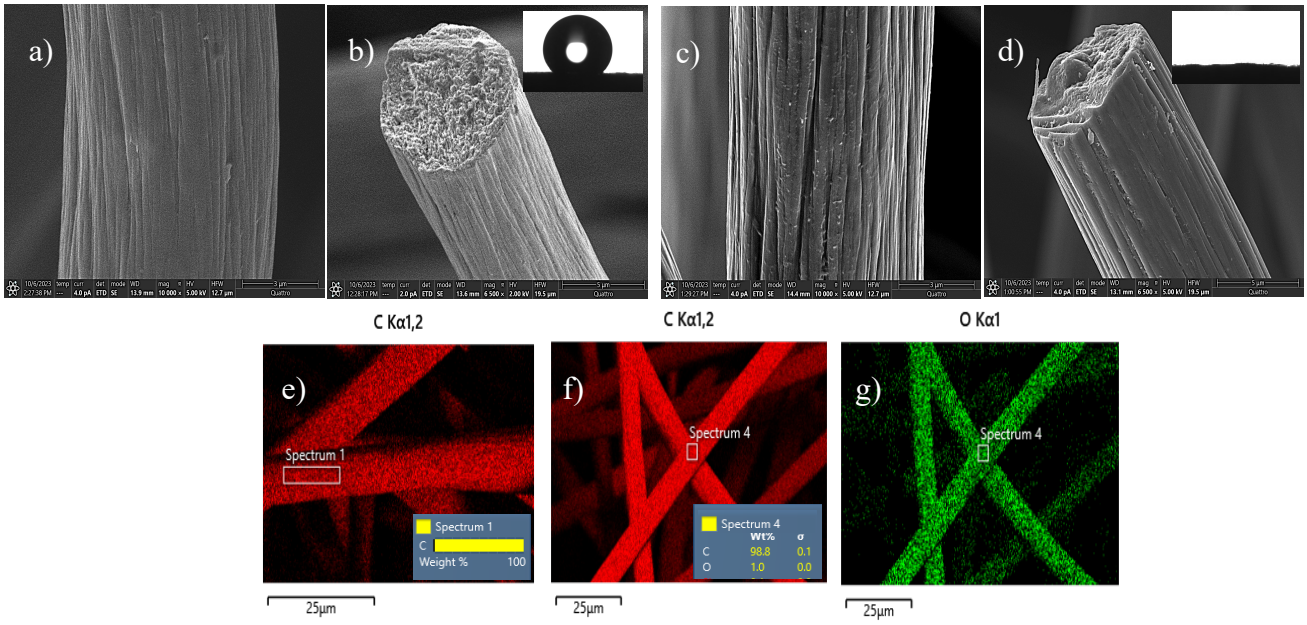

Figure 5.3 SEM images of: a) and b) pristine carbon cloth (CC); c) and d) ultrasound treated carbon cloth (UTCC); e) EDS mapping of C for pristine CC; f) and g) EDS mapping of C and O for UTCC; Inset figure 1b) and 1d): water contact angle measurements for CC and UTCC.

EDS mapping shows a homogeneous distribution of C and O elements on the UTCC electrode. In contrast, the analysis of CC indicates solely the presence of C (Figure 5.3e, Figure 5.3f, and Figure 5.3g).

To study the wettability of pristine CC and UTCC electrodes in aqueous electrolytes, we performed water contact angle measurements. Pristine CC exhibits considerable hydrophobicity, with a water drop contact angle of 135° (inset of Figure 5.3b and Figure 5.3d), whereas the water drop is absorbed rapidly on UTCC, indicating that the ultrasound treatment results in a hydrophilic surface.

The XRD patterns of pristine CC and UTCC electrodes (Figure B3a) display two broad diffraction peaks at about 25.5° and 43°, which can be assigned to the (002) and (101) diffraction planes of graphite (JCPDS card No. 75-1621). The lower intensity of the XRD peaks of the UTCC, compared to that of pristine CC, demonstrates a shorter-range order of graphitic stacking in UTCC[57, 214, 234]. Moreover, the intensity ratios of (002)/(101) for UTCC and pristine CC are 11.3 and 12.9. This illustrates the reduced orientation of the (002) plane in UTCC, attributable to exfoliation induced by ultrasonication[81].

Pristine CC and UTCC electrodes were characterized via Raman spectroscopy to assess the degree of disorder on the surface of the carbon fibers of the CC. Samples show two main bands, located at ~1351 and ~1581 cm^{-1}, attributed to disordered sp^3 hybridized carbon (D band) and graphitic sp^2 hybridized carbon (G band), respectively (Figure B3b) [214]. Generally, the intensity ratio of the D to G bands (I_D/I_G) can help to estimate the structural disorder of the carbon-based materials. The higher I_D/I_G ratio of UTCC, compared to that of pristine CC (1.05 vs. 1.01 respectively), suggests the increase of surface disorder for UTCC[81, 235]. Moreover, the increased intensity of the 2D peak located at 2700 cm^{-1} in UTCC compared to pristine CC, further suggest the increase of surface disorder[236].

The surface area and pore-size distribution of pristine CC and UTCC were measured by BET and BJH methods, (Figure B3c). The results reveal that the surface area increased from 54 to 177 $m^2 g^{-1}$, while the total pore volume increased by 50% going from pristine CC to UTCC.

The adsorption isotherms of the samples exhibit a V-type hysteresis loop, attributed to capillary condensation[237]. UTCC shows the presence of micropores (pore width, w, < 20 Å), mesopores (20 < w < 400 Å), and macropores (w > 500 Å, Figure B3d). The rich porous structure of carbon-based electrodes is expected to enhance the supercapacitive performance, particularly the high-rate

capability. It is worth mentioning that the average pore width of UTCC (about 18 Å) is well-suited for accommodating $Na^{+}_{(aq)}$ (3.6 Å) and $SO_4^{2-}{}_{(aq)}$ (3.8 Å)[180, 181].

Pristine CC, HTCC, and UTCC were characterized by XPS to investigate the effect of heat treatment and ultrasonication on surface chemical composition and bonding (Figure B4, Figure B5, Figure B6, Figure B7, and Table B2 in Appendix B).

The XPS survey spectra indicate the presence of C1s and O1s (Figure B4). It is worth mentioning that the O content in UTCC (9.6 at.%) is higher than that of CC (2.4 at.%) and HTCC (5.9 at.%, Table B2). For UTCC, in the high-resolution spectrum of C1s, we observe five different characteristic peaks, attributable to graphitic carbon (284.6 eV), sp^3 carbon (285.0 eV), C-O and/or C-O-C (286.2 eV), O–C=O (288.4 eV), and a shake-up satellite peak (291.1 eV) (Figure B7a). The O1s peak in the high-resolution spectrum for UTCC can be curve-fitted with three components, including C=O (531.4 eV), C-O and/or C-O-C (532.5 eV), and O*-C=O (533.4 eV) (Figure B7b).

XPS results confirm the successful in situ O-functionalization of the surface of UTCC, likely due to the formation of OH· radicals during ultrasonication [144, 221]

5.6.2 Electrochemical characterization of UTCC

To study the electrochemical performance of UTCC electrodes, we conducted cyclic voltammetry (CV), galvanostatic charge-discharge (GCD), and electrochemical impedance spectroscopy (EIS) characterizations using a three-electrode cell configuration in 1M $Na_2SO_{4(aq)}$ as the electrolyte.

The cyclic voltammograms of UTCC obtained at a scan rate of 10 mV s^{-1} (Figure 5.4a), exhibit a pseudo-rectangular shape from −0.2 to 0.8 V, bringing about an areal capacitance of 147 $mF\ cm^{-2}$, which is 73 times higher than that of pristine CC (2 $mF\ cm^{-2}$). In contrast to CC and HTCC, UTCC electrode exhibits increased area in CV curves and maintains similar shape characteristics (for scan rates of 2 to 100 mV s^{-1}, Figure 5.4b). At 100 mV s^{-1}, the areal capacitance of UTCC decreases to 132 mF cm^{-2} (Figure 5.4c). These results reveal the improved charge storage performance and a notable rate capability of the UTCC electrode after undergoing the surface treatment process. This enhanced performance can be attributed to the increased surface area, suitable porosity, and hydrophilicity of UTCC in comparison to CC and HTCC, contributing to the electrostatic capacitive mechanism of UTCC. Furthermore, O-including functionalities introduce faradaic processes on the UTCC surface, adding a pseudocapacitive contribution.

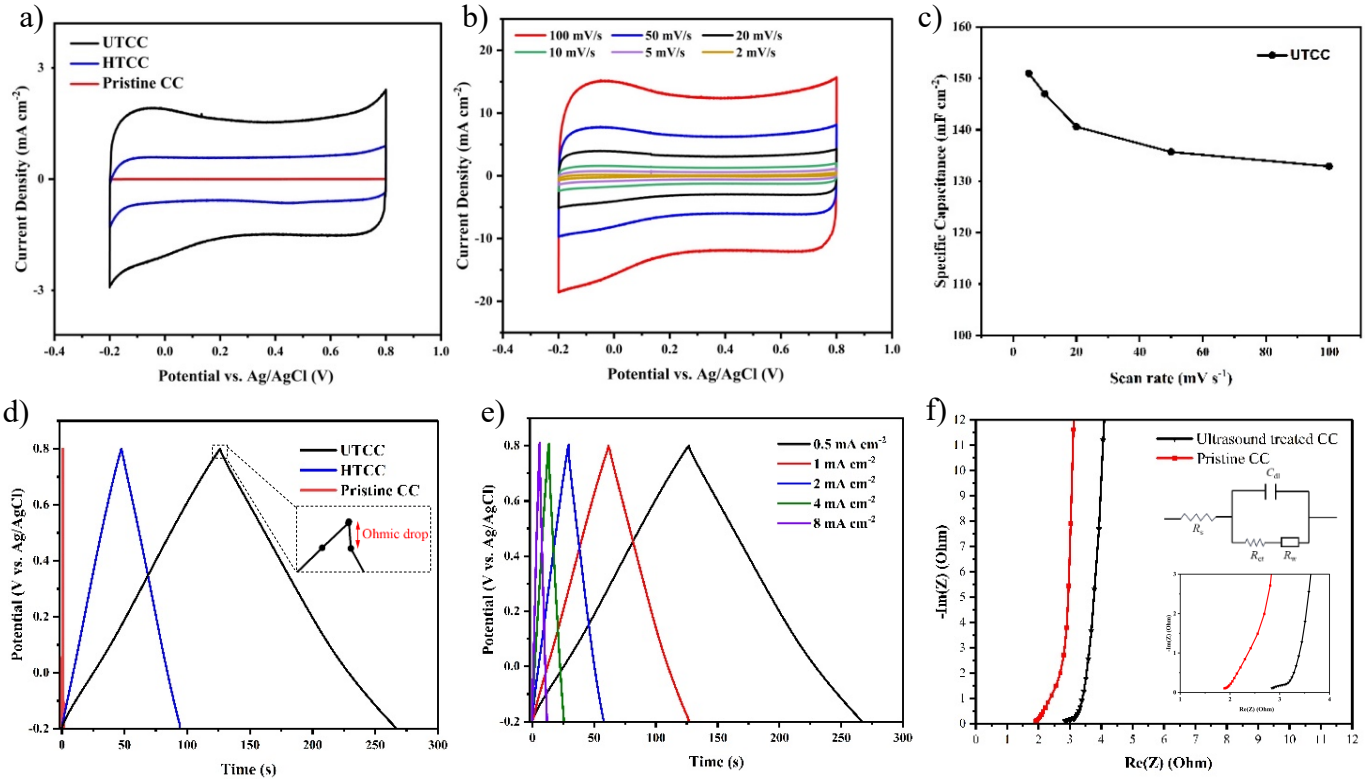

Figure 5.4 Cyclic voltammetry in three-electrode cell set-up at 10 mV s^{-1} ; b) Cyclic voltammetry at different scan rates of ultrasound treated carbon cloth (UTCC); c) Areal capacitance at different scan rates for UTCC, obtained from cyclic voltammetry; d) Galvanostatic charge/discharge curves at 0.5 mA cm^{-2}; e) Galvanostatic charge/discharge curves of UTCC at different current densities; f) Nyquist plot in the frequency range of 10^5 and 10^{-1} Hz; the inset shows an expanded view of the Nyquist plot for high frequency in 1 M $Na_2SO_{4(aq)}$, and the equivalent circuit.

We conducted GCD measurements at various current densities ranging from 0.5 to 8 mA cm^{-2}, with the cut-off potential of 1 V, to evaluate the capacitive performance of UTCC (Figure 5.4d and Figure 5.4e). The GCD curve of UTCC electrode exhibits a symmetric triangular shape with a small ohmic drop across all current regimes and a much longer discharge time (141 s) than that of the pristine CC (2 s) and HTCC (47 s) electrodes.

The slight deviation from the linear behavior in the GCD charge/discharge profile of UTCC, confirms the occurrence of redox reactions during the charging/discharging process, attributable to O-containing functional groups.

EIS measurements were carried out between 10^5 and 10^{-1} Hz to investigate charge transfer kinetics at the electrode/electrolyte interface. The UTCC electrode exhibits a low charge transfer resistance

(R_{ct}) of 0.4 Ω (Figure 2f), as determined from the diameter of the semicircle in the high-frequency range. R_{ct} originates from the occurrence of faradaic processes involving various chemical species, including oxygen, on the surface of UTCC. Notably, this semicircle is absent in the pristine CC electrode, indicating its exclusive electrostatic behavior.

The appearance of a nearly vertical line in the low-frequency region of UTCC suggests its ideal capacitive behavior. Furthermore, UTCC exhibits a slightly higher electrolyte resistance (R_e) compared to CC electrode (2.8 Ω vs. 1.8 Ω, determined from the high-frequency intercept of the Nyquist plots with the real axis) indicating that the surface treatment process has led to an increase in the electronic resistance of the electrode at least in two way: (i) the introduction of oxygen functionalities on the surface and (ii) augmentation in surface disorder levels of carbon fibers [83, 207, 238].

5.6.3 Preparation and characterization of UTCC/MWCNT:Sepia

For the preparation of MWCNT:Sepia mixtures, Sepia and MWCNT powders were mixed in various mass ratios (3:7, 1:1, and 7:3). Subsequently, the resulting mixture powders were directly added to the DIW in the ultrasonic reactor and the ultrasonication process was completed under optimized conditions (Experimental section and Supplementary note 1 in Appendix B). It is worth mentioning that neither surfactant nor organic/inorganic binder is involved in the process.

We proceeded with the morphological characterization of the novel electrode material. TEM images of MWCNT:Sepia mixture powder, obtained after ultrasonication, show dense spherical Sepia granules surrounded by an interconnected network of MWCNTs (Figure 5.5a and Figure 5.5b). Elemental mapping (Figure 5.5c) confirms the co-existence of carbon, oxygen, and nitrogen as primary constituents. The bundled structure of hollow MWCNTs exhibits an interlayer spacing that ranges from 3.33 to 6.00 Å (Figure 5.5d).

SEM images of MWCNT:Sepia on UTCC electrode reveal continuity at the interface between MWCNT/Sepia aggregates and UTCC current collector (Figure 5.5e and Figure 5.5f).

We conducted XPS experiments on MWCNT:Sepia mixture powder to gain insight into the surface elemental composition after the ultrasonication process. XPS survey spectra of MWCNT:Sepia mixture confirm the presence of carbon (C 1s), oxygen (O 1s), and nitrogen (N 1s) assigned to MWCNT and Sepia (Figure B8).

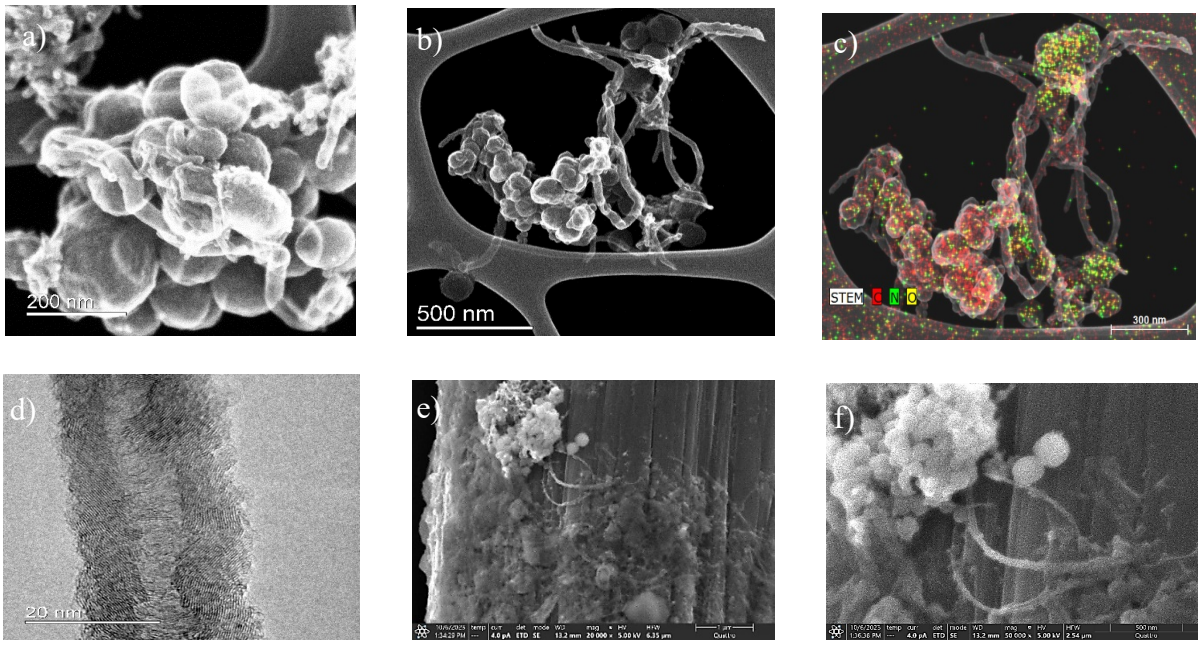

Figure 5.5 a) and b) TEM images on Cu grid of MWCNT:Sepia dispersion ; c) EDS mapping of C, N and O for MWCNT:Sepia dispersion; d) HRTEM image of the MWCNTs; e) and f) SEM images of MWCNT:Sepia on UTCC.

5.6.4 Electrochemical characterization of UTCC/MWCNT:Sepia

We employed a three-electrode cell setup to study the capacitive performance of UTCC/MWCNT:Sepia with respect to UTCC/Sepia and UTCC electrodes, using CV, GCD and EIS measurements in 1M $Na_2SO_{4(aq)}$. The voltammograms of Sepia and MWCNT:Sepia (3:7) on UTCC (Figure 5.6a), show a quasi-rectangular shape with a larger enclosed area with respect to UTCC. Superimposed on these, are two broad oxidation and reduction peaks at about 0.1 V and 0.04 V vs. Ag/AgCl, respectively, at scan rate of 10 mV s^{-1} attributable to the redox activity of quinone/hydroquinone couple in Sepia [70, 100].

Voltammograms of MWCNT:Sepia on UTCC at different scan rates ranging from 2 to 100 mV s^{-1} (Figure 5.6b), exhibit pseudocapacitive behavior with relatively negligible peak-to-peak potential separation. The latter can be associated with fast charge transport within electrodes thanks to the efficient electronic coupling at the interface of Sepia/MWCNT and UTCC current collector[229].

The areal capacitance obtained at 10 mV s^{-1} is as high as 274 $mF\ cm^{-2}$ and 183 $mF\ cm^{-2}$ for MWCNT:Sepia (3:7) and Sepia on UTCC respectively, indicating the beneficial faradaic and

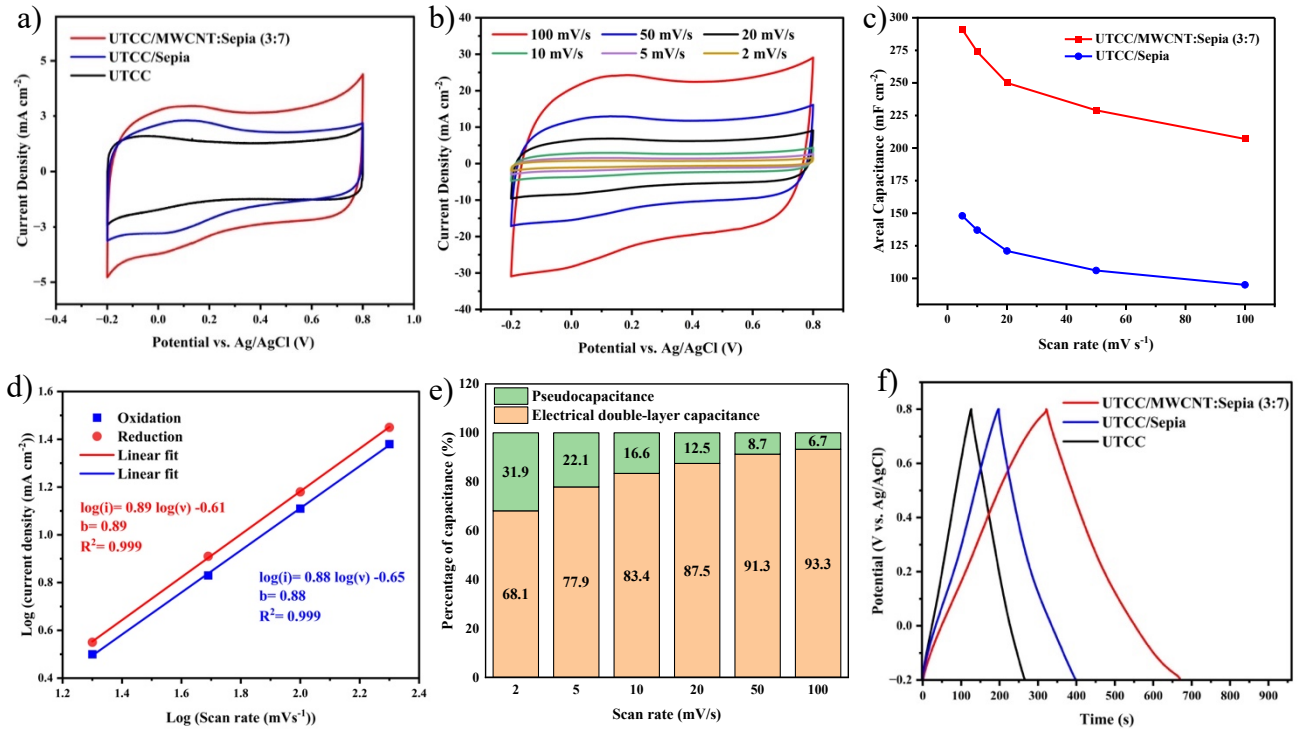

Figure 5.6 Cyclic voltammetry in three-electrode cell set-up at 10 mV s−1 ; b) Cyclic voltammetry at different scan rates MWCNT:Sepia(3:7) ; c) Areal capacitance vs. scan rate obtained from cyclic voltammetry; (d) Plots of log (current) against log (scan rate) for for MWCNT:Sepia on UTCC electrodes at different scan rates; e)Percentage of the capacitance contribution evaluated for MWCNT:Sepia on UTCC electrodes at different scan rates and based on Trasatti analysis; f) Galvanostatic charge/discharge curves at 0.5 mA cm^{-2} in 1 M $Na_2SO_{4(aq)}$.

electrostatic contributions of the novel electrode material on the charge storage performance of UTCC.

The areal capacitance decreases with increasing scan rate for both MWCNT:Sepia (3:7) and Sepia on UTCC. This is attributable to ion diffusion-limited transport at higher scan rates (Figure 5.6c). When the scan rate is increased from 5 to 100 mA cm^{-2}, a decrease in areal capacitance of 28% for MWCNT:Sepia (3:7) and 35% for Sepia on UTCC is observed which underscores the positive impact of MWCNT incorporation on the rate capability of the electrode.

The presence of spherical Sepia granules could potentially hinder ion diffusion to the UTCC surface[100]. This limitation is likely mitigated by the presence of MWCNTs owing to their high surface area, providing accessible sites for ion diffusion at high scan rates.

From the comparison of the areal capacitance of UTCC/MWCNT:Sepia in various mass ratios (3:7, 1:1, 7:3), at scan rate of $10\ mV\ s^{-1}$ (Table B3), we deduce that the optimum electrochemical performance is obtained with UTCC/MWCNT:Sepia (3:7) electrode.

To elucidate the charge transfer processes occurring at the UTCC/MWCNT:Sepia (3:7) electrodes, we explored the possible dependence of the current (i) on the sweep rate (v), using the equation $i = av^b$, where a and b are constants[43]. When the b value approaches 1, it indicates a surface-controlled process, while a value close to 0.5 is typical of a diffusion-controlled process. The calculated b values of 0.91 and 0.88 for the cathodic and anodic peaks, respectively (Figure 5.6d), indicate the dominance of surface-controlled processes, involving both electrostatic and faradaic mechanisms.

We utilized the Trasatti method to deconvolute faradaic and non-faradaic processes contributing to the total charge stored by the electrodes (Supplementary note 2 in Appendix B, Figure B9). The results indicate that the pseudocapacitance contribution (i.e. mainly from Sepia) to the total capacitance is 31.9%, at $2\ mV\ s^{-1}$ (Figure 5.6e). As expected for surface-bound redox species like Sepia, the pseudocapacitance contribution decreases with increasing scan rate, down to 6.7% at $100\ mV\ s^{-1}$. This is attributable to sluggish redox kinetics at the UTCC/MWCNT:Sepia electrode.

The GCD profile of the UTCC/MWCNT:Sepia electrode exhibits a symmetric triangular shape, featuring a very low internal resistance ohmic drop (i.e. 10 mV at 0.5 mA cm^{-2}) and a long discharge time compared to the UTCC/Sepia and UCC electrodes (Figure 5.6f). This enhanced performance can be attributed to the incorporation of MWCNTs, which facilitates rapid electronic and ionic transport within the electrode material, improving its overall charge storage performance.

The gentle slope observed in the GCD profiles of both MWCNT:Sepia and Sepia on UTCC is indicative of faradaic processes occurring at the electrodes, which aligns with the CV results.

All the GCD curves of the UTCC/MWCNT:Sepia (3:7), consistently exhibiting symmetric triangular shapes across a range of current densities from 0.5 to 10 mA cm^{-2}, indicate good reversibility during the charge/discharge process (Figure B10a).

EIS is used to evaluate charge transfer kinetics in MWCNT:Sepia and Sepia electrode materials. The Nyquist plots of both electrodes feature a semicircle (high-frequency region) due to faradaic processes associated with the quinone/hydroquinone redox couple (Figure B10b). MWCNT:Sepia

shows small charge transfer resistance (R_{ct}) of 0.2 Ω and low electrolyte resistance (R_S) of 2.4 Ω compared to that of Sepia and UTCC electrodes.

These results demonstrate that the introduction of MWCNTs into the electrode material serves two key functions: (i) facilitating electron transfer processes, and (ii) enhancing ion diffusion due to their high surface area. This dual impact significantly improves the electrode's charge storage.

5.6.5 MWCNT:Sepia symmetric semi-solid-state supercapacitors

Following the electrochemical characterization of the MWCNT:Sepia (3:7) on UTCC electrodes, we proceeded to the fabrication of symmetric semi-solid-state supercapacitors using these novel electrode materials and PVA-Na_2SO_4-based hydrogel electrolyte. The electrochemical performance of supercapacitors was evaluated in a two-electrode set-up. The cyclic voltammogram of MWCNT:Sepia-based supercapacitors, at 10 $mV\ s^{-1}$, exhibits a quasi-rectangular shape with higher voltammetric currents compared to UTCC supercapacitors attributable to the incorporation of MWCNT:Sepia into the electrode (Figure 5.7a).

Furthermore, the CV curves of the MWCNT:Sepia-based supercapacitors, obtained at various sweep rates (5 to 100 mV/s), maintain their quasi-rectangular shape even at high scan rates demonstrating good rate capability and fast charge-discharge kinetics of devices (Figure 5.7b).

GCD curves of MWCNT:Sepia-based supercapacitors at different current densities (0.5, 1, 2, 4, 8 $A\ g^{-1}$) exhibit a nearly triangular shape with a small ohmic drop of 20 mV at 0.5 $A\ g^{-1}$, corresponding to a low equivalent series resistance (ca. 2.5 Ω) (Figure 5.7c).

The specific capacitance of MWCNT:Sepia devices was calculated from the GCD profiles using the integration area under the discharge line at different current densities (Figure 5.7d). The highest specific capacitance is 118 F g^{-1}, based on the MWCNTs and Sepia mass only (45 F g^{-1}, based on the total mass of the electrodes, i.e. MWCNTs, Sepia, and UTCC) was observed at 0.5 A g^{-1}. With the increase in current density, a significant reduction in specific capacitance was observed, suggesting that the ion diffusion kinetics within the hydrogel are likely hindered at higher densities[61, 190].

Energy density and power density serve as critical parameters for assessing the performance of supercapacitors. MWCNT:Sepia (3:7) devices indicate an energy density as high as 18 W*h* kg^{-1} (ca. 7 W*h* kg^{-1}, based on the total mass of the electrodes) and power density of

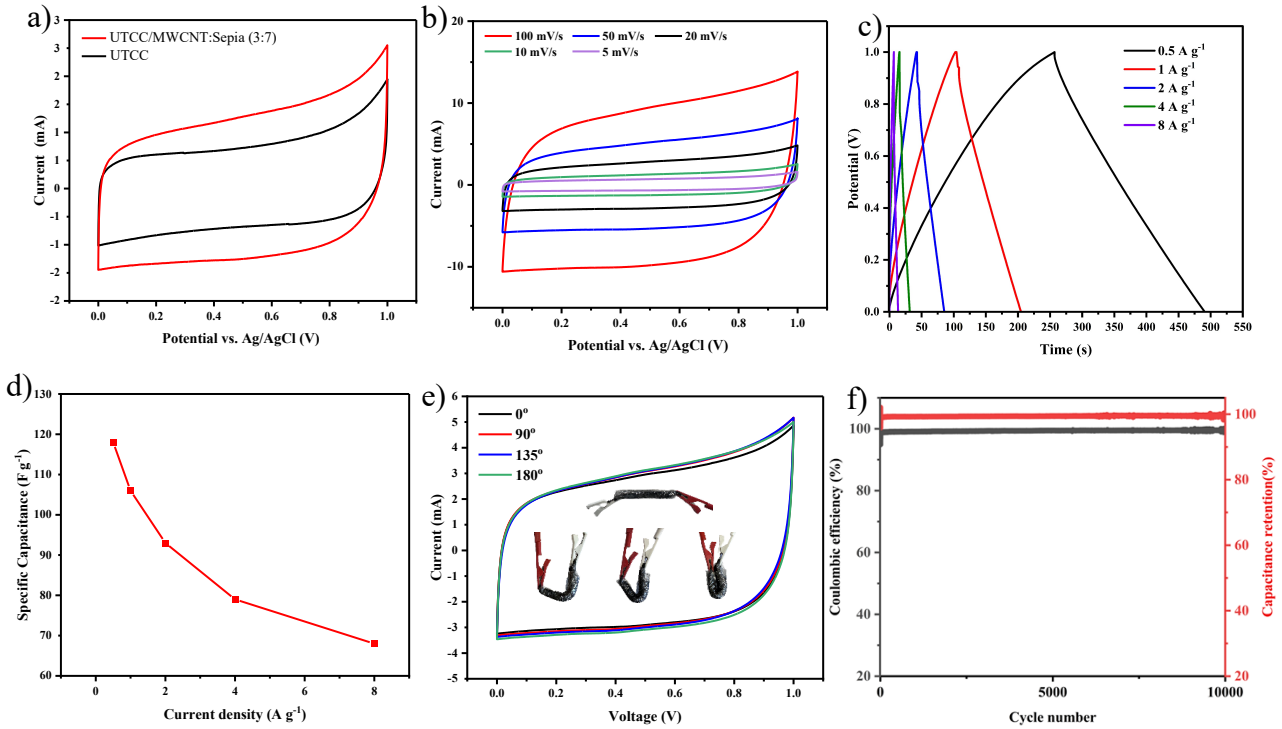

Figure 5.7 Electrochemical characterization of semi-solid-state symmetric supercapacitors: a) cyclic voltammograms at 10 mV s^{-1} ; b) Cyclic voltammograms of MWCNT:Sepia symmetric supercapacitors at different scan rates; c) Galvanostatic charge/discharge (GCD) curves for MWCNT:Sepia supercapacitors ; d) Specific capacitance for MWCNT:Sepia supercapacitors, obtained from GCD; e) cyclic voltammograms at 20 $mV\ s^{-1}$ of MWCNT:Sepia symmetric supercapacitors at different bending angles from 0° to 180°; f) Coulombic efficiency and capacitance retention for 10,000 cycles of galvanostatic charge/discharge of MWCNT:Sepia symmetric supercapacitors at 8 A g^{-1}.

18 W*h* kg^{-1} (ca. 7 W*h* kg^{-1}, based on the total mass of the electrodes) and power density of 221 W kg^{-1} (ca. 85 W kg^{-1}, based on the total mass of the electrodes) evaluated at 0.5 Ag^{-1}.

The mechanical deformation of the as-fabricated device was assessed under various bending conditions. The cyclic voltammogram curves of the device at 20 $mV\ s^{-1}$ showed negligible changes at different bending angles, ranging from 90° to 180°, demonstrating the device's robustness and mechanical flexibility (Figure 5.7e). This consistent performance under mechanical bending can be attributed to the effective immobilization of MWCNT and Sepia on the flexible UTCC substrate.

The stability test of the MWCNT:Sepia (3:7) devices carried out at 8 $A\ g^{-1}$ demonstrates 100% capacitance retention and 100% Coulombic efficiency after 10,000 galvanostatic

charging/discharging cycles (Figure 5.7f). This remarkable cycling stability is attributed to the semi-solid hydrogel electrolyte, which effectively restricts the dissolution of quinone-based molecules into the hydrogel[61, 239].

5.7 Conclusion

We employed a one-pot ultrasonication process for the modification of carbon cloth (CC) with redox-active Sepia melanin and Multiwalled Carbon Nanotubes (MWCNTs) to prepare electrode materials for sustainable electrochemical energy storage. We did not use any surfactants or binders. The ultrasonication process in water increases the surface area and porosity of the CC surface and induces its redox functionalization by O-including species. The presence of the redox active Sepia combined to conductive MWCNTs enhances the charge storage properties of the electrodes via a faradaic mechanism, in addition to the conventional electrostatic one. MWCNT:Sepia-based semi-solid-state symmetric supercapacitors reach capacitance as high as 118 F g^{-1} at 0.5 Ag^{-1}. Devices deliver a high energy density of 18 Wh kg^{-1}, power density up to 221 W kg^{-1} (evaluated at 0.5 Ag^{-1}) along with remarkable cycling stability (100% capacitance retention and Coulombic efficiency after 10,000 cycles). The supercapacitors also demonstrate consistent performance when subjected to mechanical bending at various angles.

Work is in progress to apply the ultrasonication process in presence of other bio-sourced molecules, such as indigo carmine, to assess the universality of our approach. Beyond selecting sustainable materials and processes, we foresee sustainable device end-of-life scenarios. To this purpose, we test redox-active materials and electrochemical energy storage devices based thereon for their biodegradability in industrial compost conditions.

5.8 Experimental section

5.8.1 Preparation of ultrasound-treated carbon cloth (UTCC)

Carbon cloth (CC, AvCarb G200, electrical resistivity 3 Ω mm and density 0.07 g/cm^3) was purchased from FUELCELL store, Texas, USA. After cleaning in acetone (Honeywell, VLSI, 100%) and ethanol (Commercial Alcohols, Ontario, Canada) in an ultrasonic bath (Eumax-4L) for 10 min at 40 kHz, CC was dried under vacuum for 30 min at 60 °C.

We followed a published heat treatment method for CC, with minor modifications to optimize the process [81, 86]. Typically, CC was heated to 300 °C for 1 h, at 5 °C min^{-1} in air. The resulting

material was labelled as HTCC. Afterward, HTCC underwent ultrasonication with an ultrasonic processor (VibraCell VCX 750, Sonics and Materials) working at a nominal power of 750 W and a fixed frequency of 20 kHz. The titanium alloy (Ti6Al4V) ultrasound probe (D = 19 mm) was equipped with a replaceable tip for a total length of 136 mm. The power dissipation in the system under sonication was determined with a K-type thermocouple in a glass beaker (250 ml) filled with 150 ml of deionized water (DIW). The probe, CC, and thermocouple were immersed (app. 2 cm) into DIW, and the temperature increase was recorded to derive the actual power delivered by ultrasound following the calorimetric method (Figure B11) [240].

We investigated the effects of ultrasound parameters on the areal capacitance of CC ($mF\ cm^{-2}$), calculated using equation (i). Parameters such as ultrasonication time (1, 5, 10 min), temperature (20, 40, 60 $°C$), and actual power (40, 60, 80 W) were considered during the ultrasonication treatment of CC in DIW to maximize the ultrasound-induced physical/chemical processes without compromising the mechanical integrity of CC (Supplementary note 1 in Appendix B and Figure B1)[218, 230, 231]. All the experiments were conducted under continuous ultrasound irradiation and the processing volume was constant at 150 ml of DIW. The active footprint area of CC electrodes was 1 cm^2.

5.8.2 Electron paramagnetic resonance (EPR)

The DIW sample treated by ultrasound waves during ultrasonication of CC was transferred to an electron paramagnetic resonance (EPR, Magnettech ESR5000, Bruker spectrometer) to detect the presence of hydroxyl radicals. 100 mM of radical trap DMPO (5,5-Dimethyl-1-pyrroline N-oxide, Sigma-Aldrich) was added to the sample. The power of the EPR spectrometer was set to 10 mW with a field modulation of 0.1 mT.

5.8.3 Preparation of Sepia and MWCNT:Sepia electrode materials to be deposited on UTCC

Sepia melanin was extracted from the ink sac of the cuttlefish Sepia officinalis (commercially available ink), purified and finely ground into a powder [241]. MWCNT powder was obtained as a by-product in a novel photocatalysis process, which was primarily developed for the production of gaseous hydrogen from methane. Sepia and MWCNT/Sepia electrodes were prepared by mixing Sepia with MWCNTs in different mass ratios of 3:7, 1:1, and 7:3. The mixtures were then dissolved

in 150 ml of DIW to make 1 g L^{-1} suspensions. The suspension was transferred to a 250 ml glass beaker, and CC was dipped (app. 2 cm) into the suspension to undergo the ultrasonication process for 5 min at an input power of 80 % and temperature of 40 ℃. All ultrasound parameters were set based on the optimized conditions described in supplementary note 1 in Appendix B. It is worth mentioning that no surfactants or binders of any kind were added. The samples were labeled as UTCC/Sepia, UTCC/MWCNT:Sepia (3:7), UTCC/MWCNT:Sepia (1:1), and UTCC/MWCNT:Sepia (7:3). Finally, as-prepared electrodes were rinsed gently with DIW and vacuum dried for 30 min at 60 $°C$ before morphological, chemical, and electrochemical characterizations. The mass loading of active material in all electrodes was 4.0 ±0.4 mg cm^{-2} using a microbalance (Sartorius BP 210 D).

5.8.4 Semi-solid-state symmetric supercapacitor fabrication

Polyvinyl alcohol (PVA) was purchased from Sigma-Aldrich (purity > 99% hydrolyzed, molecular weight 89,000–98,000 Da) to prepare a hydrogel, according to[61]. 2 g of PVA were dissolved in 60 mL of deionized water at 90 $°C$ and stirred for 30 min to obtain a homogeneous and transparent solution. Afterwards, 40 mL of 2.5 M Na_2SO_4(aq) (Sigma-Aldrich, purity > 99%) were added to the solution to obtain 100 mL of 1 M $Na_2SO_{4(aq)}$ and form the hydrogel. A thin film (~ 0.5 mm-thick, ionic conductivity of 0.135 $mScm^{-1}$ at 25 $°C$ and neutral pH [242]) of hydrogel was fabricated under a pressure of 700 Pa, then cut into 0.5 cm × 5 cm and sandwiched between the two electrodes of the supercapacitor (ionic conductivity is 0.135 $mScm^{-1}$ at 25 $°C$ and neutral pH).

5.8.5 Morphological and structural characterization

The morphology of MWCNT:Sepia (3:7) powder was studied using Transmission Electron Microscopy (TEM, Hitachi HF-3300) and Scanning Transmission Electron Microscopy (STEM), which was equipped with a Bruker XFlash 6T160 for energy dispersive X-ray spectroscopy (EDS). The microscope operated at an accelerating voltage of 300 kV.

The morphology of pristine CC, UTCC, and MWCNT: Sepia on UTCC were examined using a Quattro Environmental SEM (ESEM, Thermofisher Scientific) at about 10 kV voltage in backscattered mode. Samples were observed in low-vacuum mode (200 Pa). For chemical characterization of the electrode surface, we employed EDS using the same SEM equipment described above, with Aztec software (detector x-Max, Oxford, 80 mm2, 5 kV). We utilized X-ray

photoelectron spectroscopy (XPS) (VG ESCALAB 250Xi) for surface chemical analysis of modified electrodes. The X-ray source was monochromatic Al Kα, and the pressure in the analysis chamber was 10-8 Torr. Survey scans and high-resolution scans were carried out with 1 eV and 0.1 eV energy steps, respectively.

Brunauer-Emmett-Teller (BET) and Barrett-Joyner-Halenda (BJH) techniques were used to determine the surface area, pore size, and pore volume distribution of CC and UTCC by N_2 adsorption/desorption measurement (Micromeritics, model TriStar 3000). Samples were degassed at 120 $°C$ under vacuum overnight, while analysis was carried out using N_2 as an adsorbate gas at -196 $°C$; the volume of the adsorbate gas was determined at standard temperature and pressure (STP, 273 K, and atmospheric pressure).

We performed contact angle measurements for CC and UTCC, according to sessile methods, using a Data Physics contact angle measuring device, with deionized water droplets.

Raman spectra of CC and UTCC were acquired using Raman microscope Senterra (Bruker), equipped with laser excitation at 532 nm. Spectra were recorded in optical geometry 180° in the range of Raman shifts 100-3200 cm^{-1} at an optical resolution of 3-5 cm^{-1}, using a laser excitation power of 20 mW. X-ray diffraction (XRD) spectra of CC and UTCC were taken using a Bruker D8 diffractometer with a wavelength (CuK_α) of 1.54 Å. 1100 nm.

5.8.6 Electrochemical measurements

Electrochemical characteristics were investigated by cyclic voltammetry (CV), galvanostatic charge/discharge (GCD), and electrochemical impedance spectroscopy (EIS), using a biologic potentiostat (SP-300). A three-electrode cell configuration was used for the electrochemical characterization of single electrodes. Pristine CC, HTCC, and UTCC modified with Sepia and MWCNT/Sepia mixture, as working electrodes, platinum (Pt) mesh as the counter electrode, and $Ag/AgCl_{(aq)}$ in 3 M NaCl as the reference electrode in 1 M Na_2SO_4 electrolyte. EIS measurements were conducted in a 3-electrode configuration in the frequency range 10^{-1}-10^5 Hz, with a 10 mV sinusoidal perturbation, at 0 V bias. GCD was performed at current densities of 0.5, 1, 2, 4, and 8 mA cm^{-2} for a voltage scan ranging from -0.2 to 0.8 V versus Ag/AgCl. The electrode areal capacitance (C, $mF\ cm^{-2}$) was calculated at 10 mV s^{-1}, based on the cyclic voltammetry, using

$$C = \int \frac{IdV}{v\ A\ \Delta V} \tag{5.1}$$

where $\int IdV$ is the integral area of the cathodic CV discharge cycle the scan rate ($mV\ s^{-1}$), A the footprint area of the active material on the current collector (cm^2), and ΔV is the potential window (V). Full device specific capacitance (C_{GCD} , $F\ g^{-1}$), energy density (E, $Wh\ kg^{-1}$), power density (P, $W\ kg^{-1}$) were estimated from the GCD curves, using

$$C_{GCD} = I \int \left(\frac{1}{V\ (t)}\right) dt \tag{5.2}$$

$$E = \frac{I_{dis} \int vdt}{3600} \tag{5.3}$$

$$P = \frac{E}{t_{dis}} \tag{5.4}$$

where I is the applied constant-current density, t is the discharge time, and $V(t)$ is the potential as a function of t. I_{dis} represent the current of discharge (mA), $\int vdt$ is the integral area of the GCD discharge cycle, and t_{dis} denote discharge time (s), respectively[134, 135].

5.9 Supporting Information

Supporting Information is available from the Wiley Online Library or from the author.

5.10 Acknowledgments

M.H. acknowledges financial support from Hydro Quebec and CREATE SEED through PhD scholarships. C.S. acknowledges financial support from NSERC (D.G.) and the Canada Research Chair. A.G. thanks Ford Motor Canada for the financial support.

5.11 Conflict of Interest

The authors declare no conflict of interest.

CHAPTER 6 GENERAL DISCUSSION

In this PhD thesis, our approach was to explore bio-sourced organic materials for the eco-design of energy storage systems. Our study centers on two important bio-sourced quinone-based redox-active (macro)molecules: Sepia melanin and Catechin. Sepia melanin can be extracted from the ink sac of cuttlefish as byproduct from the food industries. Catechin belongs to the Tannins family (i.e., a broad class of polyphenolic biomolecules) that can be sourced from tree components (e.g., bark or leaves), fruit residues or extracted as by-product of wood or food industries. Both Sepia melanin and Catechin are abundant, non-toxic, and biodegradable, making them candidates for development of sustainable energy storage systems.

In Chapter 2, we discussed the fundamental principles of electrochemical energy storage systems and their key components. Carbon-based electrodes are extensively utilized in supercapacitors, owing to their low cost, tunable porosity, and favorable electrical conductivity. However, the inherent limitations of carbon-based electrodes, including limited surface area and inadequate wettability (i.e., poor aqueous electrolyte affinity), necessitate surface/interface engineering to effectively enhance the charge storage capacitance of the electrodes.

In Article 1, we employed a three-step hydrothermal treatment on carbon paper to enhance its surface area and modify its surface chemistry. SEM results revealed the appearance of numerous grooves on the surface of the carbon fibers following the hydrothermal treatment. BET and BJH analyses confirmed a significant increase in surface area (from 0.13 to 83 $m^2\ g^{-1}$) and a 65% improvement in total pore volume (i.e., micropores, mesopores, and macropores). Such hierarchical pore structure improved the rate capability of the electrode. Moreover, the treated carbon paper (TCP) exhibited hydrophilic behavior, as confirmed by water contact angle measurements. We also employed XPS to investigate the impact of the hydrothermal treatment on the surface chemical composition of the TCP. The results indicated that such treatment introduced oxygen and nitrogen heteroatoms onto the surface The significant improvement of the overall electrochemical performance of TCP, with specific capacitance increasing from 0.24 to 103 $F\ g^{-1}$, can be attributed to the increased surface area and the incorporation of heteroatoms, enhancing the charge storage performance in at least two ways: (i) improved electrostatic interaction and ion accumulation, and (ii) facilitated charge transfer processes involving the heteroatoms (i.e., faradaic reactions).

Subsequently, we modified the surface of the treated carbon paper (TCP) with catechin, a redox-active molecule from the Tannin family, drop-casting technique. The cyclic voltammetry profile of the Catechin-loaded treated carbon paper (Ctn/TCP) in a three-electrode configuration exhibited a quasi-rectangular shape, with superimposed oxidation and reduction peaks (i.e., characteristic of pseudocapacitive electrode materials) at 0.5 V and 0.3 V vs. Ag/AgCl, respectively, at a scan rate of 5 mV s^{-1}. Moreover, the specific capacitance obtained at 5 mV/s reached a value as high as 287 F g^{-1} (based on the mass of Catechin) for Ctn/TCP, highlighting the significant faradaic contribution of Catechin to the total charge storage performance of TCP.

The primary challenge of this study was to visualize Catechin supramolecular assemblies on TCP via SEM. Due to the low atomic numbers of Tannin constituents (e.g., C and H), direct observation using SEM was not feasible. To address this, following drop-casting, the samples were stained by immersion in a 0.1 M silver nitrate ($AgNO_3$) solution for 24 hours. Tannins have the tendency to chemically reduce metallic cations like Ag^+. Consequently, metallic Ag atoms provide sufficient contrast for SEM imaging, enabling the observation of Catechin aggregates distribution on TCP.

Following the electrochemical characterization of the Ctn/TCP electrodes, we proceeded to fabrication of semi-solid-state symmetric supercapacitors making use of a PVA-based hydrogel for the electrolyte. We employed a semi-solid-state PVA-based hydrogel (water-based gel) electrolyte to enhance cycling stability and ensure a seamless interface with the carbon electrode. In addition to its favorable ionic conductivity, the PVA-based hydrogel is considered a biodegradable polymer, to eco-design sustainable energy storage devices.

The Ctn-based semi-solid symmetric supercapacitors achieved a capacitance of up to 202 F g^{-1} at a current density of 1 A g^{-1}, along with outstanding energy density (55 Wh kg^{-1}) and power density (660 W kg^{-1}). The device featured capacitance retention and Coulombic efficiency reaching 100 %, respectively, over 20,000 cycles.

Such cycling stability has not been previously reported in bio-sourced quinone-based supercapacitors without a binder. The result is attributable to the PVA-based hydrogel, which limits the diffusion and leaching of Catechin molecules into the electrolyte.

Despite the outstanding electrochemical performance of the Catechin-based supercapacitors reported in Article 1, several challenges persisted, including: (i) the lack of mechanical flexibility and bendability of the device due to the inherent brittleness of the carbon paper electrodes, which

limited its practical applications and (ii) the poor rate response of the device at high scan rates, attributed to the high contact resistance at the Catechin interface with the carbon current collector, (iii) non-environmentally friendly characteristics of the hydrothermal treatment process, associated with high energy consumption (e.g., prolonged thermal treatment in autoclave) and the generation of acidic wastewater (e.g., resulting from the use of nitric and sulfuric acids), that fail to comply with the principles of green chemistry.

In Article 2, we present a novel pseudocapacitive electrode material based on a composite of bio-sourced, redox-active Sepia melanin and conductive multi-walled carbon nanotubes (MWCNTs). This composite was deposited onto flexible carbon cloth (CC) electrodes using ultrasonication, a quasi-waste-free surface engineering technique characterized by its low embodied energy.

The composite Sepia melanin:MWCNT electrode materials has been designed to promote (i) the formation of efficient conductive network between Sepia granules thanks to the presence of MWCNTs, and (ii) the efficiency of the electronic coupling between the CC and the Sepia melanin granules.

Moreover, the fabrication process of the composite electrode material was eco-designed, prioritizing energy efficiency, minimizing chemical waste, and avoiding the use of surfactants or organic/inorganic binders. Additionally, the MWCNTs used in this study were obtained as by-products of a photocatalytic process, further enhancing the sustainability of the electrode materials in alignment with eco-design principles.

In this study, we used commercially available carbon cloth (CC), made of carbon fibers, due to its flexibility, mechanical robustness, and favorable electronic conductivity. These attributes render it an ideal electrode for establishing a seamless interface with flexible semi-solid-state hydrogel electrolytes.

Initially, we applied a pre-heat treatment (300 °C, 1 h, in air) on pristine CC to introduce minimal oxygen-containing functional groups onto its surface. This modification aimed to enhance the wettability of the electrode, thereby improving the effectiveness of the subsequent ultrasonication process. Afterwards, we employed an ultrasonication technique in deionized water (DIW) for surface modification of CC. This approach is both waste-free and energy-efficient, eliminating the need for chemicals, surfactants, or organic/inorganic binders.

Initially, we applied a pre-heat treatment (300 °C, 1 h, in air) on pristine CC to introduce minimal oxygen-containing functional groups onto its surface. This modification aimed to enhance the wettability of the electrode, thereby improving the effectiveness of the subsequent ultrasonication process. Afterwards, we employed an ultrasonication technique in deionized water (DIW) for surface modification of CC. This approach is both waste-free and energy-efficient, eliminating the need for chemicals, surfactants, or organic/inorganic binders.

The primary challenge of this study was to identify the optimal ultrasonication parameters, including time, power, and temperature, and to evaluate their effects on the areal capacitance of the ultrasound treated carbon cloth (UTCC). The key parameters considered in this study included ultrasonication time (1-5 min), temperature (20-60 °C), and power (40-80 W). The areal capacitance of the resulting carbon cloth was determined from cyclic voltammetry obtained in a three-electrode setup. The results revealed that the optimal conditions were 60 W for the ultrasound power, 40 °C for the temperature, and 5 minutes for the ultrasonication time, bringing about an areal capacitance of 147 mF cm^{-2}, which is 73 times higher than that of pristine CC (2 mF cm^{-2}). Notably, the energy consumption of this process was merely 5 Wh.

SEM images of UTCC confirmed an increase in surface roughness of the carbon fibers, suggesting that ultrasound treatment had a significant impact on the fibers, likely through cavitation effects. Interestingly, the EDS mapping and XPS results of UTCC also confirmed the successful in-situ O-functionalization of the surface of UTCC, likely due to the generation of $OH\cdot$ radicals during ultrasonication.

The cyclic voltammograms of UTCC, obtained at a scan rate of 10 mV s^{-1}, exhibited a pseudo-rectangular shape typical of pseudocapacitive electrodes. Moreover, GCD profile of the UTCC displayed a slight deviation from linear behavior, indicating the occurrence of redox reactions during the charging and discharging processes. This deviation can be attributed to the presence of O-containing functional groups induced by the ultrasonication process.

This improved electrochemical performance can be attributed to the increased surface area, optimal porosity, and enhanced hydrophilicity of UTCC compared to pristine CC, all of which facilitate the electrostatic mechanism and ions accumulation at the surface of the UTCC. Additionally, the presence of O-containing functional groups on the UTCC enhances the pseudocapacitive contribution.

Subsequently, for the preparation of Sepia melanin:MWCNT on UTCC electrode, Sepia and MWCNT powders were blended in various mass ratios (3:7, 1:1, and 7:3). The resulting mixtures were then added directly to DIW in the ultrasonic reactor, where the ultrasonication process was conducted under the optimized conditions.

SEM and TEM images of UTCC/MWCNT:Sepia electrodes, showed that the dense, spherical Sepia melanin granules were surrounded by an interconnected network of MWCNTs, which were uniformly anchored to the carbon fibers during ultrasonication.

The CV profile of UTCC/MWCNT:Sepia electrodes exhibited a quasi-rectangular shape, with two broad oxidation and reduction peaks observed at approximately 0.1 V and 0.04 V versus Ag/AgCl, respectively, at a scan rate of 10 mV s^{-1}. These peaks are attributed to the redox activity of the quinone/hydroquinone couple present in Sepia melanin.

Comparison of the areal capacitance of UTCC/MWCNT:Sepia at different mass ratios (3:7, 1:1, 7:3) at scan rate of 10 mV s^{-1} indicated that the optimal electrochemical performance was achieved with the UTCC/MWCNT:Sepia (3:7) electrode, yielding a capacitance as high as 274 mF cm^{-2}. These results underscore the synergistic contributions of faradaic and electrostatic processes to the enhanced overall charge storage performance of the novel electrode materials.

The GCD profile of the UTCC/MWCNT:Sepia electrode showed a symmetric triangular shape, characterized by a minimal ohmic drop (10 mV at 0.5 mA cm^{-2}) and an extended discharge time compared to the UTCC/Sepia and UCC electrodes. Furthermore, EIS characterization revealed that the UTCC/MWCNT:Sepia electrode exhibited a low charge transfer resistance (R_{ct}) of 0.2 Ω and a small electrolyte resistance (R_s) of 2.4 Ω.

These results indicated that the incorporation of MWCNTs into the electrode material fulfills two critical roles: (i) enhancing electron transfer, and (ii) improving ion diffusion within electrode materials by providing accessible sites for ion diffusion at high scan rates. This dual effect leads to a notable improvement in the electrode rate capability and charge storage performance.

To assess the practical performance of the novel electrode material, we fabricated symmetric semi-solid-state supercapacitors using a PVA-Na_2SO_4-based hydrogel electrolyte. The MWCNT:Sepia-based supercapacitors achieved a capacitance of up to 118 F g^{-1} at 0.5 A g^{-1}, delivering a high energy density of 18 Wh kg^{-1} and a power density of 221 W kg^{-1} (evaluated at 0.5 A g^{-1}), along with remarkable cycling stability, characterized by 100% capacitance retention and 100%

Coulombic efficiency after 10,000 cycles. This remarkable cycling stability is attributable to the semi-solid hydrogel electrolyte, which effectively limits the dissolution of quinone-based molecules into the electrolyte during extended charging and discharging cycles. Furthermore, the devices demonstrated consistent electrochemical performance when subjected to mechanical bending at various angles (ranging from 90° to 180°), further highlighting their robustness and mechanical flexibility.

In conclusion, Article 2 introduced a novel bio-sourced quinone-based composite electrode material developed through a sustainable surface engineering approach, achieving high capacitive performance suitable for environmentally friendly electrochemical energy storage applications. The fabrication process was eco-designed by (i) incorporating organic bio-sourced redox-active materials, (ii) employing an energy-efficient surface modification technique, and (iii) mitigating chemical waste, aligning well with the principles of green chemistry.

CHAPTER 7 CONCLUSION AND RECOMMENDATIONS

This growing market for consumer electronics and portable devices places immense pressure on the supply chain of strategic and critical elements (e.g., Co, Li), whose extraction often leads to environmental, social, and geopolitical challenges. Furthermore, the vast accumulation of waste electrical and electronic equipment (WEEE) and its spent powering components worldwide poses a significant global challenge, particularly as recycling remains unviable in many regions under the current economic framework conditions. Therefore, shifting toward sustainable solutions is imperative.

Nature offers a wealth of inspiration, capable of inspiring sustainable approaches to the design and engineering of innovative solutions. In this PhD thesis, our vision is centered on the idea that by harnessing organic bio-sourced materials, we can develop greener energy storage devices that align with the principles of eco-design. This approach aims to reduce embodied energy and environmental impact while ensuring optimal electrochemical performance.

Organic bio-sourced redox-active molecules are highly promising for the development of sustainable energy storage systems, offering key advantages of abundance, low cost, solution processability, and potential biodegradability. When deposited on carbon-based electrode, redox-active molecules bring about an increase of the energy density of the electrodes since the Faradaic storage mechanism adds to the electrostatic one. The surface/interface engineering of the electrode, the molecule, and the electrolyte is essential for optimizing energy storage performance, particularly in terms of rate capability and cycling stability.

In Article 1, we reported on the surface engineering of carbon paper electrodes through hydrothermal treatment, aimed at improving wettability, increasing surface area, enhancing porous architecture, and introducing electrochemically active surface sites (i.e., O and N functionalities). Additionally, we modified the treated carbon paper electrodes with redox-active Catechin molecules, a member of the Tannin family, through solution processing from an aqueous Catechin solution. Finally, we fabricated symmetric electrochemical capacitors by interfacing these modified electrodes with a polyvinyl alcohol (PVA)-based hydrogel electrolyte.

Our morphological and electrochemical characterizations revealed key findings, including the following: the high surface area and porous architecture of treated carbon paper facilitate electrostatic interactions and ion accumulation at the electrode/electrolyte interface, thereby

enhancing the electric double-layer capacitance (EDLC) of the treated carbon paper. Additionally, the introduction of O and N surface functionalities improves charge storage properties through pseudocapacitive contributions, resulting in specific capacitances of 103 F g^{-1}.

Surface modification of treated carbon paper with Catechin further improves its charge storage performance, bringing about the specific capacitance as high as 287 F g^{-1}, indicating the beneficial Faradaic contribution of Catechin.

Moreover, symmetric semi-solid-state supercapacitors made of corresponding electrodes, reached capacitance values as high as 202 F g^{-1}, excellent cycling stability over 20,000 cycles. The devices also exhibited an energy density of 55 Wh kg^{-1} and power density of 660 W kg^{-1}.

Polymer-based semi-solid-state electrolytes effectively limit the leaching of quinone-based molecules during extended cycling, while establishing a seamless interface with current collectors and providing ion conductivity. Consequently, they can be considered a promising electrolyte for enhancing the performance of quinone-based supercapacitors without the need for organic/inorganic binders.

The findings of Article 1 contribute to the development of eco-designed, cost-efficient, and sustainable electrochemical supercapacitors utilizing redox-active bio-sourced materials. These results may serve as guidance for future studies aimed at evaluating the potential of the Tannins family, beyond Catechin for electrochemical energy storage applications. Moreover, the biodegradation of such devices presents a compelling area for further research to assess their end-of-life scenarios.

In Article 2, we reported on a novel pseudocapacitive electrode material on flexible electrodes, prepared by ultrasound-assisted modification of carbon cloth in the presence of Sepia melanin, a quinone-based macromolecule, and multiwalled carbon nanotubes (MWCNTs). Optimal parameters for the ultrasonication process (i.e., ultrasonication time, temperature, and power) were determined by evaluating the areal capacitance of the treated carbon cloth. Flexible symmetric electrochemical capacitors were then fabricated using these modified electrodes, assembled with a polyvinyl alcohol (PVA)-based hydrogel electrolyte.

The results of our study revealed that the ultrasonication process in water increases the surface area and porosity of the carbon cloth and introducing surface O-including functionalities, bring about pseudocapacitive contribution complementary to its electrostatic one. The incorporation of

MWCNTs into the composite electrode materials creates an efficient conductive network among the Sepia granules, enhancing the electronic coupling between the carbon cloth and the Sepia melanin granules. This network consequently improves the rate response of the composite electrode materials.

Additionally, MWCNT:Sepia-based semi-solid-state symmetric supercapacitors achieved capacitance as high as 118 F g^{-1}. These devices deliver a high energy density and power density (i.e., 18 Wh kg^{-1} and 221 W kg^{-1}, respectively), along with notable flexibility and cycling stability over 10,000 cycles.

This work contributes to the development of sustainable surface engineering approaches toward the eco-design of environmentally benign electrochemical energy storage devices. Our findings offer critical insights into the treatment of carbon-based electrodes, emphasizing a paradigm shift that moves beyond electrochemical performance and considering sustainability and the environmental impact of the treatment processes.

In perspective, our research provides a foundation for future studies aimed at developing scalable and streamlined one-pot treatment processes for modification of carbon-based electrodes that are energy-efficient and waste-free without the need for organic/inorganic binders or surfactants. Furthermore, additional experiments are needed to investigate the application of ultrasonication in the presence of other bio-sourced molecules, such as indigo carmine, to evaluate the universality of this approach.

Furthermore, considering the significance of anticipating end-of-life scenarios for organic electronics, it is imperative to conduct biodegradation tests in the future on bio-sourced redox-active electrochemical energy storage devices under industrial composting conditions.

REFERENCES

[1] C. Church and A. Crawford, "Minerals and the metals for the energy transition: Exploring the conflict implications for mineral-rich, fragile states," in *The geopolitics of the global energy transition*: Springer, 2020, pp. 279-304.

[2] S. Kalantzakos, "The race for critical minerals in an era of geopolitical realignments," *The International Spectator,* vol. 55, no. 3, pp. 1-16, 2020.

[3] S. M. Jowitt, "Renewable energy and associated technologies and the scarcity of metal," in *Living with Climate Change*: Elsevier, 2024, pp. 45-63.

[4] S. Nižetić, P. Šolić, D. L.-d.-I. Gonzalez-De, and L. Patrono, "Internet of Things (IoT): Opportunities, issues and challenges towards a smart and sustainable future," *Journal of cleaner production,* vol. 274, p. 122877, 2020.

[5] J. L. Calderon *et al.*, "Reviewing the material and metal security of low-carbon energy transitions," *Renewable and Sustainable Energy Reviews,* vol. 124, p. 109789, 2020.

[6] R. Moss *et al.*, "Critical Metals in the Path towards the Decarbonisation of the EU Energy Sector," *Assessing rare metals as supply-chain bottlenecks in low-carbon energy technologies. JRC Report EUR,* vol. 25994, 2013.

[7] P. Teehan and M. Kandlikar, "Comparing embodied greenhouse gas emissions of modern computing and electronics products," *Environmental science & technology,* vol. 47, no. 9, pp. 3997-4003, 2013.

[8] I. El-Mahallawi *et al.*, "Options for using electronic waste as an alloy resource: dilution with Al scrap," *Academia Engineering,* vol. 1, no. 3, 2024.

[9] V. Kumar and D. K. Verma, "e-Waste in construction: a comprehensive bibliometric analysis and review of the literature," *World Journal of Engineering,* 2024.

[10] W. O. Agbondinmwin, "FLOWS OF WASTE AND SECONDHAND ITEMS FROM DEVELOPED TO DEVELOPING COUNTRIES: A case study of e-wastes in Nigeria and China," 2024.

[11] A. Modak and P. Bhattacharjyya, "Health and Environmental Effects of E-waste Recycling Processes: Issues, Challenges, and Solutions," in *Development in E-waste Management*: CRC Press, 2023, pp. 107-125.

[12] F. Blomsma, T. Bauwens, I. Weissbrod, and J. Kirchherr, "The 'need for speed': Towards circular disruption—What it is, how to make it happen and how to know it's happening," *Business Strategy and the Environment,* vol. 32, no. 3, pp. 1010-1031, 2023.

[13] V. Kandpal, A. Jaswal, E. D. Santibanez Gonzalez, and N. Agarwal, "Circular economy principles: shifting towards sustainable prosperity," in *Sustainable Energy Transition: Circular Economy and Sustainable Financing for Environmental, Social and Governance (ESG) Practices*: Springer, 2024, pp. 125-165.

[14] M. D. Bovea and V. Pérez-Belis, "A taxonomy of ecodesign tools for integrating environmental requirements into the product design process," *Journal of Cleaner Production,* vol. 20, no. 1, pp. 61-71, 2012.

[15] J. Kuczynski and D. Boday, "Bio-based materials for high-end electronics applications," *International Journal of Sustainable Development & World Ecology,* vol. 19, no. 6, pp. 557-563, 2012.

[16] E. Di Mauro, D. Rho, and C. Santato, "Biodegradation of bio-sourced and synthetic organic electronic materials towards green organic electronics," *Nature Communications,* vol. 12, no. 1, p. 3167, 2021/05/26 2021, doi: 10.1038/s41467-021-23227-4.

[17] F. Visentin, J. Cantin, and C. Santato, "Active and Dynamic Learning in Sustainable Electronics," *Journal of Chemical Education,* vol. 101, no. 8, pp. 3156-3162, 2024.

[18] W. Wang, V. Balland, M. Branca, and B. Limoges, "A unified charge storage mechanism to rationalize the electrochemical behavior of quinone-based organic electrodes in aqueous rechargeable batteries," *Journal of the American Chemical Society,* 2024.

[19] A. Gouda, *Biosourced Quinone-Based Molecular Materials for Electrochemical Energy Storage*. Ecole Polytechnique, Montreal (Canada), 2021.

[20] S. P. Ega and P. Srinivasan, "Quinone materials for supercapacitor: Current status, approaches, and future directions," *Journal of Energy Storage,* vol. 47, p. 103700, 2022/03/01/ 2022, doi: https://doi.org/10.1016/j.est.2021.103700.

[21] J. Lemieux, D. Bélanger, and C. Santato, "Toward Biosourced Materials for Electrochemical Energy Storage: The Case of Tannins," *ACS Sustainable Chemistry & Engineering,* vol. 9, no. 17, pp. 6079-6086, 2021/05/03 2021, doi: 10.1021/acssuschemeng.1c01535.

[22] T. Ahmad and D. Zhang, "A critical review of comparative global historical energy consumption and future demand: The story told so far," *Energy Reports,* vol. 6, pp. 1973-1991, 2020/11/01/ 2020, doi: https://doi.org/10.1016/j.egyr.2020.07.020.

[23] D. H. S. Tan, A. Banerjee, Z. Chen, and Y. S. Meng, "From nanoscale interface characterization to sustainable energy storage using all-solid-state batteries," *Nature Nanotechnology,* vol. 15, no. 3, pp. 170-180, 2020/03/01 2020, doi: 10.1038/s41565-020-0657-x.

[24] Y. Jiang and J. Liu, "Definitions of Pseudocapacitive Materials: A Brief Review," *ENERGY & ENVIRONMENTAL MATERIALS,* vol. 2, no. 1, pp. 30-37, 2019, doi: https://doi.org/10.1002/eem2.12028.

[25] F. N. Ajjan, D. Mecerreyes, and O. Inganäs, "Enhancing Energy Storage Devices with Biomacromolecules in Hybrid Electrodes," *Biotechnology Journal,* vol. 14, no. 12, p. 1900062, 2019, doi: https://doi.org/10.1002/biot.201900062.

[26] F. Hussain, M. Z. Rahman, A. N. Sivasengaran, and M. Hasanuzzaman, "Chapter 6 - Energy storage technologies," in *Energy for Sustainable Development*, M. D. Hasanuzzaman and N. A. Rahim Eds.: Academic Press, 2020, pp. 125-165.

[27] M. Winter and R. J. Brodd, "What Are Batteries, Fuel Cells, and Supercapacitors?," *Chemical Reviews,* vol. 104, no. 10, pp. 4245-4270, 2004/10/01 2004, doi: 10.1021/cr020730k.

[28] Y. Ding and Z. Zhang, "Nanoporous Metals for Supercapacitor Applications," in *Nanoporous Metals for Advanced Energy Technologies*. Cham: Springer International Publishing, 2016, pp. 137-173.

[29] J. Huang, K. Yuan, and Y. Chen, "Wide Voltage Aqueous Asymmetric Supercapacitors: Advances, Strategies, and Challenges," *Advanced Functional Materials,* vol. 32, no. 4, p. 2108107, 2022, doi: https://doi.org/10.1002/adfm.202108107.

[30] S. Banerjee *et al.*, "Capacitor to Supercapacitor," in *Handbook of Nanocomposite Supercapacitor Materials I: Characteristics*, K. K. Kar Ed. Cham: Springer International Publishing, 2020, pp. 53-89.

[31] K. Fic, A. Platek, J. Piwek, and E. Frackowiak, "Sustainable materials for electrochemical capacitors," *Materials Today,* vol. 21, no. 4, pp. 437-454, 2018/05/01/ 2018, doi: https://doi.org/10.1016/j.mattod.2018.03.005.

[32] J. Castro-Gutiérrez, A. Celzard, and V. Fierro, "Energy Storage in Supercapacitors: Focus on Tannin-Derived Carbon Electrodes," (in English), *Frontiers in Materials,* Review vol. 7, no. 217, 2020-July-22 2020, doi: 10.3389/fmats.2020.00217.

[33] N. Kumar, S. B. Kim, S. Y. Lee, and S. J. Park, "Recent Advanced Supercapacitor: A Review of Storage Mechanisms, Electrode Materials, Modification, and Perspectives," (in eng), *Nanomaterials (Basel),* vol. 12, no. 20, Oct 21 2022, doi: 10.3390/nano12203708.

[34] J. R. Miller, "CAPACITORS | Overview," in *Encyclopedia of Electrochemical Power Sources*, J. Garche Ed. Amsterdam: Elsevier, 2009, pp. 587-599.

[35] S. T. Revankar, "Chapter Six - Chemical Energy Storage," in *Storage and Hybridization of Nuclear Energy*, H. Bindra and S. Revankar Eds.: Academic Press, 2019, pp. 177-227.

[36] S. Roldán, M. Granda, R. Menéndez, R. Santamaría, and C. Blanco, "Mechanisms of Energy Storage in Carbon-Based Supercapacitors Modified with a Quinoid Redox-Active Electrolyte," *The Journal of Physical Chemistry C,* vol. 115, no. 35, pp. 17606-17611, 2011/09/08 2011, doi: 10.1021/jp205100v.

[37] D. P. Chatterjee and A. K. Nandi, "A review on the recent advances in hybrid supercapacitors," *Journal of Materials Chemistry A,* 10.1039/D1TA02505H vol. 9, no. 29, pp. 15880-15918, 2021, doi: 10.1039/D1TA02505H.

[38] S. Karthikeyan, B. Narenthiran, A. Sivanantham, L. D. Bhatlu, and T. Maridurai, "Supercapacitor: Evolution and review," *Materials Today: Proceedings,* vol. 46, pp. 3984-3988, 2021/01/01/ 2021, doi: https://doi.org/10.1016/j.matpr.2021.02.526.

[39] J. Liu *et al.*, "Advanced Energy Storage Devices: Basic Principles, Analytical Methods, and Rational Materials Design," *Advanced Science,* vol. 5, no. 1, p. 1700322, 2018, doi: https://doi.org/10.1002/advs.201700322.

[40] N. R. Chodankar *et al.*, "True Meaning of Pseudocapacitors and Their Performance Metrics: Asymmetric versus Hybrid Supercapacitors," *Small,* vol. 16, no. 37, p. 2002806, 2020, doi: https://doi.org/10.1002/smll.202002806.

[41] T. Brousse, D. Bélanger, and J. W. Long, "To Be or Not To Be Pseudocapacitive?," *Journal of The Electrochemical Society,* vol. 162, no. 5, pp. A5185-A5189, 2015, doi: 10.1149/2.0201505jes.

[42] P. Bhojane, "Recent advances and fundamentals of Pseudocapacitors: Materials, mechanism, and its understanding," *Journal of Energy Storage,* vol. 45, p. 103654, 2022/01/01/ 2022, doi: https://doi.org/10.1016/j.est.2021.103654.

[43] V. Augustyn, P. Simon, and B. Dunn, "Pseudocapacitive oxide materials for high-rate electrochemical energy storage," *Energy & Environmental Science,* 10.1039/C3EE44164D vol. 7, no. 5, pp. 1597-1614, 2014, doi: 10.1039/C3EE44164D.

[44] M. Czagany *et al.*, "Supercapacitors: An Efficient Way for Energy Storage Application," *Materials,* vol. 17, no. 3, p. 702, 2024. [Online]. Available: https://www.mdpi.com/1996-1944/17/3/702.

[45] Y. Shao *et al.*, "Design and Mechanisms of Asymmetric Supercapacitors," *Chemical Reviews,* vol. 118, no. 18, pp. 9233-9280, 2018/09/26 2018, doi: 10.1021/acs.chemrev.8b00252.

[46] S. J. Panchu, K. Raju, and H. C. Swart, "Emerging Two–Dimensional Intercalation Pseudocapacitive Electrodes for Supercapacitors," *ChemElectroChem,* vol. 11, no. 15, p. e202300810, 2024, doi: https://doi.org/10.1002/celc.202300810.

[47] Y. Liu, S. P. Jiang, and Z. Shao, "Intercalation pseudocapacitance in electrochemical energy storage: recent advances in fundamental understanding and materials development," *Materials Today Advances,* vol. 7, p. 100072, 2020/09/01/ 2020, doi: https://doi.org/10.1016/j.mtadv.2020.100072.

[48] J. Zhang, M. Gu, and X. Chen, "Supercapacitors for renewable energy applications: A review," *Micro and Nano Engineering,* vol. 21, p. 100229, 2023/12/01/ 2023, doi: https://doi.org/10.1016/j.mne.2023.100229.

[49] A. Muzaffar, M. B. Ahamed, K. Deshmukh, and J. Thirumalai, "A review on recent advances in hybrid supercapacitors: Design, fabrication and applications," *Renewable and Sustainable Energy Reviews,* vol. 101, pp. 123-145, 2019/03/01/ 2019, doi: https://doi.org/10.1016/j.rser.2018.10.026.

[50] E. J. Son, J. H. Kim, K. Kim, and C. B. Park, "Quinone and its derivatives for energy harvesting and storage materials," *Journal of Materials Chemistry A,* 10.1039/C6TA03123D vol. 4, no. 29, pp. 11179-11202, 2016, doi: 10.1039/C6TA03123D.

[51] M. Amiri, G. Shul, N. Donzel, and D. Bélanger, "Aqueous electrochemical energy storage system based on phenanthroline- and anthraquinone-modified carbon electrodes," *Electrochimica Acta,* vol. 390, p. 138862, 2021/09/10/ 2021, doi: https://doi.org/10.1016/j.electacta.2021.138862.

[52] J. Castro-Gutiérrez *et al.*, "High-Rate Capability of Supercapacitors Based on Tannin-Derived Ordered Mesoporous Carbons," *ACS Sustainable Chemistry & Engineering,* vol. 7, no. 21, pp. 17627-17635, 2019/11/04 2019, doi: 10.1021/acssuschemeng.9b03407.

[53] K. Naoi, S. Suematsu, and A. Manago, "Electrochemistry of Poly(1,5-diaminoanthraquinone) and Its Application in Electrochemical Capacitor Materials," *Journal of The Electrochemical Society,* vol. 147, no. 2, p. 420, 2000/02/01 2000, doi: 10.1149/1.1393212.

[54] G. Milczarek and O. Inganäs, "Renewable cathode materials from biopolymer/conjugated polymer interpenetrating networks," (in eng), *Science,* vol. 335, no. 6075, pp. 1468-71, Mar 23 2012, doi: 10.1126/science.1215159.

[55] A. Mukhopadhyay, Y. Jiao, R. Katahira, P. N. Ciesielski, M. Himmel, and H. Zhu, "Heavy Metal-Free Tannin from Bark for Sustainable Energy Storage," *Nano Letters,* vol. 17, no. 12, pp. 7897-7907, 2017/12/13 2017, doi: 10.1021/acs.nanolett.7b04242.

[56] P. J. G. Lopes *et al.*, "Tannin-based extracts of Mimosa tenuiflora bark: features and prospecting as wood adhesives," *Applied Adhesion Science,* vol. 9, no. 1, p. 3, 2021/01/26 2021, doi: 10.1186/s40563-021-00133-y.

[57] M. Moloudi, M. S. Rahmanifar, A. Noori, X. Chang, R. B. Kaner, and M. F. Mousavi, "Bioinspired polydopamine supported on oxygen-functionalized carbon cloth as a high-performance 1.2 V aqueous symmetric metal-free supercapacitor," *Journal of Materials Chemistry A,* 10.1039/D0TA12624A vol. 9, no. 12, pp. 7712-7725, 2021, doi: 10.1039/D0TA12624A.

[58] D. Fang, J. Zhou, L. Sheng, W. Tang, and J. Tang, "Juglone bonded carbon nanotubes interweaving cellulose nanofibers as self-standing membrane electrodes for flexible high energy supercapacitors," *Chemical Engineering Journal,* vol. 396, p. 125325, 2020/09/15/ 2020, doi: https://doi.org/10.1016/j.cej.2020.125325.

[59] Y. M. Shulga *et al.*, "Preparation of graphene oxide-humic acid composite-based ink for printing thin film electrodes for micro-supercapacitors," *Journal of Alloys and Compounds,* vol. 730, pp. 88-95, 2018/01/05/ 2018, doi: https://doi.org/10.1016/j.jallcom.2017.09.249.

[60] Y. Zhou *et al.*, "Quinone-Enriched Polymer with a Large π-Conjugated Structure for High-Energy Supercapacitors: Synthesis and Electrochemical Assessment," *Energy & Fuels,* vol. 38, no. 8, pp. 7399-7411, 2024/04/18 2024, doi: 10.1021/acs.energyfuels.4c00778.

[61] M. Hoseinizadeh, K. E. Salem, A. Gouda, D. Belanger, and C. Santato, "Tannins for Sustainable Semi-solid-state Supercapacitors," *Waste and Biomass Valorization,* 2023/04/07 2023, doi: 10.1007/s12649-023-02125-4.

[62] Y. Dong, J. Zhu, Q. Li, S. Zhang, H. Song, and D. Jia, "Carbon materials for high mass-loading supercapacitors: filling the gap between new materials and practical applications," *Journal of Materials Chemistry A,* vol. 8, no. 42, pp. 21930-21946, 2020.

[63] X. He *et al.*, "Pseudocapacitance electrode and asymmetric supercapacitor based on biomass juglone/activated carbon composites," *RSC advances,* vol. 9, no. 53, pp. 30809-30814, 2019.

[64] L. Hou, C. Kong, Z. Hu, Y. Han, and B. Wu, "Redox active organic molecule-Emodin modified graphene for high-performance supercapacitors," *Journal of Electroanalytical Chemistry,* vol. 895, p. 115402, 2021/08/15/ 2021, doi: https://doi.org/10.1016/j.jelechem.2021.115402.

[65] M. Cao, W. Cheng, X. Ni, Y. Hu, and G. Han, "Lignin-based multi-channels carbon nanofibers @ SnO2 nanocomposites for high-performance supercapacitors," *Electrochimica Acta,* vol. 345, p. 136172, 2020/06/10/ 2020, doi: https://doi.org/10.1016/j.electacta.2020.136172.

[66] L. Xu, H. Yu, Y. Li, M. Jia, C. Yao, and X. Jin, "Tannic Acid-Decorated Spongy Graphene for Flexible and High Performance Supercapacitors," *Journal of The Electrochemical Society,* vol. 165, no. 9, pp. A1706-A1712, 2018, doi: 10.1149/2.0871809jes.

[67] W. Wang *et al.*, "Reduced graphene oxide film modified by tannic acid for high areal performance supercapacitors," *Journal of Solid State Electrochemistry,* 2024/07/16 2024, doi: 10.1007/s10008-024-05946-y.

[68] C. Yang *et al.*, "Flexible supercapacitors with tunable capacitance based on reduced graphene oxide/tannin composite for wearable electronics," *Journal of Electroanalytical Chemistry,* vol. 894, p. 115354, 2021/08/01/ 2021, doi: https://doi.org/10.1016/j.jelechem.2021.115354.

[69] X. Zhao, M. Gnanaseelan, D. Jehnichen, F. Simon, and J. Pionteck, "Green and facile synthesis of polyaniline/tannic acid/rGO composites for supercapacitor purpose," *Journal of Materials Science,* vol. 54, no. 15, pp. 10809-10824, 2019/08/01 2019, doi: 10.1007/s10853-019-03654-x.

[70] A. Gouda, J. Manioudakis, R. Naccache, F. Soavi, and C. Santato, "3D Network of Sepia Melanin and N- and, S-Doped Graphitic Carbon Quantum Dots for Sustainable Electrochemical Capacitors," *Advanced Sustainable Systems,* vol. 5, no. 10, p. 2100152, 2021, doi: https://doi.org/10.1002/adsu.202100152.

[71] P. Simon and Y. Gogotsi, "Materials for electrochemical capacitors," *Nature Materials,* vol. 7, no. 11, pp. 845-854, 2008/11/01 2008, doi: 10.1038/nmat2297.

[72] J. Xia, F. Chen, J. Li, and N. Tao, "Measurement of the quantum capacitance of graphene," *Nature Nanotechnology,* vol. 4, no. 8, pp. 505-509, 2009/08/01 2009, doi: 10.1038/nnano.2009.177.

[73] Y. Zhu *et al.*, "Carbon-Based Supercapacitors Produced by Activation of Graphene," *Science,* vol. 332, no. 6037, pp. 1537-1541, 2011, doi: doi:10.1126/science.1200770.

[74] M. Seredych, D. Hulicova-Jurcakova, G. Q. Lu, and T. J. Bandosz, "Surface functional groups of carbons and the effects of their chemical character, density and accessibility to ions on electrochemical performance," *Carbon,* vol. 46, no. 11, pp. 1475-1488, 2008.

[75] H. M. Jeong *et al.*, "Nitrogen-doped graphene for high-performance ultracapacitors and the importance of nitrogen-doped sites at basal planes," *Nano letters,* vol. 11, no. 6, pp. 2472-2477, 2011.

[76] S. Ghosh, S. Barg, S. M. Jeong, and K. Ostrikov, "Heteroatom-Doped and Oxygen-Functionalized Nanocarbons for High-Performance Supercapacitors," *Advanced Energy Materials,* vol. 10, no. 32, p. 2001239, 2020, doi: https://doi.org/10.1002/aenm.202001239.

[77] C. Poochai *et al.*, "High performance coin-cell and pouch-cell supercapacitors based on nitrogen-doped reduced graphene oxide electrodes with phenylenediamine-mediated organic electrolyte," *Applied Surface Science,* vol. 489, pp. 989-1001, 2019.

[78] F. Su *et al.*, "Nitrogen-containing microporous carbon nanospheres with improved capacitive properties," *Energy & Environmental Science,* 10.1039/C0EE00277A vol. 4, no. 3, pp. 717-724, 2011, doi: 10.1039/C0EE00277A.

[79] T. Lin *et al.*, "Nitrogen-doped mesoporous carbon of extraordinary capacitance for electrochemical energy storage," *Science,* vol. 350, no. 6267, pp. 1508-1513, 2015, doi: doi:10.1126/science.aab3798.

[80] W. Wang *et al.*, "A Novel Exfoliation Strategy to Significantly Boost the Energy Storage Capability of Commercial Carbon Cloth," *Advanced Materials,* vol. 27, no. 23, pp. 3572-3578, 2015, doi: https://doi.org/10.1002/adma.201500707.

[81] H.-f. Xia *et al.*, "Surface engineered carbon-cloth with broadening voltage window for boosted energy density aqueous supercapacitors," *Carbon,* vol. 162, pp. 136-146, 2020/06/01/ 2020, doi: https://doi.org/10.1016/j.carbon.2020.02.033.

[82] D.-Y. Feng, Y. Song, Z.-H. Huang, X.-X. Xu, and X.-X. Liu, "Rate capability improvement of polypyrrole via integration with functionalized commercial carbon cloth for pseudocapacitor," *Journal of Power Sources,* vol. 324, pp. 788-797, 2016/08/30/ 2016, doi: https://doi.org/10.1016/j.jpowsour.2016.05.112.

[83] G. Wang *et al.*, "Solid-state supercapacitor based on activated carbon cloths exhibits excellent rate capability," (in eng), *Adv Mater,* vol. 26, no. 17, pp. 2676-82, 2615, May 2014, doi: 10.1002/adma.201304756.

[84] Z. Miao *et al.*, "High-Performance Symmetric Supercapacitor Constructed Using Carbon Cloth Boosted by Engineering Oxygen-Containing Functional Groups," (in eng), *ACS Appl Mater Interfaces,* vol. 11, no. 19, pp. 18044-18050, May 15 2019, doi: 10.1021/acsami.9b04426.

[85] B. Ouyang, Y. Zhang, Y. Wang, Z. Zhang, H. J. Fan, and R. S. Rawat, "Plasma surface functionalization induces nanostructuring and nitrogen-doping in carbon cloth with enhanced energy storage performance," *Journal of Materials Chemistry A,* 10.1039/C6TA08155J vol. 4, no. 45, pp. 17801-17808, 2016, doi: 10.1039/C6TA08155J.

[86] Y.-J. Gu, W. Wen, and J.-M. Wu, "Simple air calcination affords commercial carbon cloth with high areal specific capacitance for symmetrical supercapacitors," *Journal of Materials Chemistry A,* 10.1039/C8TA07561A vol. 6, no. 42, pp. 21078-21086, 2018, doi: 10.1039/C8TA07561A.

[87] Z. Li, L. Wang, Y. Li, Y. Feng, and W. Feng, "Carbon-based functional nanomaterials: Preparation, properties and applications," *Composites Science and Technology,* vol. 179, pp. 10-40, 2019/07/28/ 2019, doi: https://doi.org/10.1016/j.compscitech.2019.04.028.

[88] J. Liang, Y. Jiao, M. Jaroniec, and S. Z. Qiao, "Sulfur and Nitrogen Dual-Doped Mesoporous Graphene Electrocatalyst for Oxygen Reduction with Synergistically Enhanced Performance," *Angewandte Chemie International Edition,* vol. 51, no. 46, pp. 11496-11500, 2012, doi: https://doi.org/10.1002/anie.201206720.

[89] Z.-S. Wu *et al.*, "Three-Dimensional Nitrogen and Boron Co-doped Graphene for High-Performance All-Solid-State Supercapacitors," *Advanced Materials,* vol. 24, no. 37, pp. 5130-5135, 2012, doi: https://doi.org/10.1002/adma.201201948.

[90] Y. Zhao *et al.*, "N-P-O co-doped high performance 3D graphene prepared through red phosphorous-assisted “cutting-thin” technique: A universal synthesis and multifunctional applications," *Nano Energy,* vol. 28, pp. 346-355, 2016/10/01/ 2016, doi: https://doi.org/10.1016/j.nanoen.2016.08.053.

[91] W. Chen, M. Wan, Q. Liu, X. Xiong, F. Yu, and Y. Huang, "Heteroatom-Doped Carbon Materials: Synthesis, Mechanism, and Application for Sodium-Ion Batteries," *Small Methods,* vol. 3, no. 4, p. 1800323, 2019, doi: https://doi.org/10.1002/smtd.201800323.

[92] J. Li *et al.*, "Three-dimensional nitrogen and phosphorus co-doped carbon quantum dots/reduced graphene oxide composite aerogels with a hierarchical porous structure as superior electrode materials for supercapacitors," *Journal of Materials Chemistry A,* 10.1039/C9TA08151H vol. 7, no. 46, pp. 26311-26325, 2019, doi: 10.1039/C9TA08151H.

[93] C. Han *et al.*, "Organic quinones towards advanced electrochemical energy storage: recent advances and challenges," *Journal of Materials Chemistry A,* 10.1039/C9TA05252F vol. 7, no. 41, pp. 23378-23415, 2019, doi: 10.1039/C9TA05252F.

[94] J. P. Jyothibasu, R.-H. Wang, Y.-C. Tien, C.-C. Kuo, and R.-H. Lee, "Lignin-Derived Quinone Redox Moieties for Bio-Based Supercapacitors," *Polymers,* vol. 14, no. 15, p. 3106, 2022. [Online]. Available: https://www.mdpi.com/2073-4360/14/15/3106.

[95] D. P. Dubal, N. R. Chodankar, D.-H. Kim, and P. Gomez-Romero, "Towards flexible solid-state supercapacitors for smart and wearable electronics," *Chemical Society Reviews,* vol. 47, no. 6, pp. 2065-2129, 2018.

[96] Q. Su, S. Pang, V. Alijani, C. Li, X. Feng, and K. Müllen, "Composites of graphene with large aromatic molecules," *Adv. Mater,* vol. 21, no. 31, pp. 3191-3195, 2009.

[97] H. Liu, X. Cheng, Y. Chong, H. Yuan, J.-Q. Huang, and Q. Zhang, "Advanced electrode processing of lithium ion batteries: A review of powder technology in battery fabrication," *Particuology,* vol. 57, pp. 56-71, 2021/08/01/ 2021, doi: https://doi.org/10.1016/j.partic.2020.12.003.

[98] M. Jia, M. Wang, and Y. Zhou, "A flexible supercapacitor electrode based on carbonized cotton fiber/juglone-modified graphene hydrogel," *Journal of Materials Science,* vol. 57, no. 47, pp. 21654-21666, 2022/12/01 2022, doi: 10.1007/s10853-022-08010-0.

[99] D. Xu, C. Zhang, and Y. Li, "Molecular engineering redox-active organic materials for nonaqueous redox flow battery," *Current Opinion in Chemical Engineering,* vol. 37, p. 100851, 2022/09/01/ 2022, doi: https://doi.org/10.1016/j.coche.2022.100851.

[100] A. Gouda, A. Masson, M. Hoseinizadeh, F. Soavi, and C. Santato, "Biosourced quinones for high-performance environmentally benign electrochemical capacitors via interface engineering," *Communications Chemistry,* vol. 5, no. 1, p. 98, 2022/08/20 2022, doi: 10.1038/s42004-022-00719-y.

[101] M. d'Ischia, A. Napolitano, A. Pezzella, P. Meredith, and M. Buehler, "Melanin Biopolymers: Tailoring Chemical Complexity for Materials Design," *Angewandte Chemie International Edition,* vol. 59, no. 28, pp. 11196-11205, 2020, doi: https://doi.org/10.1002/anie.201914276.

[102] D. Niyonkuru *et al.*, "A nanoscale study of the structure and electrical response of Sepia eumelanin," *Nanoscale Advances,* 10.1039/D3NA00355H vol. 5, no. 19, pp. 5295-5300, 2023, doi: 10.1039/D3NA00355H.

[103] P. Kumar *et al.*, "Melanin-based flexible supercapacitors," *Journal of Materials Chemistry C,* 10.1039/C6TC03739A vol. 4, no. 40, pp. 9516-9525, 2016, doi: 10.1039/C6TC03739A.

[104] H. A. Galeb *et al.*, "Melanins as Sustainable Resources for Advanced Biotechnological Applications," (in eng), *Glob Chall,* vol. 5, no. 2, p. 2000102, Feb 2021, doi: 10.1002/gch2.202000102.

[105] E. Vahidzadeh, A. P. Kalra, and K. Shankar, "Melanin-based electronics: From proton conductors to photovoltaics and beyond," (in eng), *Biosens Bioelectron,* vol. 122, pp. 127-139, Dec 30 2018, doi: 10.1016/j.bios.2018.09.026.

[106] J. V. Paulin *et al.*, "Eumelanin-based multisensory platform: A case of study for photolithographic patterning," *Applied Materials Today,* vol. 28, p. 101525, 2022/08/01/ 2022, doi: https://doi.org/10.1016/j.apmt.2022.101525.

[107] Y. J. Kim, W. Wu, S.-E. Chun, J. F. Whitacre, and C. J. Bettinger, "Biologically derived melanin electrodes in aqueous sodium-ion energy storage devices," *Proceedings of the National Academy of Sciences,* vol. 110, no. 52, pp. 20912-20917, 2013, doi: doi:10.1073/pnas.1314345110.

[108] F. Cheng *et al.*, "Squid inks-derived nanocarbons with unique “shell@pearls” structure for high performance supercapacitors," *Journal of Power Sources,* vol. 354, pp. 116-123, 2017/06/30/ 2017, doi: https://doi.org/10.1016/j.jpowsour.2017.04.016.

[109] R. Xu, A. Gouda, M. F. Caso, F. Soavi, and C. Santato, "Melanin: A Greener Route To Enhance Energy Storage under Solar Light," (in eng), *ACS Omega,* vol. 4, no. 7, pp. 12244-12251, Jul 31 2019, doi: 10.1021/acsomega.9b01039.

[110] N. Al-Shamery *et al.*, "Sustainable organic electrodes using black soldier fly-derived melanin for zinc-ion hybrid capacitors," *Communications Materials,* vol. 5, no. 1, p. 156, 2024/08/17 2024, doi: 10.1038/s43246-024-00602-4.

[111] A. K. Das, M. N. Islam, M. O. Faruk, M. Ashaduzzaman, and R. Dungani, "Review on tannins: Extraction processes, applications and possibilities," *South African Journal of Botany,* vol. 135, pp. 58-70, 2020/12/01/ 2020, doi: https://doi.org/10.1016/j.sajb.2020.08.008.

[112] K. Chira, G. Schmauch, C. Saucier, S. Fabre, and P.-L. Teissedre, "Grape Variety Effect on Proanthocyanidin Composition and Sensory Perception of Skin and Seed Tannin Extracts from Bordeaux Wine Grapes (Cabernet Sauvignon and Merlot) for Two Consecutive Vintages (2006 and 2007)," *Journal of Agricultural and Food Chemistry,* vol. 57, no. 2, pp. 545-553, 2009/01/28 2009, doi: 10.1021/jf802301g.

[113] T. Sepperer *et al.*, "Purification of industrial tannin extract through simple solid-liquid extractions," *Industrial Crops and Products,* vol. 139, p. 111502, 2019/11/01/ 2019, doi: https://doi.org/10.1016/j.indcrop.2019.111502.

[114] A. Arbenz and L. Avérous, "Chemical modification of tannins to elaborate aromatic biobased macromolecular architectures," *Green Chemistry,* 10.1039/C5GC00282F vol. 17, no. 5, pp. 2626-2646, 2015, doi: 10.1039/C5GC00282F.

[115] A. Pizzi, "Chapter 8 - Tannins: Major Sources, Properties and Applications," in *Monomers, Polymers and Composites from Renewable Resources*, M. N. Belgacem and A. Gandini Eds. Amsterdam: Elsevier, 2008, pp. 179-199.

[116] M. Y. GUO Linxin, QIANG Taotao, REN Longfang, "Review on structure modification of plant tannins," *CIESC Journal,* vol. 72, no. 5, pp. 2448-2464, 2021-05-05 2021, doi: 10.11949/0438-1157.20201355.

[117] K. B. Martinez, J. D. Mackert, and M. K. McIntosh, "Chapter 18 - Polyphenols and Intestinal Health," in *Nutrition and Functional Foods for Healthy Aging*, R. R. Watson Ed.: Academic Press, 2017, pp. 191-210.

[118] T. Mori and T. Town, "Chapter 100 - A Naturally Occurring β-Secretase Modulator, Tannic Acid, Improves Behavioral Impairment and Mitigates Alzheimer-Like Pathology," in *Diet and Nutrition in Dementia and Cognitive Decline*, C. R. Martin and V. R. Preedy Eds. San Diego: Academic Press, 2015, pp. 1069-1079.

[119] Z. Osman, A. Pizzi, M. E. Elbadawi, J. Mehats, W. Mohammed, and B. Charrier, "Effect of Technological Factors on the Extraction of Polymeric Condensed Tannins from Acacia Species," *Polymers,* vol. 16, no. 11, p. 1550, 2024. [Online]. Available: https://www.mdpi.com/2073-4360/16/11/1550.

[120] A. Pizzi, "Tannins: Prospectives and Actual Industrial Applications," (in eng), *Biomolecules,* vol. 9, no. 8, Aug 5 2019, doi: 10.3390/biom9080344.

[121] Y. Zhou *et al.*, "Synthesis and capability evaluation of quinone-enriched polymer with extended π-conjugated and contorted structures for efficient energy storage," *Electrochimica Acta,* vol. 476, p. 143693, 2024/02/01/ 2024, doi: https://doi.org/10.1016/j.electacta.2023.143693.

[122] T. Cai *et al.*, "Stable cycling of small molecular organic electrode materials enabled by high concentration electrolytes," *Energy Storage Materials,* vol. 31, pp. 318-327, 2020.

[123] L. Jiao *et al.*, "A novel organic molecule electrode based on organic polymer functionalized graphene for supercapacitor with high-performance," *Journal of Energy Storage,* vol. 52, p. 104777, 2022/08/01/ 2022, doi: https://doi.org/10.1016/j.est.2022.104777.

[124] X.-P. Gao and H.-X. Yang, "Multi-electron reaction materials for high energy density batteries," *Energy & Environmental Science,* 10.1039/B916098A vol. 3, no. 2, pp. 174-189, 2010, doi: 10.1039/B916098A.

[125] I. K. Ilic *et al.*, "Sustainable Cathodes for Lithium-Ion Energy Storage Devices Based on Tannic Acid—Toward Ecofriendly Energy Storage," *Advanced Sustainable Systems,* vol. 5, no. 1, p. 2000206, 2021, doi: https://doi.org/10.1002/adsu.202000206.

[126] H. Tonnoir, D. Huo, R. L. S. Canevesi, V. Fierro, A. Celzard, and R. Janot, "Tannin-based hard carbons as high-performance anode materials for sodium-ion batteries," *Materials Today Chemistry,* vol. 23, p. 100614, 2022/03/01/ 2022, doi: https://doi.org/10.1016/j.mtchem.2021.100614.

[127] M.-Y. Jia, L.-S. Xu, Y. Li, C.-L. Yao, and X.-J. Jin, "Synthesis and characterization of graphene/carbonized paper/tannic acid for flexible composite electrodes," *New Journal of Chemistry,* 10.1039/C8NJ02898B vol. 42, no. 17, pp. 14576-14585, 2018, doi: 10.1039/C8NJ02898B.

[128] J. Y. Oh *et al.*, "Metal–Phenolic Carbon Nanocomposites for Robust and Flexible Energy-Storage Devices," *ChemSusChem,* vol. 10, no. 8, pp. 1675-1682, 2017, doi: https://doi.org/10.1002/cssc.201601615.

[129] N. Elgrishi, K. J. Rountree, B. D. McCarthy, E. S. Rountree, T. T. Eisenhart, and J. L. Dempsey, "A Practical Beginner's Guide to Cyclic Voltammetry," *Journal of Chemical Education,* vol. 95, no. 2, pp. 197-206, 2018/02/13 2018, doi: 10.1021/acs.jchemed.7b00361.

[130] P. Simon and Y. Gogotsi, "Perspectives for electrochemical capacitors and related devices," *Nature Materials,* vol. 19, no. 11, pp. 1151-1163, 2020/11/01 2020, doi: 10.1038/s41563-020-0747-z.

[131] S. A. Arote, "Electrochemical energy storage mechanisms and performance assessments: an overview," *Electrochemical Energy Storage Devices and Supercapacitors*: IOP Publishing, 2021, pp. 1-1-1-34. [Online]. Available: https://dx.doi.org/10.1088/978-0-7503-3103-6ch1

[132] G. C. Allan and J. T. Woodcock, "A review of the flotation of native gold and electrum," *Minerals Engineering,* vol. 14, no. 9, pp. 931-962, 2001/09/01/ 2001, doi: https://doi.org/10.1016/S0892-6875(01)00103-0.

[133] D. S. Macedo, T. Rodopoulos, M. Vepsäläinen, S. Bajaj, and C. F. Hogan, "More Accurate Measurement of Return Peak Current in Cyclic Voltammetry Using Diffusional Baseline Fitting," *Analytical Chemistry,* vol. 96, no. 4, pp. 1530-1537, 2024/01/30 2024, doi: 10.1021/acs.analchem.3c04181.

[134] N. Jäckel, P. Simon, Y. Gogotsi, and V. Presser, "Increase in Capacitance by Subnanometer Pores in Carbon," *ACS Energy Letters,* vol. 1, no. 6, pp. 1262-1265, 2016/12/09 2016, doi: 10.1021/acsenergylett.6b00516.

[135] T. S. Mathis, N. Kurra, X. Wang, D. Pinto, P. Simon, and Y. Gogotsi, "Energy Storage Data Reporting in Perspective—Guidelines for Interpreting the Performance of Electrochemical Energy Storage Systems," *Advanced Energy Materials,* vol. 9, no. 39, p. 1902007, 2019, doi: https://doi.org/10.1002/aenm.201902007.

[136] B.-A. Mei, O. Munteshari, J. Lau, B. Dunn, and L. Pilon, "Physical Interpretations of Nyquist Plots for EDLC Electrodes and Devices," *The Journal of Physical Chemistry C,* vol. 122, no. 1, pp. 194-206, 2018/01/11 2018, doi: 10.1021/acs.jpcc.7b10582.

[137] A. C. Lazanas and M. I. Prodromidis, "Electrochemical Impedance Spectroscopy─A Tutorial," *ACS Measurement Science Au,* vol. 3, no. 3, pp. 162-193, 2023/06/21 2023, doi: 10.1021/acsmeasuresciau.2c00070.

[138] T. Schoetz, L. W. Gordon, S. Ivanov, A. Bund, D. Mandler, and R. J. Messinger, "Disentangling faradaic, pseudocapacitive, and capacitive charge storage: A tutorial for the characterization of batteries, supercapacitors, and hybrid systems," *Electrochimica Acta,* vol. 412, p. 140072, 2022/04/20/ 2022, doi: https://doi.org/10.1016/j.electacta.2022.140072.

[139] Q. Wu *et al.*, "Cyclic stability of supercapacitors: materials, energy storage mechanism, test methods, and device," *Journal of Materials Chemistry A,* 10.1039/D1TA06815F vol. 9, no. 43, pp. 24094-24147, 2021, doi: 10.1039/D1TA06815F.

[140] Poonam, K. Sharma, A. Arora, and S. K. Tripathi, "Review of supercapacitors: Materials and devices," *Journal of Energy Storage,* vol. 21, pp. 801-825, 2019/02/01/ 2019, doi: https://doi.org/10.1016/j.est.2019.01.010.

[141] D. Y. Hoo *et al.*, "Ultrasonic cavitation: An effective cleaner and greener intensification technology in the extraction and surface modification of nanocellulose," *Ultrasonics Sonochemistry,* vol. 90, p. 106176, 2022/11/01/ 2022, doi: https://doi.org/10.1016/j.ultsonch.2022.106176.

[142] A. R. Deshmukh, P. K. Chaturvedi, S.-Y. Lee, W.-Y. Park, and B. S. Kim, "One-Step Green Production of Biocompatible Functionalized Few-Layer Graphene/Boron Nitride Nanosheet Hybrids Using Tannic Acid-Based Liquid-Phase Exfoliation," *ACS Sustainable Chemistry & Engineering,* vol. 10, no. 29, pp. 9573-9583, 2022/07/25 2022, doi: 10.1021/acssuschemeng.2c02484.

[143] E. A. Neppiras, "Acoustic cavitation," *Physics Reports,* vol. 61, no. 3, pp. 159-251, 1980/05/01/ 1980, doi: https://doi.org/10.1016/0370-1573(80)90115-5.

[144] S. Manickam *et al.*, "Ultrasonics and sonochemistry: Editors' perspective," *Ultrasonics Sonochemistry,* vol. 99, p. 106540, 2023/10/01/ 2023, doi: https://doi.org/10.1016/j.ultsonch.2023.106540.

[145] N. Kutlu *et al.*, "Impact of ultrasonication applications on color profile of foods," *Ultrasonics Sonochemistry,* vol. 89, p. 106109, 2022/09/01/ 2022, doi: https://doi.org/10.1016/j.ultsonch.2022.106109.

[146] S. Pye, F. G. N. Li, J. Price, and B. Fais, "Achieving net-zero emissions through the reframing of UK national targets in the post-Paris Agreement era," *Nature Energy,* vol. 2, no. 3, p. 17024, 2017/03/06 2017, doi: 10.1038/nenergy.2017.24.

[147] W. D. Fletcher and C. B. Smith, *Reaching Net Zero: What it Takes to Solve the Global Climate Crisis*. Elsevier, 2020.

[148] H. D. Yoo, E. Markevich, G. Salitra, D. Sharon, and D. Aurbach, "On the challenge of developing advanced technologies for electrochemical energy storage and conversion," *Materials Today,* vol. 17, no. 3, pp. 110-121, 2014/04/01/ 2014, doi: https://doi.org/10.1016/j.mattod.2014.02.014.

[149] D. Bogdanov *et al.*, "Low-cost renewable electricity as the key driver of the global energy transition towards sustainability," *Energy,* vol. 227, p. 120467, 2021/07/15/ 2021, doi: https://doi.org/10.1016/j.energy.2021.120467.

[150] R. Kötz and M. Carlen, "Principles and applications of electrochemical capacitors," *Electrochimica Acta,* vol. 45, no. 15, pp. 2483-2498, 2000/05/03/ 2000, doi: https://doi.org/10.1016/S0013-4686(00)00354-6.

[151] M. Sarno, "Chapter 22 - Nanotechnology in energy storage: the supercapacitors," in *Studies in Surface Science and Catalysis*, vol. 179, A. Basile, G. Centi, M. D. Falco, and G. Iaquaniello Eds.: Elsevier, 2020, pp. 431-458.

[152] R. Wang, M. Yao, and Z. Niu, "Smart supercapacitors from materials to devices," *InfoMat,* vol. 2, no. 1, pp. 113-125, 2020, doi: https://doi.org/10.1002/inf2.12037.

[153] E. Pomerantseva, F. Bonaccorso, X. Feng, Y. Cui, and Y. Gogotsi, "Energy storage: The future enabled by nanomaterials," *Science,* vol. 366, no. 6468, p. eaan8285, 2019, doi: doi:10.1126/science.aan8285.

[154] C. An, Y. Zhang, H. Guo, and Y. Wang, "Metal oxide-based supercapacitors: progress and prospectives," *Nanoscale Advances,* 10.1039/C9NA00543A vol. 1, no. 12, pp. 4644-4658, 2019, doi: 10.1039/C9NA00543A.

[155] J. H. Park, O. O. Park, K. H. Shin, C. S. Jin, and J. H. Kim, "An Electrochemical Capacitor Based on a Ni(OH)[sub 2]/Activated Carbon Composite Electrode," *Electrochemical and Solid-State Letters,* vol. 5, no. 2, p. H7, 2002, doi: 10.1149/1.1432245.

[156] C. Zhao, X. Jia, K. Shu, C. Yu, G. G. Wallace, and C. Wang, "Conducting polymer composites for unconventional solid-state supercapacitors," *Journal of Materials Chemistry A,* 10.1039/C9TA13432H vol. 8, no. 9, pp. 4677-4699, 2020, doi: 10.1039/C9TA13432H.

[157] Q. Jiang, N. Kurra, M. Alhabeb, Y. Gogotsi, and H. N. Alshareef, "All Pseudocapacitive MXene-RuO2 Asymmetric Supercapacitors," *Advanced Energy Materials,* vol. 8, no. 13, p. 1703043, 2018, doi: https://doi.org/10.1002/aenm.201703043.

[158] Y.-J. Hsiao and L.-Y. Lin, "Enhanced Surface Area, Graphene Quantum Dots, and Functional Groups for the Simple Acid-Treated Carbon Fiber Electrode of Flexible Fiber-Type Solid-State Supercapacitors without Active Materials," *ACS Sustainable Chemistry & Engineering,* vol. 8, no. 6, pp. 2453-2461, 2020/02/17 2020, doi: 10.1021/acssuschemeng.9b06569.

[159] H. Nishide, "Organic redox polymers as electrochemical energy materials," *Green Chemistry,* 10.1039/D2GC00981A vol. 24, no. 12, pp. 4650-4679, 2022, doi: 10.1039/D2GC00981A.

[160] H. Yang *et al.*, "Molecular engineering of carbonyl organic electrodes for rechargeable metal-ion batteries: fundamentals, recent advances, and challenges," *Energy & Environmental Science,* 10.1039/D1EE00419K vol. 14, no. 8, pp. 4228-4267, 2021, doi: 10.1039/D1EE00419K.

[161] R. Chen, H. Ling, Q. Huang, Y. Yang, and X. Wang, "Interface Engineering on Cellulose-Based Flexible Electrode Enables High Mass Loading Wearable Supercapacitor with Ultrahigh Capacitance and Energy Density," *Small,* vol. 18, no. 9, p. 2106356, 2022, doi: https://doi.org/10.1002/smll.202106356.

[162] G. Würger, L. J. McGaw, and J. N. Eloff, "Tannin content of leaf extracts of 53 trees used traditionally to treat diarrhoea is an important criterion in selecting species for further work," *South African Journal of Botany,* vol. 90, pp. 114-117, 2014/01/01/ 2014, doi: https://doi.org/10.1016/j.sajb.2013.11.003.

[163] A. U. N. Tinkílíç, "Spectrophotometric determination of the tannin contents of various Turkish black tea, beer and wine samples," *International Journal of Food Sciences and Nutrition,* vol. 52, no. 3, pp. 289-294, 2001/01/01 2001, doi: 10.1080/09637480120044147.

[164] H.-F. Gu, C.-M. Li, Y.-j. Xu, W.-f. Hu, M.-h. Chen, and Q.-h. Wan, "Structural features and antioxidant activity of tannin from persimmon pulp," *Food Research International,* vol.

41, no. 2, pp. 208-217, 2008/01/01/ 2008, doi: https://doi.org/10.1016/j.foodres.2007.11.011.

[165] L. Falcão and M. E. M. Araújo, "Vegetable Tannins Used in the Manufacture of Historic Leathers," (in eng), *Molecules (Basel, Switzerland),* vol. 23, no. 5, p. 1081, 2018, doi: 10.3390/molecules23051081.

[166] M. Fraga-Corral *et al.*, "Traditional Applications of Tannin Rich Extracts Supported by Scientific Data: Chemical Composition, Bioavailability and Bioaccessibility," (in eng), *Foods (Basel, Switzerland),* vol. 10, no. 2, p. 251, 2021, doi: 10.3390/foods10020251.

[167] Y. Zhao, C. Fang, C. Jin, Z. Bao, G. Yang, and Y. Jin, "Catechin from green tea had the potential to decrease the chlorpyrifos induced oxidative stress in larval zebrafish (Danio rerio)," *Pesticide Biochemistry and Physiology,* p. 105028, 2021/12/28/ 2021, doi: https://doi.org/10.1016/j.pestbp.2021.105028.

[168] S. Alipoori, S. Mazinani, S. H. Aboutalebi, and F. Sharif, "Review of PVA-based gel polymer electrolytes in flexible solid-state supercapacitors: Opportunities and challenges," *journal of energy storage,* vol. 27, p. 101072, 2020.

[169] X. Fan *et al.*, "Porous nanocomposite gel polymer electrolyte with high ionic conductivity and superior electrolyte retention capability for long-cycle-life flexible zinc–air batteries," *Nano Energy,* vol. 56, pp. 454-462, 2019/02/01/ 2019, doi: https://doi.org/10.1016/j.nanoen.2018.11.057.

[170] X. Cheng, J. Pan, Y. Zhao, M. Liao, and H. Peng, "Gel Polymer Electrolytes for Electrochemical Energy Storage," *Advanced Energy Materials,* vol. 8, no. 7, p. 1702184, 2018, doi: https://doi.org/10.1002/aenm.201702184.

[171] J. Castillo *et al.*, "Safe, Flexible, and High-Performing Gel-Polymer Electrolyte for Rechargeable Lithium Metal Batteries," *Chemistry of Materials,* vol. 33, no. 22, pp. 8812-8821, 2021/11/23 2021, doi: 10.1021/acs.chemmater.1c02952.

[172] K. Sun *et al.*, "High energy density of quasi-solid-state supercapacitor based on redox-mediated gel polymer electrolyte," *RSC Advances,* 10.1039/C6RA06797B vol. 6, no. 60, pp. 55225-55232, 2016, doi: 10.1039/C6RA06797B.

[173] A. G. Destaye, C.-K. Lin, and C.-K. Lee, "Glutaraldehyde Vapor Cross-linked Nanofibrous PVA Mat with in Situ Formed Silver Nanoparticles," *ACS Applied Materials & Interfaces,* vol. 5, no. 11, pp. 4745-4752, 2013/06/12 2013, doi: 10.1021/am401730x.

[174] O. Alonso-López, S. López-Ibáñez, and R. Beiras, "Assessment of Toxicity and Biodegradability of Poly(vinyl alcohol)-Based Materials in Marine Water," (in eng), *Polymers (Basel),* vol. 13, no. 21, Oct 29 2021, doi: 10.3390/polym13213742.

[175] R. K. Morris, A. P. Hilker, T. M. Mattice, S. M. Donovan, M. T. Wentzel, and P. H. Willoughby, "Simple and Versatile Protocol for Preparing Self-Healing Poly(vinyl alcohol) Hydrogels," *Journal of Chemical Education,* vol. 96, no. 10, pp. 2247-2252, 2019/10/08 2019, doi: 10.1021/acs.jchemed.9b00161.

[176] Y. Gogotsi and P. Simon, "True Performance Metrics in Electrochemical Energy Storage," *Science,* vol. 334, no. 6058, pp. 917-918, 2011, doi: doi:10.1126/science.1213003.

[177] D. G. Barrett, T. S. Sileika, and P. B. Messersmith, "Molecular diversity in phenolic and polyphenolic precursors of tannin-inspired nanocoatings," *Chemical Communications,* 10.1039/C4CC02961E vol. 50, no. 55, pp. 7265-7268, 2014, doi: 10.1039/C4CC02961E.

[178] Z. Song *et al.*, "A universal strategy to obtain highly redox-active porous carbons for efficient energy storage," *Journal of Materials Chemistry A,* 10.1039/C9TA13520K vol. 8, no. 7, pp. 3717-3725, 2020, doi: 10.1039/C9TA13520K.

[179] S. Song, F. Ma, G. Wu, D. Ma, W. Geng, and J. Wan, "Facile self-templating large scale preparation of biomass-derived 3D hierarchical porous carbon for advanced supercapacitors," *Journal of Materials Chemistry A,* 10.1039/C5TA04721H vol. 3, no. 35, pp. 18154-18162, 2015, doi: 10.1039/C5TA04721H.

[180] Y. Li, C. Zhang, Y. Jiang, T.-J. Wang, and H. Wang, "Effects of the hydration ratio on the electrosorption selectivity of ions during capacitive deionization," *Desalination,* vol. 399, pp. 171-177, 2016/12/01/ 2016, doi: https://doi.org/10.1016/j.desal.2016.09.011.

[181] K. Fic, G. Lota, M. Meller, and E. Frackowiak, "Novel insight into neutral medium as electrolyte for high-voltage supercapacitors," *Energy & Environmental Science,* 10.1039/C1EE02262H vol. 5, no. 2, pp. 5842-5850, 2012, doi: 10.1039/C1EE02262H.

[182] Y. Fang, Q. Zhang, and L. Cui, "Recent progress of mesoporous materials for high performance supercapacitors," *Microporous and Mesoporous Materials,* vol. 314, p. 110870, 2021/02/01/ 2021, doi: https://doi.org/10.1016/j.micromeso.2020.110870.

[183] Y. Zhang *et al.*, "Review of macroporous materials as electrochemical supercapacitor electrodes," *Journal of Materials Science,* vol. 52, no. 19, pp. 11201-11228, 2017/10/01 2017, doi: 10.1007/s10853-017-0955-3.

[184] T. Liu, B. Lee, B. G. Kim, M. J. Lee, J. Park, and S. W. Lee, "In Situ Polymerization of Dopamine on Graphene Framework for Charge Storage Applications," *Small,* vol. 14, no. 34, p. 1801236, 2018, doi: https://doi.org/10.1002/smll.201801236.

[185] H. Yoon *et al.*, "Pseudocapacitive slurry electrodes using redox-active quinone for high-performance flow capacitors: an atomic-level understanding of pore texture and capacitance enhancement," *Journal of Materials Chemistry A,* 10.1039/C5TA05403F vol. 3, no. 46, pp. 23323-23332, 2015, doi: 10.1039/C5TA05403F.

[186] H.-J. Kim and Y.-K. Han, "How can we describe the adsorption of quinones on activated carbon surfaces?," *Current Applied Physics,* vol. 16, no. 10, pp. 1437-1441, 2016/10/01/ 2016, doi: https://doi.org/10.1016/j.cap.2016.08.009.

[187] A. Maleki, D. Nematollahi, J. Clausmeyer, J. Henig, N. Plumeré, and W. Schuhmann, "Electrodeposition of Catechol on Glassy Carbon Electrode and Its Electrocatalytic Activity Toward NADH Oxidation," *Electroanalysis,* vol. 24, no. 10, pp. 1932-1936, 2012, doi: https://doi.org/10.1002/elan.201200251.

[188] S. Ardizzone, G. Fregonara, and S. Trasatti, ""“Inner” and “outer” active surface of RuO2 electrodes," *Electrochimica Acta,* vol. 35, no. 1, pp. 263-267, 1990/01/01/ 1990, doi: https://doi.org/10.1016/0013-4686(90)85068-X.

[189] A. M. Zardkhoshoui and S. S. Hosseiny Davarani, "An efficient hybrid supercapacitor based on Zn–Mn–Ni–S@NiSe core–shell architectures," *Sustainable Energy & Fuels,* 10.1039/D0SE01665A vol. 5, no. 3, pp. 900-913, 2021, doi: 10.1039/D0SE01665A.

[190] Q. Zheng *et al.*, "High performance solid-state supercapacitors based on highly conductive organogel electrolyte at low temperature," *Journal of Power Sources,* vol. 524, p. 231102, 2022/03/15/ 2022, doi: https://doi.org/10.1016/j.jpowsour.2022.231102.

[191] W. Li, A. Xu, Y. Zhang, Y. Yu, Z. Liu, and Y. Qin, "Metal-organic framework-derived Mn3O4 nanostructure on reduced graphene oxide as high-performance supercapacitor electrodes," *Journal of Alloys and Compounds,* vol. 897, p. 162640, 2022/03/15/ 2022, doi: https://doi.org/10.1016/j.jallcom.2021.162640.

[192] S. Mondal, U. Rana, and S. Malik, "Reduced Graphene Oxide/Fe3O4/Polyaniline Nanostructures as Electrode Materials for an All-Solid-State Hybrid Supercapacitor," *The Journal of Physical Chemistry C,* vol. 121, no. 14, pp. 7573-7583, 2017/04/13 2017, doi: 10.1021/acs.jpcc.6b10978.

[193] M. R. Biradar, A. V. Salkar, P. P. Morajkar, S. V. Bhosale, and S. V. Bhosale, "Designing neurotransmitter dopamine-functionalized naphthalene diimide molecular architectures for high-performance organic supercapacitor electrode materials," *New Journal of Chemistry,* 10.1039/D1NJ00269D vol. 45, no. 21, pp. 9346-9357, 2021, doi: 10.1039/D1NJ00269D.

[194] Z. J. Zhang, G. L. Deng, X. Huang, X. Wang, J. M. Xue, and X. Y. Chen, "Highly boosting the supercapacitor performance by polydopamine-induced surface modification of carbon materials and use of hydroquinone as an electrolyte additive," *Electrochimica Acta,* vol. 339, p. 135940, 2020/04/10/ 2020, doi: https://doi.org/10.1016/j.electacta.2020.135940.

[195] A. H. Muhr and J. M. V. Blanshard, "Diffusion in gels," *Polymer,* vol. 23, no. 7, pp. 1012-1026, 1982/07/01/ 1982, doi: https://doi.org/10.1016/0032-3861(82)90402-5.

[196] M. A. Lauffer, "Theory of diffusion in gels," *Biophysical Journal,* vol. 1, no. 3, pp. 205-213, 1961.

[197] D. Gielen, F. Boshell, D. Saygin, M. D. Bazilian, N. Wagner, and R. Gorini, "The role of renewable energy in the global energy transformation," *Energy Strategy Reviews,* vol. 24, pp. 38-50, 2019/04/01/ 2019, doi: https://doi.org/10.1016/j.esr.2019.01.006.

[198] E. T. Sayed *et al.*, "Renewable Energy and Energy Storage Systems," *Energies,* vol. 16, no. 3, p. 1415, 2023. [Online]. Available: https://www.mdpi.com/1996-1073/16/3/1415.

[199] J.-H. Lee, G. Yang, C.-H. Kim, R. L. Mahajan, S.-Y. Lee, and S.-J. Park, "Flexible solid-state hybrid supercapacitors for the internet of everything (IoE)," *Energy & Environmental Science,* 10.1039/D1EE03567C vol. 15, no. 6, pp. 2233-2258, 2022, doi: 10.1039/D1EE03567C.

[200] Z. Zhai *et al.*, "A review of carbon materials for supercapacitors," *Materials & Design,* vol. 221, p. 111017, 2022/09/01/ 2022, doi: https://doi.org/10.1016/j.matdes.2022.111017.

[201] L.-F. Chen *et al.*, "Synthesis of Nitrogen-Doped Porous Carbon Nanofibers as an Efficient Electrode Material for Supercapacitors," *ACS Nano,* vol. 6, no. 8, pp. 7092-7102, 2012/08/28 2012, doi: 10.1021/nn302147s.

[202] K. Komatsubara *et al.*, "Highly Oriented Carbon Nanotube Supercapacitors," *ACS Applied Nano Materials,* vol. 5, no. 1, pp. 1521-1532, 2022/01/28 2022, doi: 10.1021/acsanm.1c04236.

[203] B. Z. Yang *et al.*, "Binder-Free ω-Li3V2O5 Catalytic Network with Multi-Polarization Centers Assists Lithium–Sulfur Batteries for Enhanced Kinetics Behavior," *Advanced Functional Materials,* vol. 32, no. 8, p. 2110665, 2022, doi: https://doi.org/10.1002/adfm.202110665.

[204] Y. Q. Mi *et al.*, "In Situ Polymerized 1,3-Dioxolane Electrolyte for Integrated Solid-State Lithium Batteries," *Angewandte Chemie International Edition,* vol. 62, no. 12, p. e202218621, 2023, doi: https://doi.org/10.1002/anie.202218621.

[205] D. Zhang, C. Tan, W. Zhang, W. Pan, Q. Wang, and L. Li, "Expanded Graphite-Based Materials for Supercapacitors: A Review," *Molecules,* vol. 27, no. 3, p. 716, 2022. [Online]. Available: https://www.mdpi.com/1420-3049/27/3/716.

[206] X. Liu, W. Xu, D. Zheng, Z. Li, Y. Zeng, and X. Lu, "Carbon cloth as an advanced electrode material for supercapacitors: progress and challenges," *Journal of Materials Chemistry A,* 10.1039/D0TA03463K vol. 8, no. 35, pp. 17938-17950, 2020, doi: 10.1039/D0TA03463K.

[207] S. Zhang *et al.*, "Commercial carbon cloth: An emerging substrate for practical lithium metal batteries," *Energy Storage Materials,* vol. 48, pp. 172-190, 2022/06/01/ 2022, doi: https://doi.org/10.1016/j.ensm.2022.03.014.

[208] Q. Wang *et al.*, "Thermally Activated Multilayered Carbon Cloth as Flexible Supercapacitor Electrode Material with Significantly Enhanced Areal Energy Density," *ChemElectroChem,* vol. 6, no. 6, pp. 1768-1775, 2019, doi: https://doi.org/10.1002/celc.201801642.

[209] M. Xiang, L. He, N. Wang, J. Chen, and W. Hu, "Hydrothermally etching commercial carbon cloth to form a porous structure for flexible zinc-ion hybrid supercapacitors," *Applied Surface Science,* vol. 613, p. 156093, 2023/03/15/ 2023, doi: https://doi.org/10.1016/j.apsusc.2022.156093.

[210] Y. Han *et al.*, "Enhancing the Capacitive Storage Performance of Carbon Fiber Textile by Surface and Structural Modulation for Advanced Flexible Asymmetric Supercapacitors," *Advanced Functional Materials,* vol. 29, no. 7, p. 1806329, 2019, doi: https://doi.org/10.1002/adfm.201806329.

[211] N. R. Chodankar, S.-H. Ji, and D.-H. Kim, "Surface Modified Carbon Cloth via Nitrogen Plasma for Supercapacitor Applications," *Journal of The Electrochemical Society,* vol. 165, no. 11, p. A2446, 2018/08/09 2018, doi: 10.1149/2.0181811jes.

[212] H. Zhang, C. An, A. Yuan, Q. Deng, and J. Ning, "A non-conventional way to modulate the capacitive process on carbon cloth by mechanical stretching," *Electrochemistry Communications,* vol. 89, pp. 43-47, 2018/04/01/ 2018, doi: https://doi.org/10.1016/j.elecom.2018.02.017.

[213] C. Shen, Y. Xie, B. Zhu, M. Sanghadasa, Y. Tang, and L. Lin, "Wearable woven supercapacitor fabrics with high energy density and load-bearing capability," *Scientific Reports,* vol. 7, no. 1, p. 14324, 2017/10/30 2017, doi: 10.1038/s41598-017-14854-3.

[214] W. Zhu *et al.*, "Surface Engineering of Carbon Fiber Paper toward Exceptionally High-Performance and Stable Electrochemical Nitrite Sensing," *ACS Sensors,* vol. 4, no. 11, pp. 2980-2987, 2019/11/22 2019, doi: 10.1021/acssensors.9b01474.

[215] X. Zhou *et al.*, "Porous Mo–Co–S Nanosheets on Carbon Cloth for All-Solid-State Flexible Asymmetric Supercapacitors," *Advanced Materials Interfaces,* vol. 6, no. 22, p. 1901138, 2019, doi: https://doi.org/10.1002/admi.201901138.

[216] W. Wang *et al.*, "Uniformly highly dispersed hollow NiCo2S4 nanospheres anchored on carbon cloth as cathodes for high-performance hybrid supercapacitors," *Journal of Energy Storage,* vol. 85, p. 110948, 2024/04/30/ 2024, doi: https://doi.org/10.1016/j.est.2024.110948.

[217] M. Gao *et al.*, "Novel cyclic ultrasound-assisted liquid phase exfoliation of graphene in deionized water: A parameter study," *Materials Letters,* vol. 337, p. 134011, 2023/04/15/ 2023, doi: https://doi.org/10.1016/j.matlet.2023.134011.

[218] S. Shi, R. Zhong, L. Li, C. Wan, and C. Wu, "Ultrasound-assisted synthesis of graphene@MXene hybrid: A novel and promising material for electrochemical sensing," *Ultrasonics Sonochemistry,* vol. 90, p. 106208, 2022/11/01/ 2022, doi: https://doi.org/10.1016/j.ultsonch.2022.106208.

[219] M. Telkhozhayeva *et al.*, "Higher Ultrasonic Frequency Liquid Phase Exfoliation Leads to Larger and Monolayer to Few-Layer Flakes of 2D Layered Materials," *Langmuir,* vol. 37, no. 15, pp. 4504-4514, 2021/04/20 2021, doi: 10.1021/acs.langmuir.0c03668.

[220] X. Gu *et al.*, "Method of ultrasound-assisted liquid-phase exfoliation to prepare graphene," *Ultrasonics Sonochemistry,* vol. 58, p. 104630, 2019/11/01/ 2019, doi: https://doi.org/10.1016/j.ultsonch.2019.104630.

[221] K. Muthoosamy and S. Manickam, "State of the art and recent advances in the ultrasound-assisted synthesis, exfoliation and functionalization of graphene derivatives," *Ultrasonics Sonochemistry,* vol. 39, pp. 478-493, 2017/11/01/ 2017, doi: https://doi.org/10.1016/j.ultsonch.2017.05.019.

[222] L. Yang *et al.*, "Emergence of melanin-inspired supercapacitors," *Nano Today,* vol. 37, p. 101075, 2021/04/01/ 2021, doi: https://doi.org/10.1016/j.nantod.2020.101075.

[223] L. Yang *et al.*, "Synthetic Biopigment Supercapacitors," *ACS Applied Materials & Interfaces,* vol. 11, no. 33, pp. 30360-30367, 2019/08/21 2019, doi: 10.1021/acsami.9b10956.

[224] D. Niyonkuru *et al.*, "Locating the bandgap edges of eumelanin thin films for applications in organic electronics," *Journal of Chemical Technology & Biotechnology,* vol. 97, no. 4, pp. 837-843, 2022, doi: https://doi.org/10.1002/jctb.7011.

[225] E. Di Mauro, C. Santato, G. Soliveri, and R. Xu, "Natural melanin pigments and their interfaces with metal ions and oxides: emerging concepts and technologies," *MRS Communications,* vol. 7, no. 2, pp. 141-151, 2017, doi: 10.1557/mrc.2017.33.

[226] A. Gouda, S. R. Bobbara, M. Reali, and C. Santato, "Light-assisted melanin-based electrochemical energy storage: physicochemical aspects," *Journal of Physics D: Applied Physics,* vol. 53, no. 4, p. 043003, 2019/11/18 2020, doi: 10.1088/1361-6463/ab508b.

[227] Z. Ma, R. Zheng, Y. Liu, Y. Ying, and W. Shi, "Carbon nanotubes interpenetrating MOFs-derived Co-Ni-S composite spheres with interconnected architecture for high performance hybrid supercapacitor," *Journal of Colloid and Interface Science,* vol. 602, pp. 627-635, 2021/11/15/ 2021, doi: https://doi.org/10.1016/j.jcis.2021.06.027.

[228] M. Wang, J. Yang, S. Liu, M. Li, C. Hu, and J. Qiu, "Nitrogen-doped hierarchically porous carbon nanosheets derived from polymer/graphene oxide hydrogels for high-performance supercapacitors," *Journal of Colloid and Interface Science,* vol. 560, pp. 69-76, 2020/02/15/ 2020, doi: https://doi.org/10.1016/j.jcis.2019.10.037.

[229] C. Bathula *et al.*, "Sonochemically exfoliated polymer-carbon nanotube interface for high performance supercapacitors," *Journal of Colloid and Interface Science,* vol. 606, pp. 1792-1799, 2022/01/15/ 2022, doi: https://doi.org/10.1016/j.jcis.2021.08.136.

[230] A. Kaur *et al.*, "Temperature as a key parameter for graphene sono-exfoliation in water," *Ultrasonics Sonochemistry,* vol. 90, p. 106187, 2022/11/01/ 2022, doi: https://doi.org/10.1016/j.ultsonch.2022.106187.

[231] J. A. Morton *et al.*, "An eco-friendly solution for liquid phase exfoliation of graphite under optimised ultrasonication conditions," *Carbon,* vol. 204, pp. 434-446, 2023/02/01/ 2023, doi: https://doi.org/10.1016/j.carbon.2022.12.070.

[232] A. Miyaji, M. Kohno, Y. Inoue, and T. Baba, "Hydroxyl radical generation by dissociation of water molecules during 1.65 MHz frequency ultrasound irradiation under aerobic conditions," *Biochemical and Biophysical Research Communications,* vol. 483, no. 1, pp. 178-182, 2017/01/29/ 2017, doi: https://doi.org/10.1016/j.bbrc.2016.12.171.

[233] Y. Xu, H. Cao, Y. Xue, B. Li, and W. Cai, "Liquid-Phase Exfoliation of Graphene: An Overview on Exfoliation Media, Techniques, and Challenges," *Nanomaterials,* vol. 8, no. 11, p. 942, 2018. [Online]. Available: https://www.mdpi.com/2079-4991/8/11/942.

[234] G. Zhang *et al.*, "High-Performance and Ultra-Stable Lithium-Ion Batteries Based on MOF-Derived ZnO@ZnO Quantum Dots/C Core–Shell Nanorod Arrays on a Carbon Cloth Anode," *Advanced Materials,* vol. 27, no. 14, pp. 2400-2405, 2015, doi: https://doi.org/10.1002/adma.201405222.

[235] S. Meng *et al.*, "Metal-free and flexible surface-enhanced Raman scattering substrate based on oxidized carbon cloth," *Carbon,* vol. 189, pp. 152-161, 2022/04/15/ 2022, doi: https://doi.org/10.1016/j.carbon.2021.12.055.

[236] T. Xiong, T. L. Tan, L. Lu, W. S. V. Lee, and J. Xue, "Harmonizing Energy and Power Density toward 2.7 V Asymmetric Aqueous Supercapacitor," *Advanced Energy Materials,* vol. 8, no. 14, p. 1702630, 2018, doi: https://doi.org/10.1002/aenm.201702630.

[237] C. Buttersack, "Modeling of type IV and V sigmoidal adsorption isotherms," *Physical Chemistry Chemical Physics,* 10.1039/C8CP07751G vol. 21, no. 10, pp. 5614-5626, 2019, doi: 10.1039/C8CP07751G.

[238] L. Zhang, X. Yu, P. Zhu, R. Sun, and C.-p. Wong, "Surface functional treatment of carbon fiber with ultra wide potential range in neutral electrolyte for high performance supercapacitor," *Journal of Electroanalytical Chemistry,* vol. 876, p. 114478, 2020/11/01/ 2020, doi: https://doi.org/10.1016/j.jelechem.2020.114478.

[239] B. Amsden, "Diffusion in Polyelectrolyte Hydrogels: Application of an Obstruction-Scaling Model to Solute Diffusion in Calcium Alginate," *Macromolecules,* vol. 34, no. 5, pp. 1430-1435, 2001/02/01 2001, doi: 10.1021/ma001450e.

[240] R. F. Contamine, A. M. Wilhelm, J. Berlan, and H. Delmas, "Power measurement in sonochemistry," *Ultrasonics Sonochemistry,* vol. 2, no. 1, pp. S43-S47, 1995/01/01/ 1995, doi: https://doi.org/10.1016/1350-4177(94)00010-P.

[241] M. Reali *et al.*, "Electronic Transport in the Biopigment Sepia Melanin," *ACS Applied Bio Materials,* vol. 3, no. 8, pp. 5244-5252, 2020/08/17 2020, doi: 10.1021/acsabm.0c00373.

[242] P.-H. Wang, C.-H. Lin, L.-H. Tseng, and T.-C. Wen, "Superior hydrogel electrolytes in both ionic conductivity and electrochemical window from the immobilized pair ions for carbon-based supercapacitors," *Journal of the Taiwan Institute of Chemical Engineers,* vol. 118, pp. 152-158, 2021.

[243] M. Maoela *et al.*, "Electroanalytical Determination of Catechin Flavonoid in Ethyl Acetate Extracts of Medicinal Plants," *Int. J. Electrochem. Sci. International Journal,* vol. 4, pp. 1497-1510, 11/01 2009.

[244] Y. Hu, T. Zhang, X. Gong, Z. Wang, M. Wang, and S. Zhang, "Roles of Ultrasound on Hydroxyl Radical Generation and Bauxite Desulfurization from Water Electrolysis," *Journal of The Electrochemical Society,* vol. 165, no. 5, p. E177, 2018/03/28 2018, doi: 10.1149/2.0701805jes.

[245] A. V. Tyurnina *et al.*, "Ultrasonic exfoliation of graphene in water: A key parameter study," *Carbon,* vol. 168, pp. 737-747, 2020/10/30/ 2020, doi: https://doi.org/10.1016/j.carbon.2020.06.029.

[246] R. W. N. Nugroho, B. L. Tardy, S. M. Eldin, R. A. Ilyas, M. Mahardika, and N. Masruchin, "Controlling the critical parameters of ultrasonication to affect the dispersion state, isolation, and chiral nematic assembly of cellulose nanocrystals," *Ultrasonics Sonochemistry,* vol. 99, p. 106581, 2023/10/01/ 2023, doi: https://doi.org/10.1016/j.ultsonch.2023.106581.

[247] Y. D. Huang, L. Liu, J. H. Qiu, and L. Shao, "Influence of ultrasonic treatment on the characteristics of epoxy resin and the interfacial property of its carbon fiber composites," *Composites Science and Technology,* vol. 62, no. 16, pp. 2153-2159, 2002/12/01/ 2002, doi: https://doi.org/10.1016/S0266-3538(02)00148-3.

APPENDIX A SUPPORTING INFORMATION ARTICLE 1

Tannins for sustainable semi-solid-state supercapacitors

Molood Hoseinizadeh[1], Kholoud Salem[2], Abdelaziz Gouda[1,3], Daniel Belanger[4], Clara Santato[1, *]

[1]Department of Engineering Physics, Polytechnique Montreal, Canada

[2]Energy Materials Laboratory (EML), School of Sciences and Engineering, The American University in Cairo, New Cairo, Egypt

[3]Solar Fuels Group, Department of Applied Chemistry and Chemical Engineering, University of Toronto, Canada

[4]Département de Chimie, Université du Québec à Montréal, Canada

*Corresponding author: Clara Santato

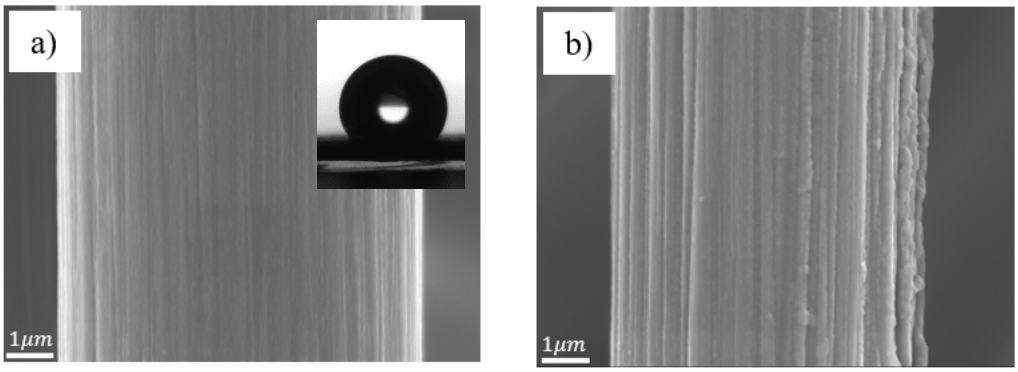

Figure A. 1 SEM images of: a) Carbon Paper (CP); b) Treated Carbon Paper (TCP), at 5 kV. Inset figure A. 1a): contact angle measurement for carbon paper.

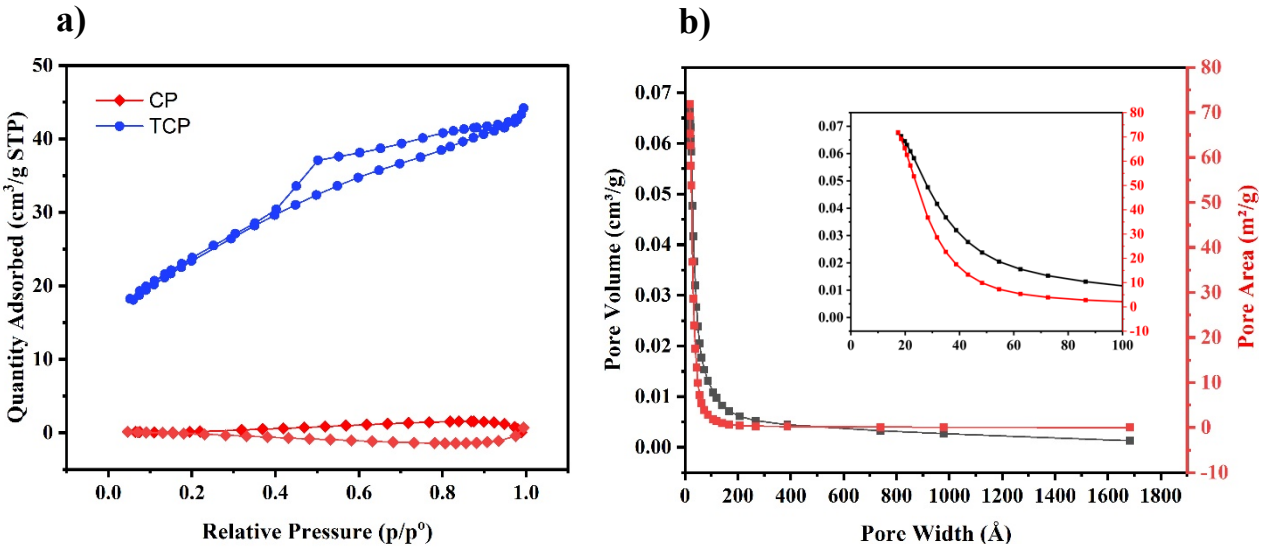

Figure A. 2 a) N2 adsorption/desorption isotherms of Carbon Paper (CP) and Treated Carbon Paper (TCP), b) pore size distribution for TCP. Inset figure A. 2b) magnified figure A. 2 for micro- and meso-pores distribution.

Table A. 1 Summary of BET results indicating the structural properties of Carbon Paper (CP) and Treated Carbon Paper (TCP). The nanopore surface area results from the sum of the surface areas of mesopores and macropores.

Sample*	**BET surface area ($m^2 g^{-1}$)**	**Micropore surface area ($m^2 g^{-1}$)**	**Nanopore surface area ($m^2 g^{-1}$)**	**Total Pore Volume ($cm^3 g^{-1}$)**	**Average pore diameter ($Å$)**
CP	0.13	2.90	0.90	1.05×10^{-3}	319.1
TCP	83.20	3.86	71.89	68.3×10^{-3}	32.8

* At least 3 weight measurements were taken for each sample, with a standard deviation of 5%

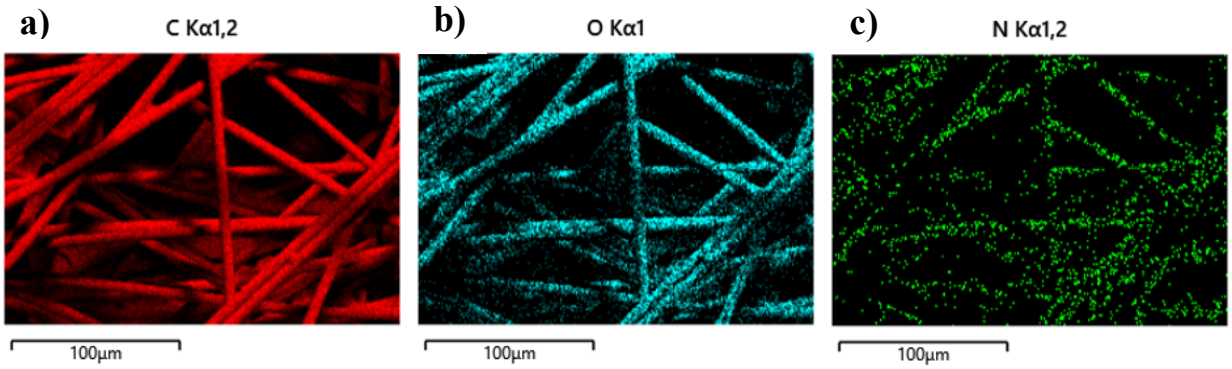

Figure A. 3 EDS mapping of C, O, N, for Treated Carbon Paper, at 5 kV.

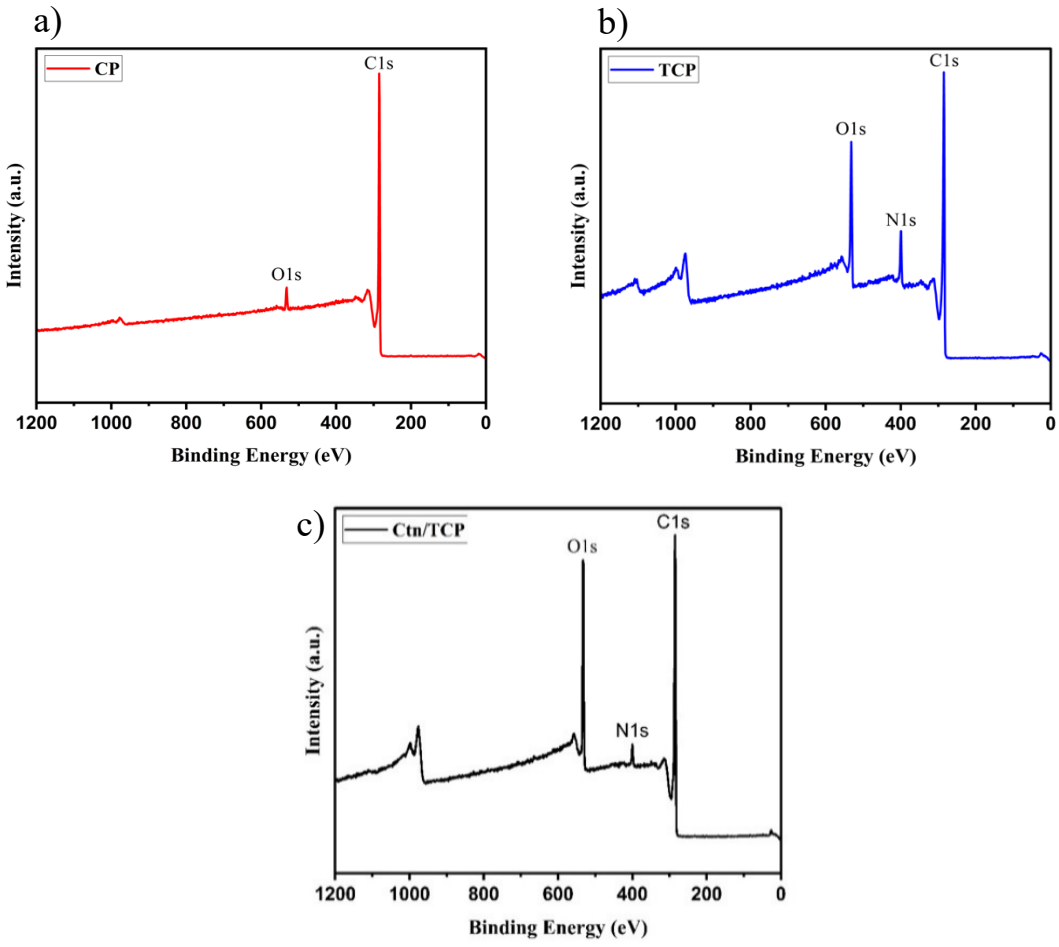

Figure A. 4 XPS survey spectra of a) Carbon Paper (CP), b) Treated Carbon Paper (TCP) and c) Catechin-loaded Treated Carbon Paper (Ctn/TCP)

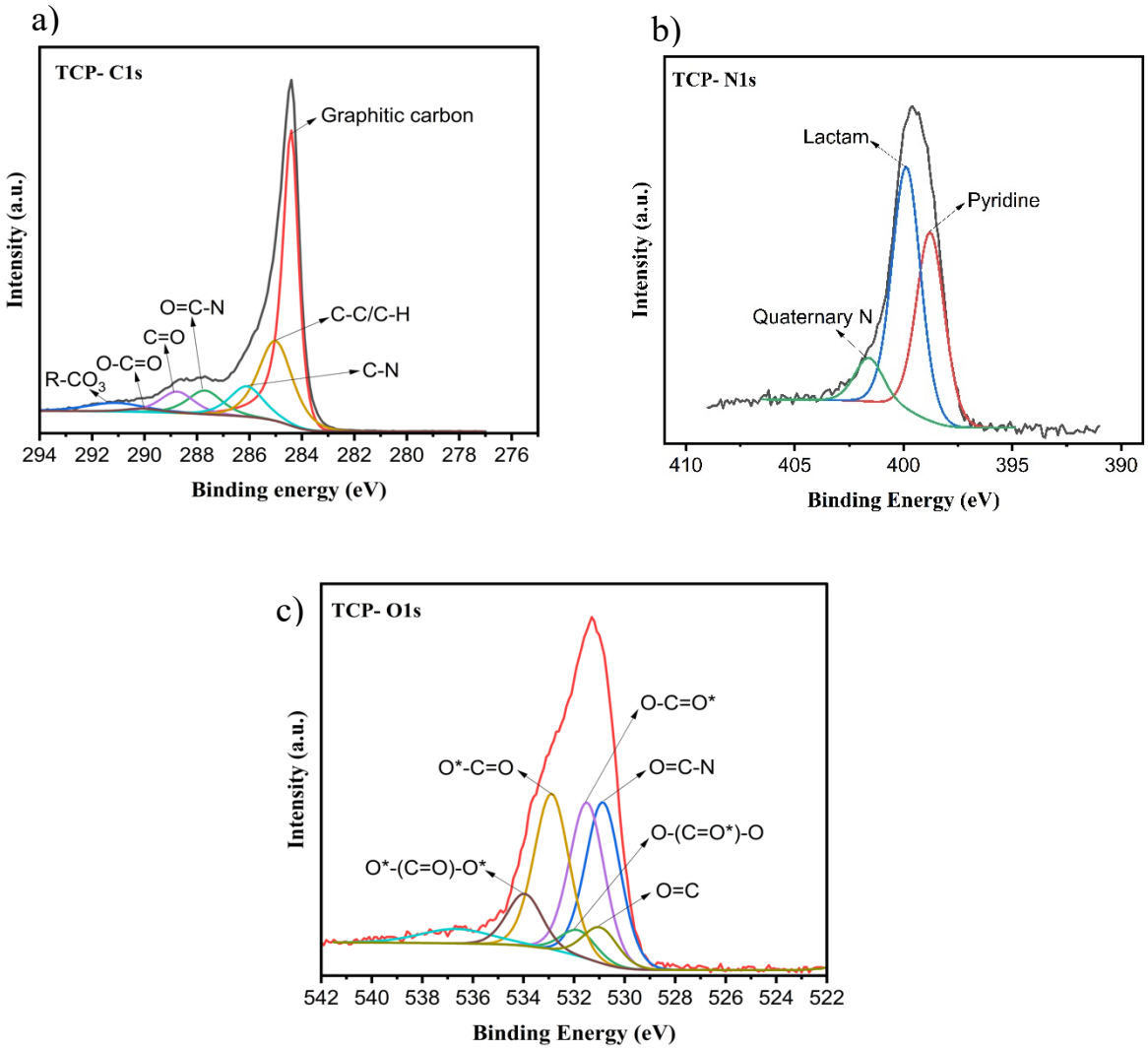

Figure A. 5 Core level XPS spectra of a) C1s, b) N1s and c) O1s for Treated Carbon Paper (TCP).

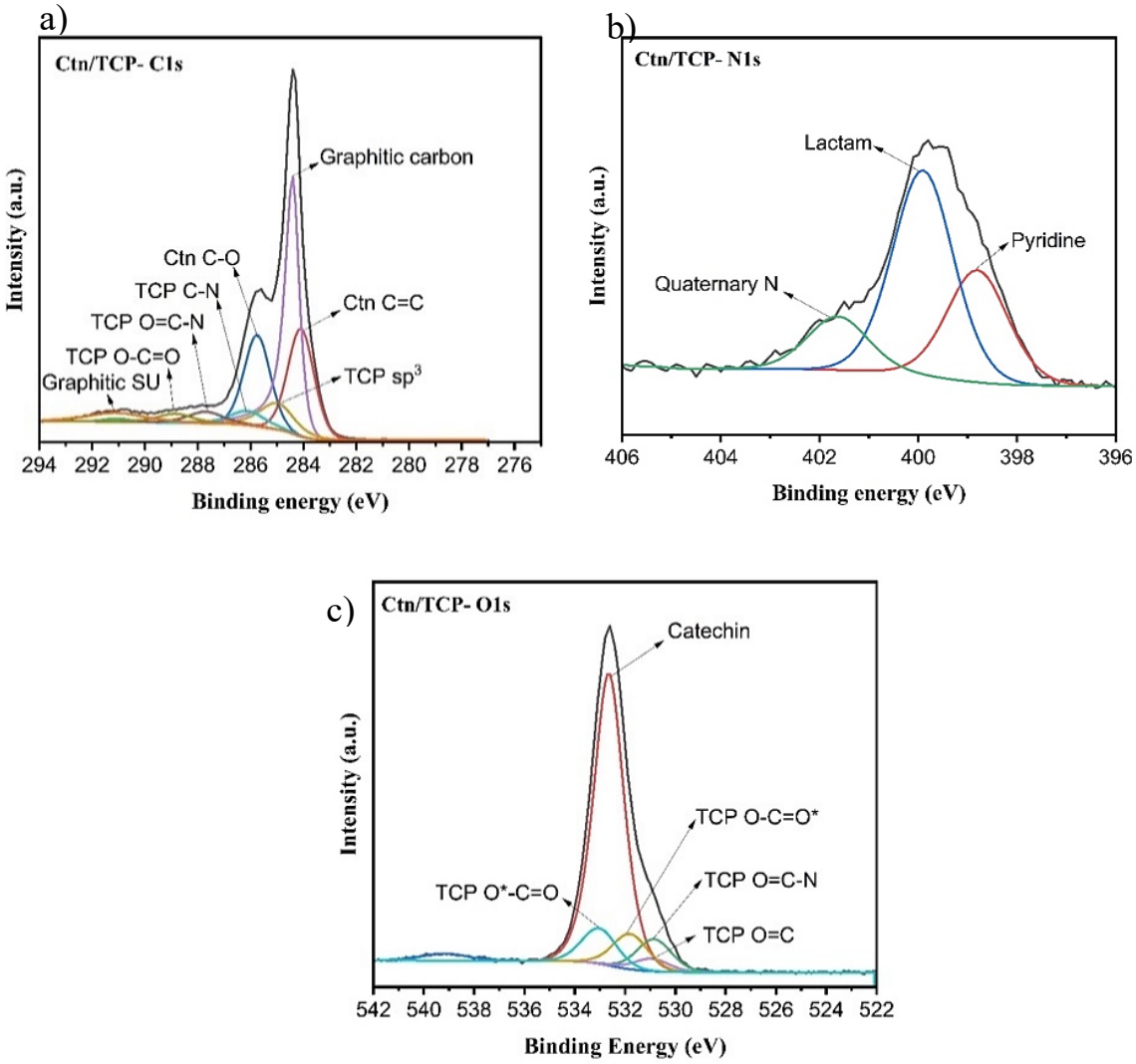

Figure A. 6 Core level XPS spectra of a) C1s, b) N1s and c) O1s for Catechin-loaded Treated Carbon Paper (Ctn/TCP).

Table A. 2 Elemental composition from XPS of the carbon paper (CP), Treated Carbon Paper (TCP), Catechin-loaded Treated Carbon Paper (Ctn/TCP).

		Atomic percent (at.%)		
Element	**Binding energy (eV)**	**CP**	**TCP**	**Ctn/TCP**
C 1s	284.8	96.5	75.6	76.5
O 1s	532.3	3.9	15.5	20.1
N 1s	399.5	NA	8.9	3.5

Supplementary note 1: FTIR characterization of Catechin (Ctn)

In the range of 3000-3500 cm^{-1}, a strong broad absorption peak was observed for Catechin, due to the presence of three secondary and two tertiary OH groups. In the range of 700 - 2000 cm^{-1}, there are a few characteristic peaks observed for Catechin including: at 760 cm^{-1} for C-H out of plane bending, at 880 cm^{-1} and 990 cm^{-1} for out of plane C=C–H bending, between 1050 – 1200 cm^{-1} for C-O stretching of secondary and tertiary alcohols, at 1150 cm^{-1} for aromatic OH, at 1290 cm^{-1} for C-O in alcohols, at 1370 cm^{-1} for OH bending of phenols, at 1470 cm^{-1} for C-H in alkanes, 1520 $cm^{-1}$for C=C belonging to the aromatic ring and 1610 cm^{-1} for C=C stretching of conjugated alkenes. The missing strong C=O stretching peak of a quinone moiety in the 1700 cm^{-1} region suggests the starting Catechin powder is in the reduced form (hydroquinone) before to electrochemical analysis[243].

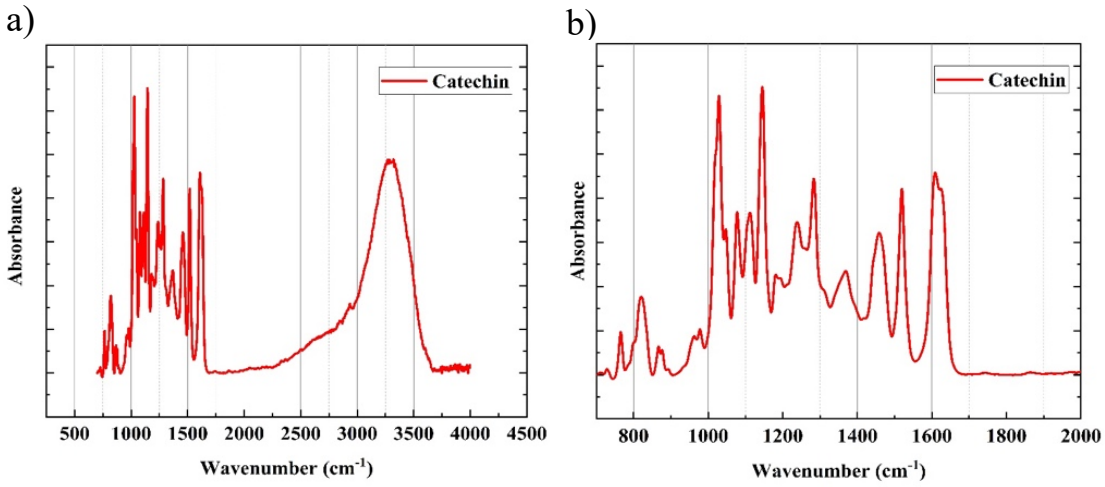

Figure A. 7 FTIR analysis of Catechin (Ctn) in the range of a) 500-4000 cm^{-1} and b) 700-2000 cm^{-1}.

Supplementary note 2: Evaluation of the faradic and non-faradic capacitance contribution

To deconvolute faradaic and non-faradaic contributions to the total charge storage, we used the Trasatti method[188]. We initially calculated the areal capacitance (C) from the cyclic voltammetries at different scan rates, using:

$$C = \frac{S}{2\,\nu\,\Delta V}$$

where C is the areal capacitance (mF cm^{-2}), ΔV the potential window (V), S is the area enclosed by the cyclic voltammograms (mA V cm^{-2}) and ν the potential scan rate (V s^{-1}). We assumed that ion diffusion follows a semi-infinite diffusion pattern such that a linear correlation between the reciprocal of the calculated areal capacitance (C^{-1}) and the square root of scan rates ($v^{1/2}$) is expected (Figure A8a), as follows:

$$C^{-1} = constant\ \ \nu^{1/2} + C_T^{-1}$$

where C_T represents maximum capacitance (sum of electrical double-layer capacitance (C_{EDL}) and pseudo-capacitance (C_{PS})).

We assessed the maximum C_{EDL} and maximum C_{PC} by plotting the linear relation between the calculated areal capacitances (C) vs. the reciprocal of the square root of scan rate ($\nu^{-1/2}$)(Figure A8b), described by the following equation:

$$C = constant\ \nu^{-1/2} + C_{EDL}$$

where C_{EDL} is evaluated from the linear fitting and extrapolating the fitting line to y-axis and C_T can be assessed by subtraction of C_{EDL} from C_T.

The percentage of each capacitance contribution can be evaluated as follows:

$$C_{EDL}\% = \frac{C_{EDL}}{C_T} \times 100$$

$$C_{PC}\% = \frac{C_{PC}}{C_T} \times 100$$

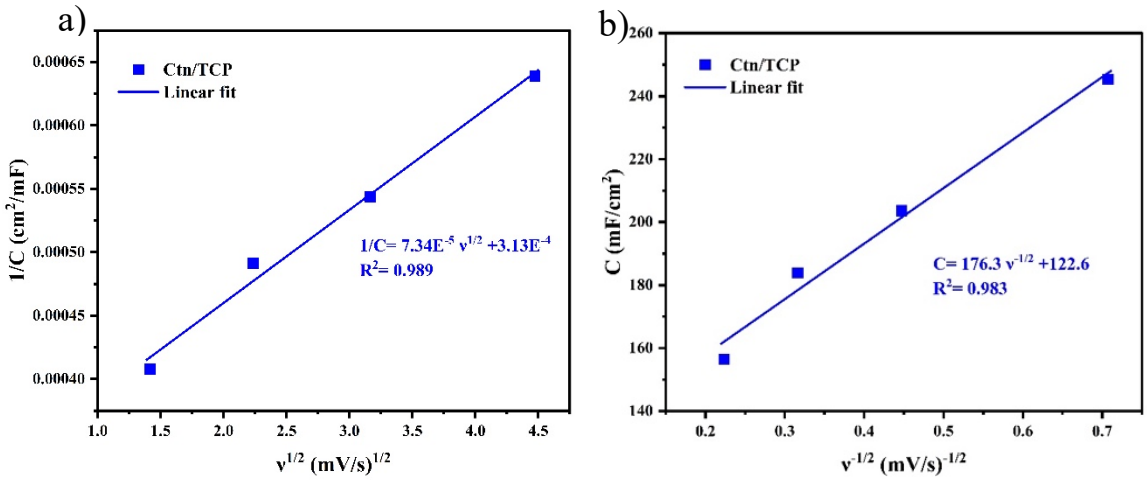

Figure A. 8 Plots of reciprocal of areal capacitance (C^{-1}) vs. square root of scan rate ($v^{1/2}$). (b) Plots of areal capacitance (C) vs. reciprocal of square root of the scan rate ($v^{-1/2}$). The solid lines are linear fitting of data points, and the linear fit equation with root mean square is shown in the inset.

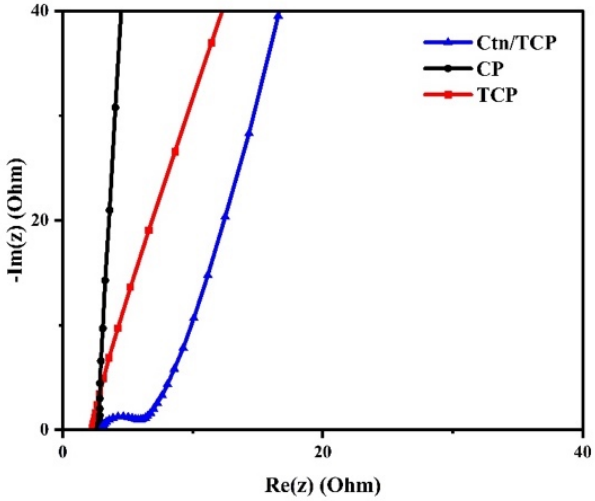

Figure A. 9 Nyquist plot of the carbon paper (CP), Treated Carbon Paper (TCP), Catechin-loaded TCP (Ctn/TCP) in three-electrode cell set-up in 0.5M Na_2SO_4 (aq)

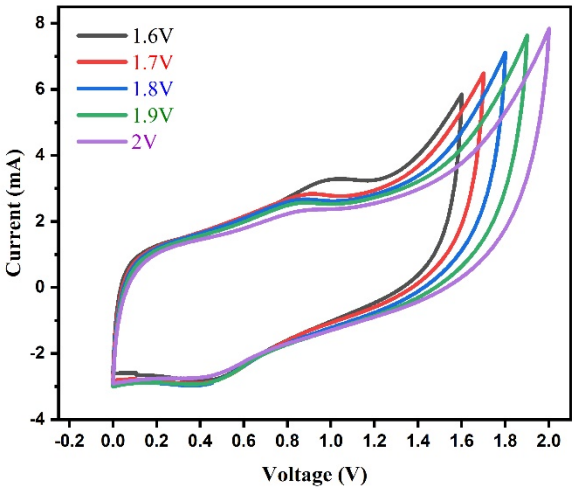

Figure A. 10 Cyclic voltammograms of a Catechin-loaded Treated Carbon Paper (Ctn/TCP) symmetric solid-state supercapacitor at different voltage windows from 1.6 to 2 V at a scan rate of 5 mV/s.

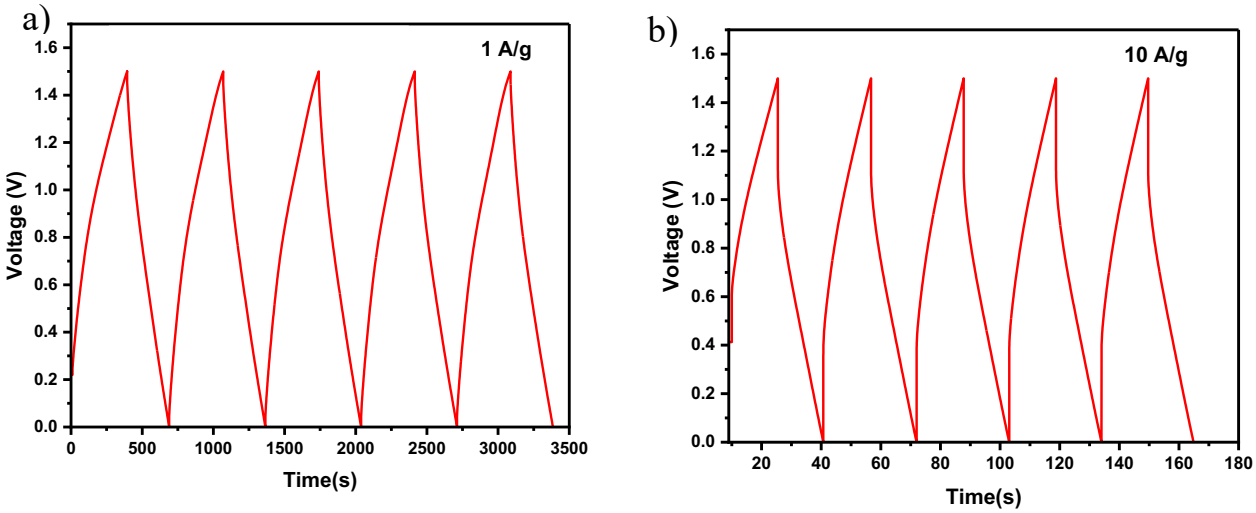

Figure A. 11 Galvanostatic charge/discharge curves for Catechin-loaded Treated Carbon Paper (Ctn/TCP) symmetric solid-state supercapacitors at a) 1 A/g and b) 10 A/g.

Table A. 3 Electrochemical performance of State-of-the-art of organic bio-sourced-based supercapacitors in the literature

Electrode material	***Electrolyte***	***Performance***				***Capacitance retention***	***Published Year***	***Ref.***
		Capacitance	***Chargin g voltage***	***Energy Density***	***Power density***			
Juglone modified CNT-bacterial cellulose/ activated carbon	*H_2SO_4/PVA hydrogel*	*NA*	*2 V*	*40 W h kg^{-1} at 10 A g^{-1}*	*1 000 W kg^{-1} at 10 A g^{-1}*	*80% after 10 000 cycles*	*2020*	*[58]*
Juglone modified activated carbon/activated carbon	*H_2SO_4 1M*	*66 F g^{-1} at 0.3 A g^{-1}*	*1.2 V*	*12 W h kg^{-1} at 3 A g^{-1}*	*180 W kg^{-1} at 3 A g^{-1}*	*77% after 3 000 cycles*	*2019*	*[63]*
Emodin-Graphene nanosheet/ Caffeic acid-graphene hydrogel	*H_2SO_4 1M*	*88 F g^{-1} at 10 mV s^{-1}*	*1.8 V*	*33 W h kg^{-1} at 0.5 A g^{-1}*	*800 W kg^{-1} at 0.5 A g^{-1}*	*80% after 7 000 cycles*	*2021*	*[64]*
Lignin-based carbon nanofiber-SnO_2	*Na_2SO_4 1M*	*NA*	*1.8 V*	*11.5 W h kg^{-1} at 1 A g^{-1}*	*451 W kg^{-1} at 1 A g^{-1}*	*91.3% after 10 000 cycles*	*2020*	*[65]*
polydopamine supported on functionalized carbon cloth	*H_2SO_4/PVA hydrogel*	*61 F g^{-1} at 1 A g^{-1}*	*1.2 V*	*11.7 W h kg^{-1} at 1 A g^{-1}*	*6400 W kg^{-1} at 1 A g^{-1}*	*81% after 10 000 cycles*	*2021*	*[57]*
Tannic acid/ graphene	*$H2_5O_4$ /PVA hydrogel*	*195 F g^{-1} at 0.5 A g^{-1}*	*1 V*	*37 W h kg^{-1} at 20 A g^{-1}*	*4476 W kg^{-1} at 20 A g^{-1}*	*84% after 8 000 cycles*	*2018*	*[66]*
PANI/Tannic acid/rGO	*H_2SO_4 /PVA hydrogel*	*56 F g^{-1} at 0.5 A g^{-1}*	*1.6 V*	*1.68 W h kg^{-1} at 0.5 A g^{-1}*	*115 W kg^{-1} at 0.5 A g^{-1}*	*NA*	*2019*	*[69]*
Sepia on treated carbon paper	*Na_2SO_4 0.5 M*	*NA*	*1.6 V*	*20 W h kg^{-1}*	*46 W kg^{-1}*	*100% after 50 000 cycles*	*2022*	*[100]*
Catechin/Tannic acid on treated carbon paper	*Na_2SO_4 0.5 M*	*NA*	*1.6 V*	*23 W h kg^{-1}*	*26 kW kg^{-1}*	*100% after 10 000 cycles*	*2022*	*[100]*
Catechin on treated carbon paper	***Na_2SO_4/PVA hydrogel***	***202 F g^{-1} at 1 A g^{-1}***	***1.5 V***	***55 W h kg^{-1} at 1 A g^{-1}***	***660 W kg^{-1} at 1 A g^{-1}***	***99.6% after 20 000***	***This work***	

APPENDIX B SUPPORTING INFORMATION ARTICLE 2

Ultrasound-Assisted Deposition of Sepia Melanin and Multiwalled Carbon Nanotubes on Carbon Cloth: Toward Sustainable Surface Engineering for Flexible Supercapacitors

Molood Hoseinizadeh[1]*, Nila Davari[2], Abdelaziz Gouda[3]*, Hamza Hyat[1], Mohini Sain[3], Daria C.Boffito[2], Clara Santato[1]*

[1]Department of Engineering Physics, Polytechnique Montreal, H3T 1J4, Canada

[2]Department of Chemical Engineering, Polytechnique Montreal, H3T 1J4, Canada

[3]Department of Applied Chemistry and Chemical Engineering, University of Toronto, M5R 0A3, Canada

* Corresponding authors: Molood Hoseinizadeh; Abdelaziz Gouda; Clara Santato

Supplementary Note 1: Optimization of ultrasound parameters

We optimized the ultrasonication parameters, including *time*, *actual power*, and *temperature*, to evaluate their impact on the areal capacitance of carbon cloth (CC, Table B. 1). To determine the areal capacitance of CC under different ultrasonication treatment conditions, we employed cyclic voltammetry (CV) using a three-electrode cell configuration in 1M $Na_2SO_{4(aq)}$ as the electrolyte. The areal capacitance was calculated using equation (i) provided in Supplementary Note 2.

Increasing the ultrasonication time from 1 to 5 minutes increases the areal capacitance of the carbon cloth from $52\ mF\ cm^{-2}$ to $76\ mF\ cm^{-2}$, at a constant *actual* power of 40 W and temperature of 20 °C (Figure B. 1a). Extending the ultrasonication time to 10 minutes, caused a significant (60%) reduction in areal capacitance, primarily attributed to the loss of mechanical integrity of the CC. To determine the optimal temperature for the 5 min ultrasonication treatment under *actual* ultrasound power of 40 W, we evaluated the areal capacitance. The results indicate that 40 °C represents the optimal temperature for the ultrasonication treatment of CC (Figure B. 1b). This implies that the efficiency of ultrasonication treatment diminishes at higher temperatures due to reduced cavitation effects[244, 245]. We explored sonolysis effects on the areal capacitance of CC at actual powers of 40 W, 60 W, and 80 W (Figure B. 1c). The CC electrode achieves an areal capacitance as high as 147 $mF\ cm^{-2}$ under the optimal ultrasonication treatment conditions, i.e.

actual ultrasound power of 60 W, temperature of 40 °C, and 5 min ultrasonication time. Increasing the ultrasound power to 80 W leads to a decrease in areal capacitance, likely due to the breaking and fragmentation of carbon fibers[246, 247]. According to the results, the energy consumption of ultrasound treatment of CC under optimized conditions is 5 Wh.

Table B. 1 Effects of ultrasonication time, temperature, and actual power, on the areal capacitance of carbon cloth. Run 8 represents optimal conditions.

Run	Time (min)	Temperature (℃)	Actual power (W)	Areal capacitance (mF cm^{-2})
1	1	20	40	52
2	5	20	40	76
3	10	20	40	60
4	5	20	40	76
5	5	40	40	85
6	5	60	40	71
7	5	40	40	85
8	**5**	**40**	**60**	**147**
9	5	40	80	67

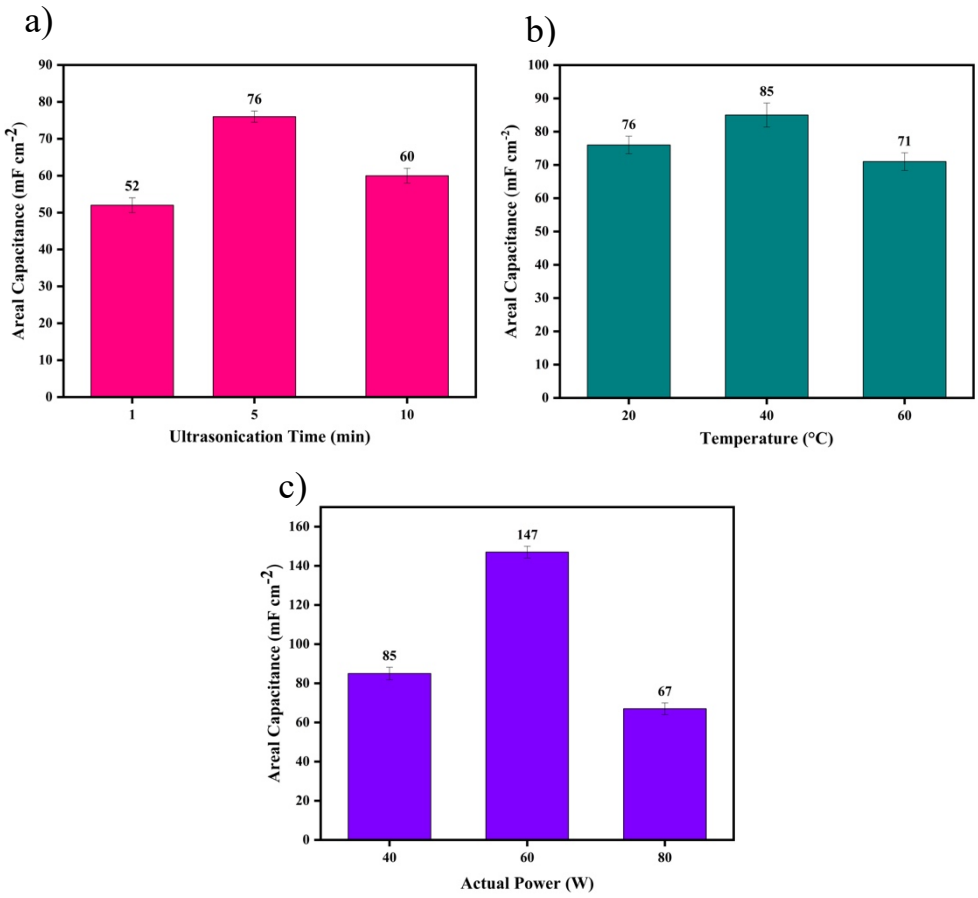

Figure B. 1 Effects of: a) ultrasonication time, b) temperature during ultrasonication treatment, and c) actual power of ultrasound, on the areal capacitance of carbon cloth (CC).

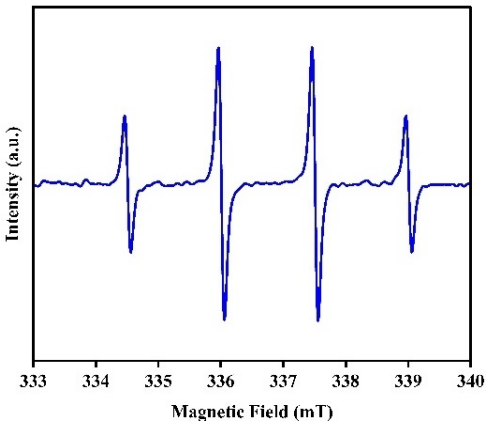

Figure B. 2 EPR spectrum of hydroxyl radicals formed during ultrasonic irradiation of water sample exposed to the ultrasonication treatment of carbon cloth (CC) under optimized conditions (see Table B. 1).

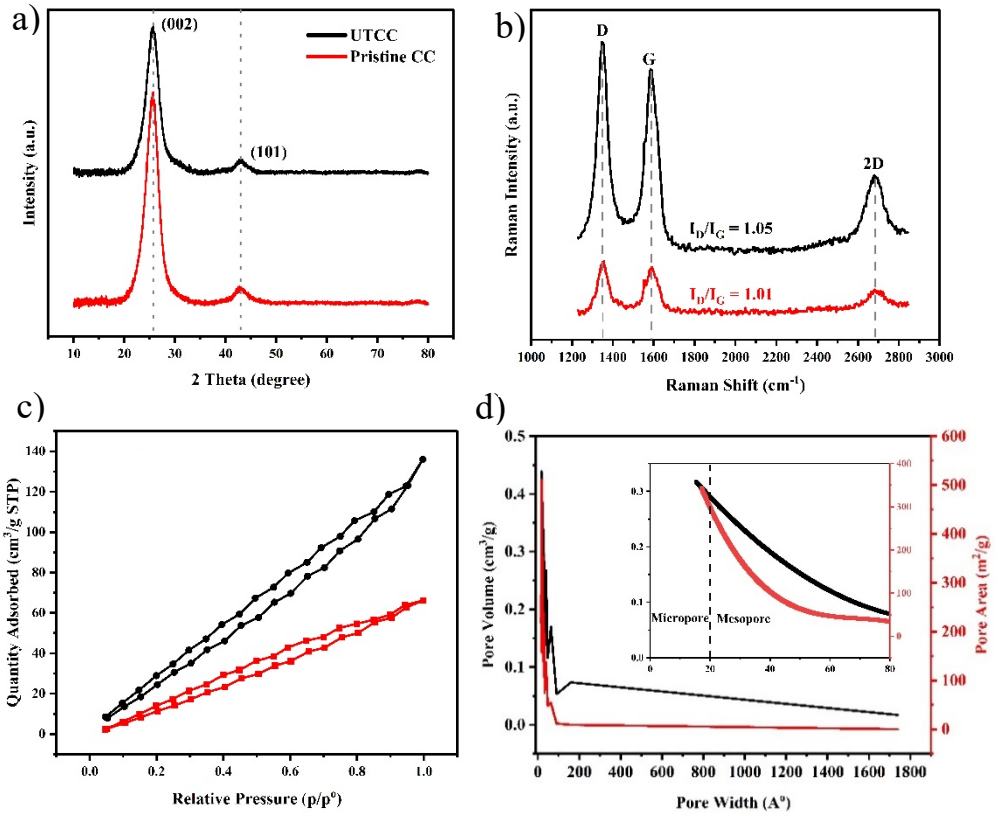

Figure B. 3 a) XRD patterns for pristine carbon cloth (CC) and ultrasound treated carbon cloth (UTCC); b) Raman spectra for CC and UTCC; c) N2 adsorption/desorption isotherms of CC and UTCC; d) pore size distribution for UTCC; Inset figure d) magnified figure for micro and mesopores distribution of UTCC.

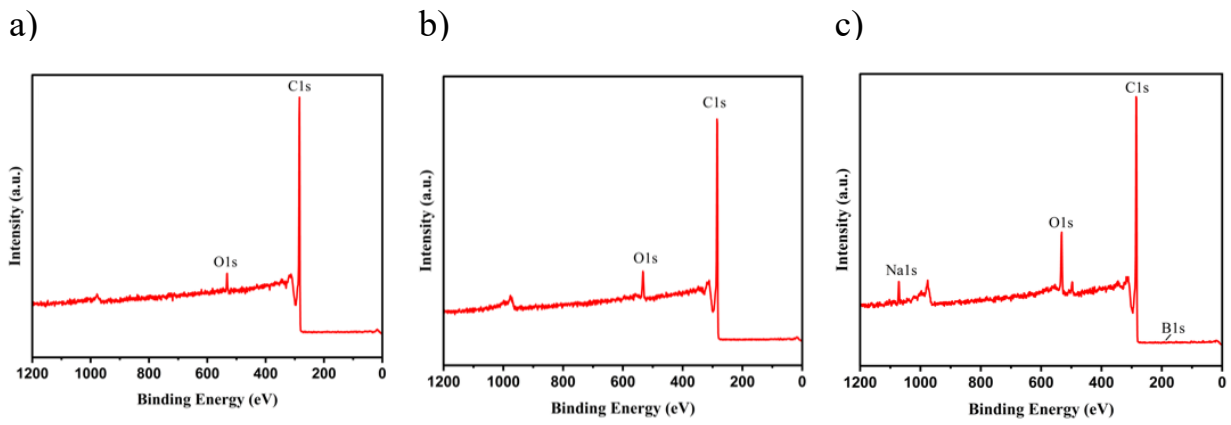

Figure B. 4 XPS survey spectra of: a) pristine carbon cloth (CC); b) heat treated carbon cloth (HTCC); c) ultrasound treated carbon cloth (UTCC).

Table B. 2 Elemental composition from XPS of the pristine carbon cloth (CC), heat-treated carbon cloth (HTCC), and ultrasound-treated carbon cloth (UTCC).

		Atomic percent (at.%)		
Element	Binding energy (eV)	Pristine CC	Heat treated CC	Ultrasound treated CC
C 1s	284.3	99.6	94.1	87.8
O 1s	532.2	2.4	5.9	9.6
Na 1s	1071.6	NA	NA	1.4
B 1s	192.4	NA	NA	0.7
Si 2p	102.7	NA	NA	0.5

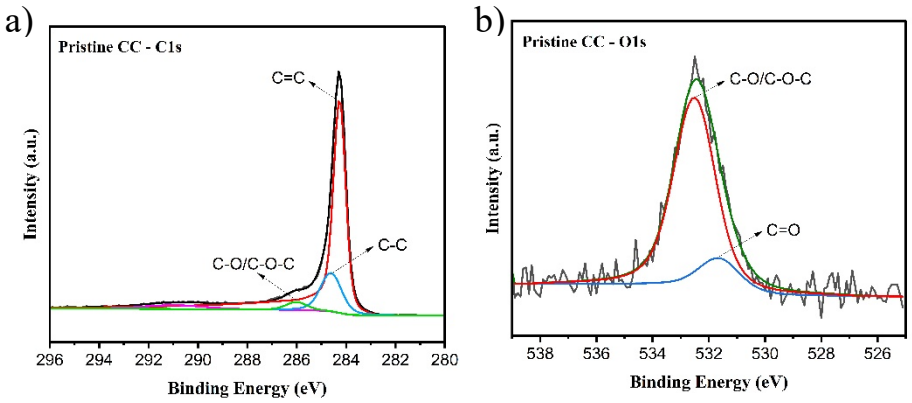

Figure B. 5 Core level XPS spectra of: a) C1s, b) O1s, for pristine carbon cloth (CC).

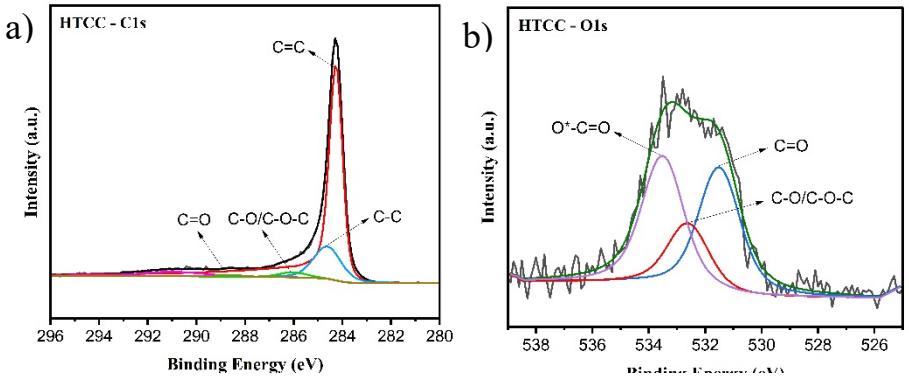

Figure B. 6 Core level XPS spectra of: a) C1s, b) O1s, for heat treated carbon cloth (HTCC).

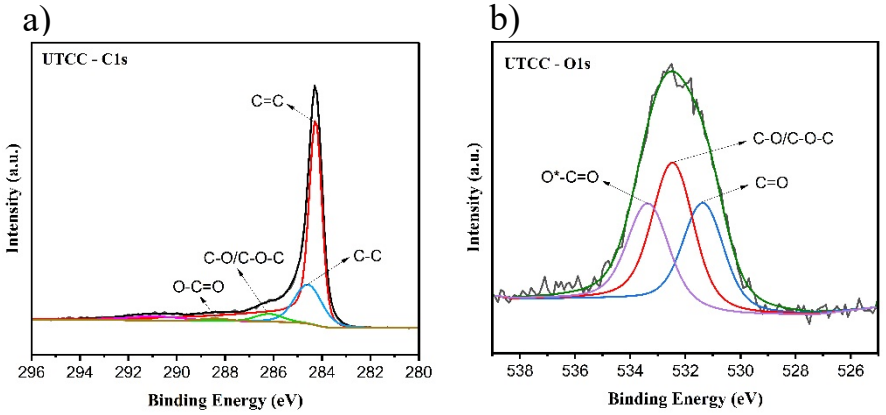

Figure B. 7 Core level XPS spectra of: a) C1s, b) O1s, for ultrasound treated carbon cloth (UTCC).

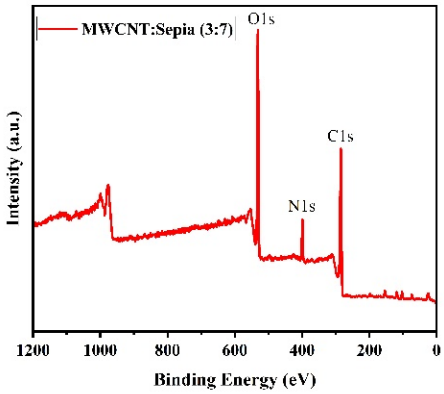

Figure B. 8 XPS survey spectra of MWCNT:Sepia (3:7).

Table B. 3 Areal capacitance of UTCC/Sepia and UTCC/MWCNT:Sepia with different mass ratios.

Sample name	**Areal capacitance** $[mF\ cm^{-2}]$
UTCC/MWCNT:Sepia (7:3)	129
UTCC/MWCNT:Sepia (1:1)	136
UTCC/MWCNT:Sepia (3:7)	274
UTCC/Sepia	183

Supplementary Note 2: Evaluation of the faradaic and non-faradaic capacitance contribution

To deconvolute faradaic and non-faradaic contributions to the total charge storage, we used the Trasatti method[188]. We initially calculated the areal capacitance (C) from the cyclic voltammetry at different scan rates, using:

$$C = \int \frac{IdV}{\nu\, A\, \Delta V} \qquad \text{(i)}$$

where $\int IdV$ is the integral CV curve area, ν the scan rate ($mV\ s^{-1}$), A the footprint area of the active material on the current collector (cm^2), and ΔV is the potential window (V). We assumed that ion diffusion follows a semi-infinite diffusion pattern such that a linear correlation between the reciprocal of the calculated areal capacitance (C^{-1}) and the square root of scan rates ($v^{1/2}$) is expected (Figure B9a), as follows:

$$C^{-1} = constant\ \nu^{1/2} + C_T^{-1}$$

where C_T represents total capacitance (i.e. sum of electrical double-layer capacitance (C_{EDL}) and pseudo-capacitance (C_{PC})).

We assessed the maximum C_{EDL} and maximum C_{PC} by plotting the linear relation between the calculated areal capacitances (C) vs. the reciprocal of the square root of scan rate ($\nu^{-1/2}$, Figure B9b), described by the following equation:

$$C = constant\ \nu^{-1/2} + C_{EDL}$$

where C_{EDL} is evaluated from the linear fitting and extrapolating the fitting line to the y-axis and C_T can be assessed by subtraction of C_{EDL} from C_T.

The percentage of each capacitance contribution can be evaluated as follows:

$$C_{EDL}\% = \frac{C_{EDL}}{C_T} \times 100$$

$$C_{PC}\% = \frac{C_{PC}}{C_T} \times 100$$

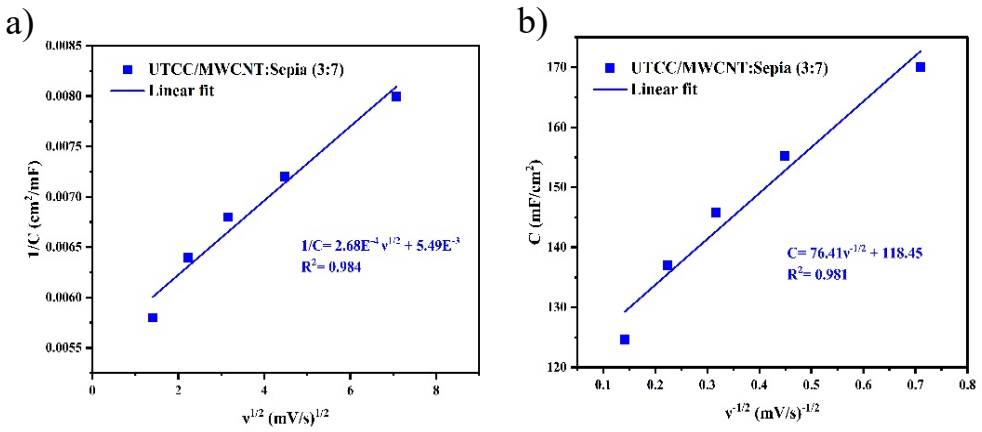

Figure B. 9 a) Plots of reciprocal of areal capacitance (C^{-1}) vs. square root of scan rate ($v^{1/2}$); b) Plots of areal capacitance (C) vs. reciprocal of square root of the scan rate ($v^{-1/2}$). The solid lines are linear fitting of data points, and the linear fit equation with root mean square is shown in the inset.

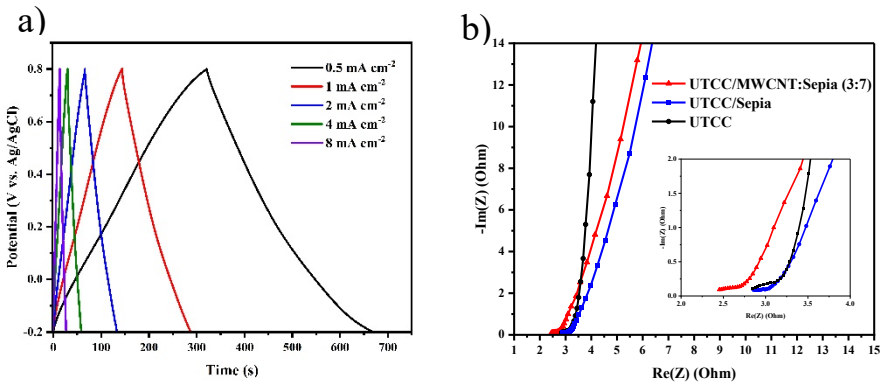

Figure B. 10 a) Galvanostatic charge/discharge curves of UTCC/MWCNT:Sepia(3:7); (b) Nyquist plot in the frequency range of 10^5 and 10^{-1} Hz; the inset shows an expanded view of the Nyquist plot for high frequency current density in 1 M $Na_2SO_{4(aq)}$

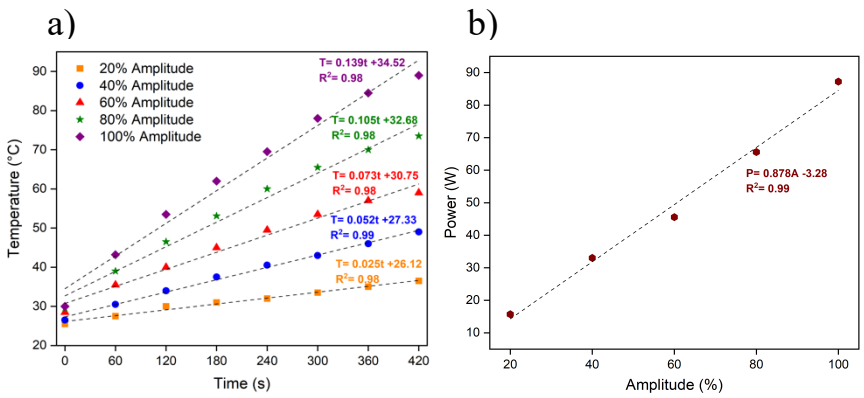

Figure B. 11 Ultrasound calibration: a) Temperature vs. time, b) Actual power vs. amplitude.